Michael Richter, BSc

Systematic Variations of Paper Properties and their Effect on High Speed Inkjet Print Curl

MASTER'S THESIS

to achieve the university degree of

Diplom-Ingenieur

Master's degree programm: Chemical and Process Engineering

submitted to

Graz University of Technology

Supervisor

Assoc. Prof. Dipl.-Ing. Dr. techn. Ulrich Hirn

Institute of Paper, Pulp and Fiber Technology

Graz, February 2018

AFFIDAVIT

I declare that I have authored this thesis independently, that I have not used other than the declared sources/resources, and that I have explicitly indicated all material which has been quoted either literally or by content from the sources used. The text document uploaded to TUGRAZonline is identical to the present master‘s thesis.

Date	Signature

Science knows no country,
because knowledge belongs to humanity,
and is the torch which illuminates the world.

Louis Pasteur

¡Muchisimas gracias a mis queridos amigos de ERASMUS que me han iluminado el mundo y siguen ampliando mi horizonte persistentemente!

Abstract

Liquid-paper interactions are known to cause dimensional stability issues in High Speed Inkjet Printing processes.

This thesis investigated the paper related reasons for curl behaviour in inkjet printing. Based on Eucalyptus kraft pulp, six individual handsheet series were manufactured, each focussing on one paper property or constituent. The trials of refining levels, PCC as fillers, furnish mixtures of kraft pulp and BCTMP, additional fines content and AKD-sizing were entirely produced by using a conventional Rapid Köthen Sheetformer. In a further trial, oriented sheets with a $TSI_{MD/CD}$ ratio of 1.7 to 1.9 were produced on a Dynamic Sheetformer. Sheet density was adapted by wet pressing at three levels between 0 and 150 bar.

The laboratory sheets were tested on a lab-scale pilot curl test setup using industrial inkjet print heads. By means of a laser displacement sensor, the extent and rate of the deformation was measured. Additional measurements were conducted regarding wet expansion of paper samples in ink and stiffness loss due to printing. The same water-based ink was used in every experiment.

The results show a considerable initial curl towards non-printed side, reaching its maximum 1-2 seconds after printing. At the end of the measurement after 4 minutes, an upwards curl towards printed side is observed. The extent of maximum curl and end curl are not correlated, both phenomenons are controlled by different mechanisms.

AKD sized papers with $Cobb_{60}$ values between 22-54 g/m^2 reduce both the initial and end curl revealing the positive impact of a superior hydrophobisation on dimensional stability. Sheets with BCTMP content observe a severe end curl but a lower maximum curl. Two-sidedness effects are mainly seen in the filler and fines trials but also within the other trials. The dynamic sheets exhibit an equally low end curl in MD and CD but no fiber orientation two-sidedness. Increasing sheet density directly correlates with a higher initial curl but barely affects the magnitude of end curl.

A high modulus of elasticity mostly leads to a diminishing initial curl and a subsequent extended end curl. However, the sizing and fines trials do not show this behaviour. Correlations between investigated Key Performance Indicators are generally not found for all trials.

Kurzfassung

Die Dimensionsstabilität von Papieren während des High Speed Inkjet-Drucks wird oftmals negativ beeinflusst durch Wechselwirkungen zwischen der Flüssigkeit und dem Papier.

Im Zuge dieser Arbeit wurden die auf Papiereigenschaften zurückzuführenden Ursachen für das Curl Verhalten im Inkjet-Druck untersucht. Dazu wurden sechs verschiedene Eigenschaften beziehungsweise Papierbestandteile in ebenso vielen Serien an Laborblättern isoliert voneinander variiert. Ausgehend von einem aus 100% Eukalyptus Zellstoff bestehenden Laborblatt, wurden Testreihen mit unterschiedlicher Mahlung, verschiedenen Füllstoffgehältern, Holzstoffanteilen, zusätzlichen Feinstoffen und AKD-Leimung mithilfe eines Rapid Köthen Blattbildners durchgeführt. Zusätzlich wurden orientierte Blätter mit einem $TSI_{MD/CD}$ Verhältnis von 1.7-1.9 auf einem Dynamischen Blattbildner produziert. Die Blattdichte wurde durch Nasspressen mit 0, 75 und 150 bar variiert.

Mithilfe eines Curl-Setups im Labormaßstab, das mit industriellen Druckköpfen und einem Lasersensor ausgestattet war, konnten Ausmaß und Geschwindigkeit des durch den Druck hervorgerufenen Curls gemessen werden. Weiters wurden Papierproben hinsichtlich ihrer Ausdehnung bei Eintauchen in Tinte und dem Steifigkeitsverlust während des Drucks untersucht. Für alle Versuche wurde dieselbe wasserbasierende Tinte verwendet.

Die Ergebnisse zeigen einen erheblichen initialen Curl zur unbedruckten Seite, der nach 1-2 Sekunden voll ausgebildet ist. Am Testende nach 4 Minuten verbleibt ein entgegengesetzter Curl zur bedruckten Seite. Den beiden Phänomenen liegen unterschiedliche Mechanismen zu Grunde, ihre Dimensionen korrelieren nicht zueinander.

Die AKD geleimten Papiere mit $Cobb_{60}$ Werten zwischen 22-54 g/m^2 reduzieren sowohl den initialen als auch den finalen Curl, was den positiven Effekt einer Hydrophobierung auf die Dimensionsstabilität unterstreicht. Papiere mit BCTMP-Gehalt zeigen einen starken finalen aber schwachen initialen Curl. Zweiseitigkeitseffekte sind verstärkt in den Füll- und Feinstoffversuchen zu beobachten. Die orientierten Blätter zeigen einen gleichermaßen geringen finalen Curl in MD und CD aber keine Zweiseitigkeit der Faserorientierung. Eine erhöhte Blattdichte beinflusst den finalen Curl nicht, führt jedoch zu einem stärkeren initialen Curl.

Ein höherer Elastizitätsmodul vermindert den initialen Curl und verstärkt den finalen Curl. In Leimungs- und Feinstoff-Versuchsreihen ist dieser Zusammenhang jedoch nicht zu sehen. Im Allgemeinen sind die gefundenen Korrelationen zwischen den untersuchten Leistungskennzahlen nicht für alle sechs Testreihen vorhanden.

Acknowledgments

The completion of this thesis and the entire degree course would not have been achieved without the support and collaboration of many people to whom I want to express my sincere gratitude at this point. In particular, I want to thank a group of people actively contributing to this graduation project.

First of all, I want gratefully acknowledge my supervisor Assoc. Prof. Dr. Ulrich Hirn for his trust, the professional support and all the instructive discussions during the realisation of this thesis. He always took his time for my concerns and gave me the decisive hints to proceed. It was really inspiring working together with international researchers within the Christian Doppler Laboratory and having the chance to spend three months in Venlo for carrying out experiments.

I want to thank all colleagues at Océ and especially Ern Clevers, MSc. for a pleasant working environment and a very interesting insight into inkjet printing mechanisms. Ern constantly triggered my motivation to think about the fundamental reasons for deformation issues and offered me many beneficial advices.

I want to express my extend gratitude to Dr. Wolfgang Fischer and above all Pascal Pucher from Sappi Gratkorn for providing me the opportunity of using the Dynamic Sheet Former. The oriented sheets were entirely produced by Pascal due to his experiences, which enables me to get anisotropic sheets in the predetermined grammage range. Otherwise, a realisation of this task would not have been possible.

My sincere gratitude goes to Heidemarie Reiter from Mondi for providing me essential papermaking constituents and valuable information on handsheet production.

I am very thankful to DI Daniel Mandlez for his support in the separation of fines.

I want gratefully acknowledge Bianca, Harry, Irmi, Kerstin, Manu, Rosie and Sarah for lightening my workload and particularly Heidi for her patience and support whenever I was in troubles.

My deep gratitude to Claudia, Kerstin and Esther for arranging all organisational issues.

I want to thank all colleagues of the APV Activitas and the IPZ for the mutual support, fellowship and many collective activities.

Special thanks go to Sascha Feyrer for many debates on fundamental principles after isolated laboratory sessions in the Netherlands.

Last but not least, I want to express my profound gratitude to my family and friends for their support throughout my years of studying in Graz and Zaragoza. Their unconditional encouragement during intensive and time-consuming periods enabled a successful accomplishment of my studies and the most formative years of my life.

Contents

List of abbreviations

AKD	Alkyl Ketene Dimer
ASA	Alkenyl Succinic Anhydride
BCTMP	Bleached Chemo Thermo Mechanical Pulp
BS	Bottom Side
CD	Cross Direction
CDL	Christian Doppler Laboratory
CI	Confidence Interval
CMC	Carboxy Methyl Cellulose
DSF	Dynamic Sheet Former
FO	Fiber Orientation
GCC	Ground Calcium Carbonate
HSI	High Speed Inkjet
KPI	Key Performance Indicator
LWC	Light Weight Coated
MAD	Median Absolute Deviation
MD	Machine Direction
PCC	Precipitated Calcium Carbonate
PVOH	Polyvinyl Alcohol
SC	Super Calandered
SEM	Scanning Electron Microscope
TI	Tensile Strenght Index
TMP	Thermo Mechanical Pulp
TS	Top Side
TSI	Tensile Stiffness Index

1 Introduction

When printing ink (e.g. in High Speed Inkjet (HSI) Printing) on a paper sample, it deforms differently on the printed and non-printed side. This behaviour is caused by an unbalanced hygroexpansion in the z-direction of the sample and leads to the formation of curl. Since the curl may lead to paper transport problems and damage to the print heads, the reasons for this kind of paper deformation were studied as part of the Christian Doppler Laboratory (CDL) for Fiber Swelling and Paper Performance at TU Graz (Graz University of Technology) in collaboration with Océ Venlo and Mondi Uncoated Fine Paper.

In total, four Master's projects within the CDL have dealt with curl issues. One focused on dried-in strains due to the industrial paper manufacturing process [1]. The second investigated long and short term curl of printed uncoated fine paper on a high speed inkjet test setup [2]. In the third thesis, paper properties responsible for blanco deformation in an industrial cut sheet printing device were analysed [3].

The aim of this work was to find correlations between specific paper properties and the curl formation during the printing process. The practical part of the work consisted in preparing handsheets with previously defined characteristics and test them on a pilot curl test setup at Océ and at the Institute of Pulp, Paper and Fiber Technology at TU Graz. By using the curl test setup, the magnitude and rate of print curl was measured and the relation to specific paper properties was investigated. Additional trials were performed investigating hydroexpansion in ink and loss of stiffness due to printing.

2 Theory - Fundamentals on paper physics and inkjet printing

The first part of this chapter gives a basic overview of the inner structure of a paper sheet regarding fibers and their orientation, filler, fines and internal sizing. The second part deals with the dimensional stability of a paper sheet focusing on four different mechanisms creating paper curl. Finally a brief introduction to inkjet printing will be provided.

2.1 Paper structure

Paper from industrial production frequently shows two-sidedness in z-direction due to unequally distributed paper constituents. Furthermore a homogeneous paper sheet is highly desired for the majority of applications, nevertheless it is barely feasible to get rid of a certain paper anisotropy. There is at least always a characteristical difference of paper properties in Machine Direction (MD) and Cross Direction (CD). This difference originates e.g. from the preferential alignment of the fibers in MD the magnitude of which is known under the term *Fiber Orientation (FO) anisotropy* [4]. A further issue that contributes to the inhomogeneity of a paper sheet arises when adding filler and fines to the furnish. These additives provoke variations of the properties over the thickness of the paper, mainly depending on the configuration of the wire section of the papermachine [5]. A detailed explanation on the mentioned aspects is given here.

Sheet forming. The fiber mat creation starts with jetting a diluted suspension of the mixed paper constituents (at approximately 1% solids content) on the forming fabric of the wire section. This step is nowadays often realised by a hydraulic headbox with dilution profiling. Applying this dilution enables a reduction of small-scale local grammage variations, known as *formation*. Small-scale here refers to deviations in a range of 0.1-20 mm.

Three major hydrodynamic processes are contributing to the formation of the fiber network. These are dewatering, oriented shear and turbulence. Elongational stretching of the fibers in the nozzle of the headbox can be considered an additional forth impact [6]. All occurring effects are illustrated in Figure 1.

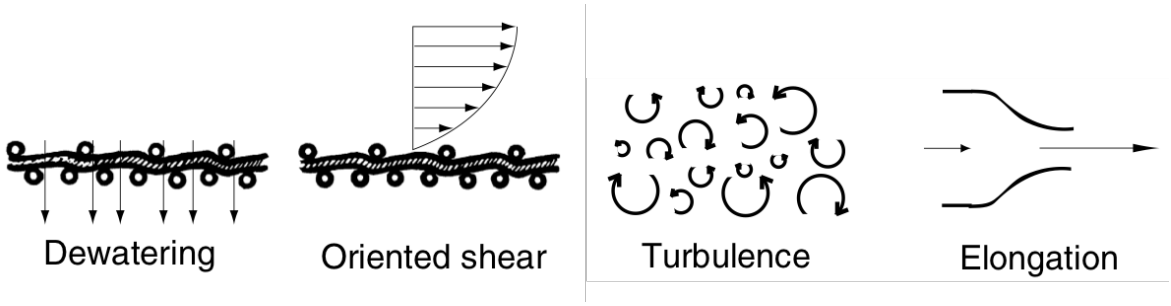

Figure 1. Four hydrodynamic principles that enhance an even fiber distribution [6].

Dewatering is the main purpose of the wire section. In order to achieve this, a high amount of water is initially removed by the jet impingement. The induced downward flow through the fiber mat and the forming fabric is further enhanced on Fourdrinier machines by foils and suction boxes [7]. A reduced flow resistance at regions of a low local grammage allow a *hydrodynamic smoothing*. Free moveable fibers are preferentially deposited in these low grammage areas and consequently homogenize the overall fiber distribution [5]. It has to be pointed out that any manipulation of the fiber network can only be achieved as long as the fibers are in aqueous suspension and the thickening fiber mat has not become too rigid.

Oriented shear. As a second effect, the oriented shear destructs and aligns fiber flocs. Only already slightly immobilized flocs can be broken by the acting shear stress. The affordable shear field or velocity gradient is created by a jet-to-wire speed difference. Concerning the fiber orientation, the jet-to-wire ratio plays a major role and will be discussed in 2.1.1.

Turbulence in this context refers to stochastic variations in flow velocity. On the positive side, turbulence augments a deflocculation in the headbox and the wire. Notwithstanding, once the fibers are deposited on the wire and drainage is in progress, turbulence has a counteracting effect on the formation [8]. But it concurrently reduces FO due to a reduction of the oriented shear flow [9].

Elongational flow. Another aspect contributing to a further enhancement of formation is the contraction of the suspension jet in the headbox. The converging headbox nozzle leads to jet-acceleration and thus creates elongational flow leading to breaking of fiber flocs [6]. Also fibers are oriented in elongational flow direction leading to a higher FO in the produced paper.

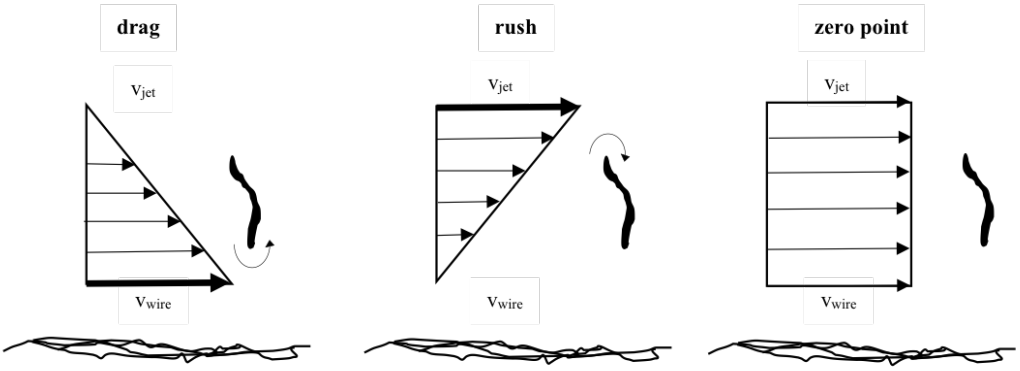

Figure 2. Jet-to-wire ratios <0 (*drag*) and ratios >0 (*rush*) lead to an alignment in MD. If velocities are equal, fibers are oriented randomly.

2.1.1 Fiber orientation and its effect on paper properties

The fiber orientation is used as a main parameter to characterize the anisotropy of a paper sheet. Its fundamental cause can be described by the suspension flow during web forming on the papermachine. As mentioned above, the jet-to-wire ratio is of particular importance when talking about alignment of fibers in MD. The speed difference between the suspension jet and the wire causes an immobilization of one end of an individual fiber. While one end gets stuck to the thickening fiber network, the other still moveable end is exposed to the shear field. Owing to that, the fiber undergoes a rotation in the direction of the shear flow [8]. In particular, there are three adjustable states. First, the wire speed is higher than the jet speed (*drag*), means a rotation of the lower end of the fiber, compare Figure 2. In the second case, the upper end of the fiber moves faster due to a higher suspension velocity (*rush*) and the fiber rotates the other way round but also in MD. Third, equal wire and jet speed do not generate any systematic fiber rotation or orientation [10].

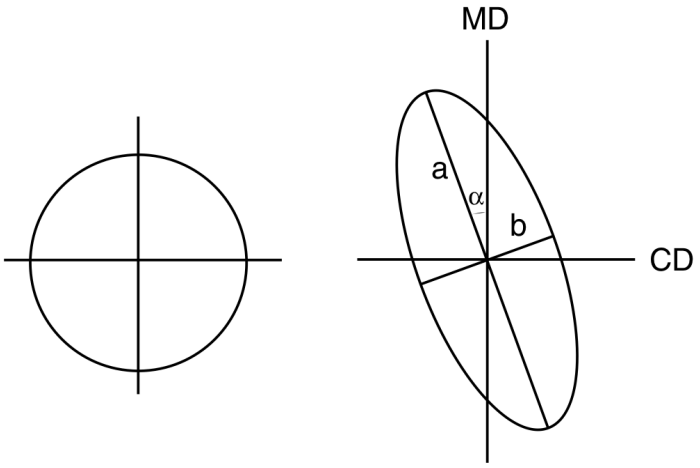

Figure 3. Comparison of a FO-index ($= a/b$) and FO-angle (α) for an isotropic sheet (left) vs. an anisotropic sheet (right) [6].

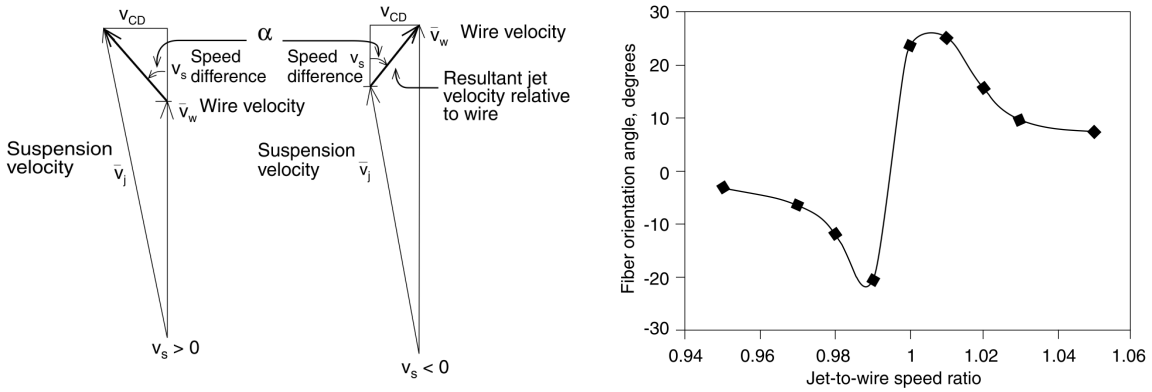

(a) The FO angle is determined by the direction of suspension flow relative to the wire.

(b) Highest FO angles are caused by minimal jet-to-wire speed differences.

Figure 4. Impact of the jet-to-wire-ratio on the fiber orientation [5].

Definition of fiber orientation index and angle. To quantify the magnitude of the fiber orientation, the frequency distribution of the orientation of all present fibers in a sheet is plotted in a polar digram. Then an ellipse is fitted to the frequency distribution. As illustrated in Figure 3 an isotropic sheet (e.g. laboratory handsheet) shows no observable orientation and thus a circular shape in this diagram. In contrast, an industrial paper forms an ellipse whose principal axis a represents the main orientation direction of fibers. The fiber orientation index or FO anisotropy is defined as ratio a/b, in which b is the conjugate axis of the ellipse [11].

While in ideal conditions the main orientation axis a and the MD coincide, there is frequently a certain deviation characterized by the fiber orientation angle α. This misalignment is mainly affected by the relations between suspension and wire velocity as illustrated in Figure 4a. Even very small angular deviations between jet and wire cause a considerable misalignment (α in Fig. 4a) due to the induced cross flow. This CD velocity component v_{CD} also covers transverse flows on the wire section as a result of generated turbulences. If the velocity differences $v_s > 0$ (*rush*) the FO angle α is positive in the mathematical sense. A correspondingly negative misalignment is provoked in the *drag* state ($v_{wire} > v_{suspension} \rightarrow v_s < 0$). At minimal speed ratios v_s close to 0 the cross flow v_{CD} plays a major role resulting in higher FO angles (compare Figure 4b). In fact, fiber orientation angle is commonly not constant across the web due to higher local dilutions or basis weight adjustments [5, 6].

Two-sidedness of FO index and angle. The fiber orientation distribution in z-direction mainly depends on initial drainage, immobilization speed of the fiber mat and thus on former type and installed turbulence generators. Figure 5 compares the impact of *drag* and *rush* state on the FO index variation over the sheet thickness for three pilot formers. All types show minor orientation on both bottom and top surface.

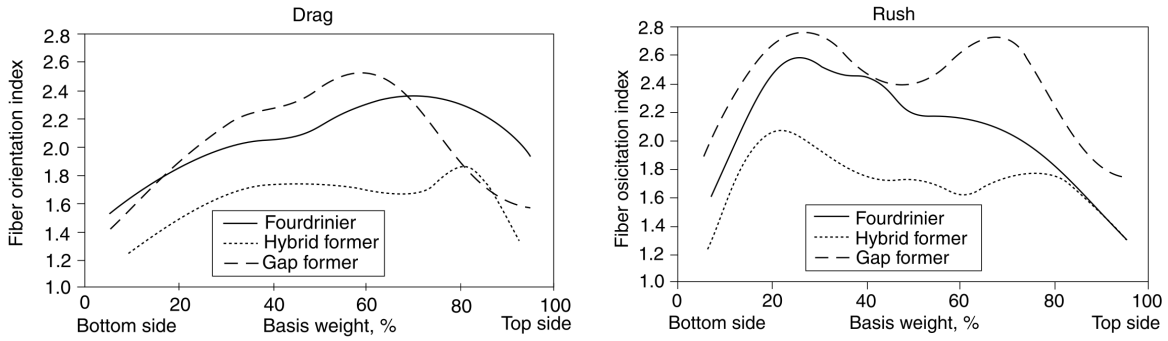

Figure 5. Comparison of 3 pilot former concepts regarding variation of FO index through sheet thickness for small jet-to-wire speed difference and both *drag* and *rush* [5].

On a Fourdrinier, this is due to fast initial dewatering on the bottom side and viscous braking forces on the top side. FO anisotropy increases under *drag* and decreases under *rush* conditions because of a decelerating suspension speed. Subsequently, the velocity gradient between wire and jet rises in case of *drag* and accordingly diminishes for *rush*.

On a gap former, a rather symmetrical fiber orientation index is achieved as a result of the comparable drainage to both sides. The variation in the center of the sheet is explained by a building pressure field in the gap decreasing the local suspension velocity there.

A hybrid former develops a fairly uniform FO index with one peak on top side for *drag* and bottom side for *rush* [5, 8].

The FO angle depends on mass flow and is very unstable.

Effect of fiber orientation on paper properties. A preferred alignment of fibers in MD causes major differences first in mechanical properties and second in dimensional stability. On the one hand, anisotropy is often desired regarding tensile strength, bending stiffness or energy absorption capacity due to a preferential load direction (e.g. in converting or printing processes).

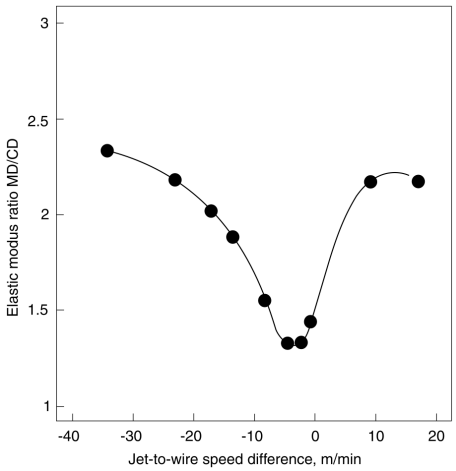

Figure 6. MD to CD ratio of the elastic modulus as a function of the jet-to-wire speed difference [5].

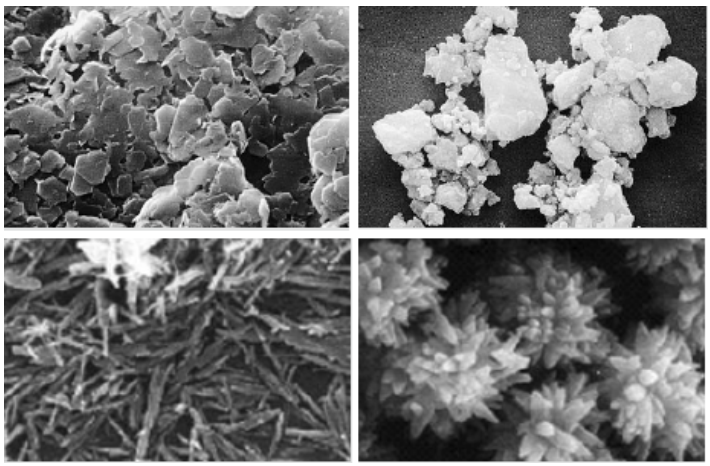

Figure 7. SEM images of various fillers. Clay (top left), GCC (top right), aragonite PCC (bottom left), scalenohedral PCC (bottom right) [12].

Figure 6 illustrates for instance the MD to CD ratio of the elastic modulus which is alternatively used to characterize the magnitude of the fiber orientation. On the other hand, FO anisotropy and its variation in z-direction have an intensified effect on inhomogeneous shrinkage and subsequently curl and buckling behaviour. A detailed discussion on the deformation issue will be given in section 2.2.

2.1.2 Sheet two-sidedness caused by fillers and fines

Since the early days of papermaking, additives have been used with the objective of improving product and process parameters. Indeed, economical considerations as well as functional properties (e.g. brightness, gloss, opacity and printability) play a decisive role. Mineral fillers and pigments represent the primary component in terms of quantity. In principle, a terminological distinction between fillers and pigments is made due to their purpose and price, even though the mineral origin is often the same. Consequently, the term pigment is used for more expensive, synthetic products (e.g. Precipitated Calcium Carbonate (PCC), TiO_2, silicates) and in coating colors. Depending on the desired product properties, particle size, size distribution and shape are of great importance. The range of particle sizes is about 0.5 to 3 μm, where coating color pigments are by tendency smaller than fillers. In order to manipulate filler characteristics and to obtain specail properties for a certain application, raw material is e.g. ground or precipitated (Ground Calcium Carbonate (GCC) or PCC) [12]. Figure 7 illustrates commonly used filler minerals.

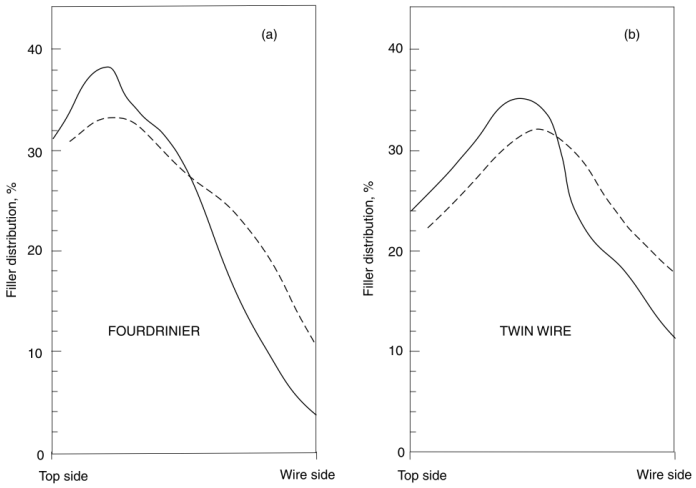

Figure 8. Filler distributions over sheet thickness on a Fourdrinier vs. gap former (twin wire) using SEM/EDS measurement from cross-sections (solid lines) and ash content of freeze-split layers (dashed lines) [5].

Types and impact of fillers. A major group of fillers are calcium carbonate derivatives obtained from deposits of chalk, limestone and marble. The ground natural product GCC is a prime example of a blocky filler material spreading apart the paper structure. This increase in bulk and phase transitions enhances permeability, liquid absorption, light scattering and opacity. However, tensile strength, bending stiffness and further mechanical properties are impaired due to the reduced amount of fiber-fiber bonds. Clay is a typical platy particle leading to a higher surface smoothness and gloss than blocky particles. In addition, deterioration of paper strength is lower. The synthetic PCC may be produced in many shapes. They can vary from needle-like aragonite crystals to scalenohedral shapes. Because of this versatility they have gained ascending attention in a wide range of applications [4, 10, 12].

Other materials are talc, titanium dioxide (TiO_2), synthetic silicates and gypsum. Titanium dioxide has an outstanding optical performance in paper grades but owing to its high price only a limited field of application.

Filler distribution is not constant over the sheet thickness. The resulting two-sidedness is illustrated in Figure 8. A sheet produced on a Fourdrinier shows a distinctive peak in the distribution close to the top side. In comparison, a gap former leads to a rather symmetrical filler distribution with a maximum in the centre of the sheet. During sheet forming, filler particles penetrate through the fiber network and wire due to drainage flow. The dimensional gap between fillers (d_{50}=1-3 μm) and fibers (d=30-50 μm) complicates the retention. It is improved by means of chemical aids, e.g. modified starch or synthetic organic polymers. The higher retention is achieved due to flocculation mechanisms (e.g. bridging or patching). However, a certain unevenness in z-direction and loss of fillers close to the wire occurs [5, 10].

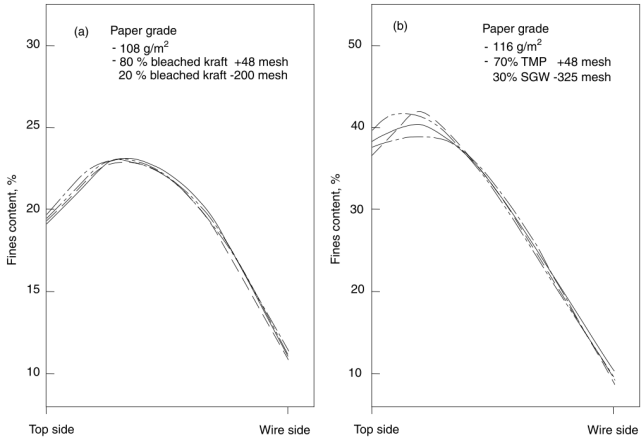

Figure 9. Fines distributions in z-direction for **(a)** chemical pulp and **(b)** mechanical pulp. The dashed lines represent various wet pressing pulses [5].

Fines. The term fines refers to fiber fragments passing the 200 mesh screen in Bauer McNett fractionation. It is distinguished between fines present in the virgin stock, called *primary fines* and *secondary fines* which are produced during refining. Primary fines contain mainly parenchyma cells from the wood. The percentage of primary fines in chemical pulps is quite low with about 2% compared to up to 15% after beating the raw material. This rise in fines originates from a peeling of of fibrillar material off the fiber wall during beating [13].

Fines from mechanical pulp are further categorized in *"flaky fines"* with poor bonding capacity and the well-bonding *"fibrillar fines"* [14].

Fines are generally responsible for a densification of the paper sheet. On the one hand, this is due to filling up free voids in the network. On the other hand, their high specific surface area plays a major role. It is up to 4 to 20 times higher than the 1 m^2/g of a typical fiber. This enables fines to strengthen fiber-fiber bonds by building bridges and getting them into closer contact during drying. In particular, even small quantities of fibrillar fines from chemical pulp bond completely to the fibers. Strength properties are therefore notable improved. In contrast, flake-like mechanical fines may hamper fiber bondings because of their lignin content. This category of fines act as spacers between fibers. Simultaneously, the light-scattering coefficient increases due to a higher specific surface area [13, 15].

Figure 9 shows fines distributions for chemical and mechanical pulp furnishes. Paper was in both cases produced on a Fourdrinier former. The distribution curves are comparable to the filler distribution mentioned previously above. Thus, the occurring two-sidedness has similar effects on an uneven deformation.

Two-sidedness of both fillers and fines may cause dimensional stability problems in converting or printing processes. Deformations like curl and buckling develop due to uneven swelling and shrinking behaviour over the sheet thickness. A deeper insight into stability issues will be given in section 2.2.

2.1.3 Effect of internal sizing on the paper properties

Paper is basically hydrophilic due to the chemical structure of pulp fibers. Both its main components, cellulose as well as hemicellulose are easily wetted. As a consequence, paper has an intrinsic tendency to absorb liquid water or water vapour from a humid environment. However, for numerous applications a limited water absorbency is required in order to fulfil printability and dimensional stability requirements. This is achieved by sizing agents either added to the pulp during stock formation or applied directly to the paper surface on the papermachine [10].

Surface sizing is a common step before coating. The main purposes are to strengthen and seal the surface and diminish penetration of liquids or coating substrates into paper. This is realised by the application of polymers with the capacity of forming hydrogen bonds with the fibers (e.g. starch, Carboxy Methyl Cellulose (CMC) and Polyvinyl Alcohol (PVOH)) [16].

In the following, the focus will be on *internal sizing*. The three major sizing agents here are rosin acids in combination with aluminium sulphate (known as *"papermaker's alum"*), Alkyl Ketene Dimer (AKD) and Alkenyl Succinic Anhydride (ASA). Rosin sizing is usually only applicable under acidic conditions which is incompatible with the increasing usage of calcium carbonate as filler. Long time stability of papers at a low pH is further diminished. Consequently, neutral synthetic agents AKD and ASA have become standard. Both form covalent bonds with the cellulosic fiber surface leading to a desired hydrophobisation [17]. In order to enable this direct reaction, it is essential to prepare emulsifications of ASA and dispersions of AKD. This is commonly realised by using cationic starch further intensifying the attachment to the anionic fiber surface.

ASA is a liquid under standard conditions, it is very sensitive to hydrolysis. Thus, it is emulsified in water close to the dosage station and sterically protected by cationic starch. Due to electrostatic interactions, ASA droplets are deposited on the fiber surface in the wet end. During heating and drying the previously attached sizing agent is spreading over the fibers and finally reacts with the hydroxyls yield ester bonds. The *curing* of ASA is extremely fast, it is finished after the end of the paper machine. [17].

AKD sizing mechanisms are comparable to ASA sizing as indicated in Figure 10. However, the curing to its full sizing potential is time consuming (up to a couple of days). The fatty-acid structure of AKD has both a hydrophilic and hydrophobic end. During curing the hydrophobic tail is oriented away from the fiber surface resulting in a water repellency. One documented drawback is a size reversion in combination with PCC as filler material. Still moveable AKD molecules may penetrate into the porous PCC particles deteriorating sizing efficiency. Though rate of hydrolysis is lower than for ASA, the produced ketons may cause runnability problems [10, 17].

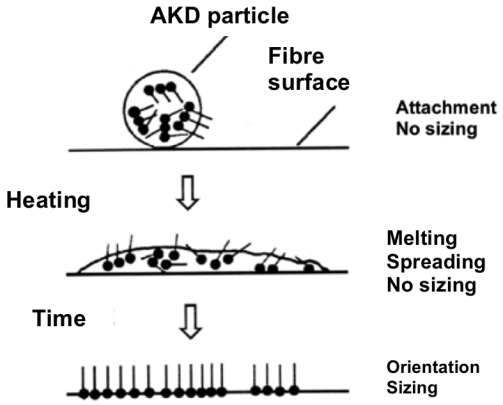

Figure 10. Illustration of AKD sizing mechanism [17].

The most common method to analyse liquid penetration into paper products is the Cobb-Test. It enables a quantification of the absorbed amount of liquid over 30 or 60 seconds, respectively.

Sizing related to inkjet printing. Regarding inkjet printing processes, a high print sharpness on the surface without bleeding of the ink is desired. On the one hand, liquid should quickly penetrate into the pores to get a fast ink setting. On the other hand, fiber swelling should be prevented to ensure a good dimensional stability of the printed papers. Because of these contradictory requirements, a proper sizing of inkjet papers is challenging [10].

Kilpeläinen and Manner [18] show low wicking (x,y-spreading of ink) results with high sizing degrees achieved by internal ASA sizing and a hydrophilic styrene acrylate (SA) surface sizing. Though, bleeding, the intermingling of ink, gets worse correspondingly. This is due to an increased ink penetration time. It is further detected that there is a lack of general correlation between paper properties and printing quality. Different inks require different base paper properties.

Glittenberg and Bergh [19], Stankovská et al. [20] emphasize the significance of a sufficient absorption and immobilisation of ink in the (uncoated) paper surface layer. Simultaneously, base paper should be increasingly hydrophobic towards the centre of the sheet. Bares and Rennels [21] also describe this requirement by defining the liquid penetration rate as major influence regarding print quality. A deep penetration into paper leads to a low print density and narrow colour gamut (the reproducible range of colours) [22].

2.2 Dimensional stability and mechanism of curl

As already mentioned, paper reacts very sensitive to changes in relative humidity. Climate variations consequently provoke a change in moisture content of the paper due to absorption and desorption of water. Depending on an uneven swelling behaviour in z-direction of the sheet, these may lead to out-of plane deformations. Pulp fibers essentially swell and shrink upt to 20% in transverse direction, in comparison to just 1% in longitudinal direction [23]. Thus, a strong fiber orientation is responsible for a pronounced expansion in CD and only a minor dimensional change in MD (3-5 times less). Type of fibers, filler and fines content and their distribution are additionally contributing to the *hygroexpansion* of paper. Hygroexpansivity β is quantified by the ratio of the hygroexpansive strain ε_h to the change in moisture content Δmc:

$$\beta = \frac{\varepsilon_h}{\Delta mc} \tag{2.1}$$

Filled papers generally lead to less hygroexpansion due to no swelling of fillers, reduced fiber bondings and a lower stress transfer capacity. In contrast, fines increase β due to densification of the sheet (subsection 2.1.3). Fibers with high hemicellulose content and amorphous cellulose regions have a higher swelling capacity than fibers with high lignin content and mainly crystalline cellulose [23, 24]. In amorphous regions, more hydroxyl groups are accessible for the water to form hydrogen bonds [25].

Beside the *hygro*expansion related to moisture absorption, *hydro*expansion means the dimensional change due to liquid water uptake. Larsson [26] reported a slower absorption into lignin and hemicellulose-rich Thermo Mechanical Pulp (TMP)-papers compared to papers made of kraft pulp. More fines further reduced the rate.

Dimensional stability is of particular importance in converting and printing processes where paper is exposed to liquid application and heating from one or both sides. Among three common issues namely *curl*, *cockling* and *fluting* the current work addresses the curl phenomenon. It occurs in machine direction, cross direction or diagonal to it, as illustrated in Figure 11. A curl towards top-side of the sheet (*"bowl"*) is defined as positive. In contrast, a paper with a convex cylindrical shape (towards bottom-side) is negative by definition. Regarding the diagonal form, a positive or negative angular are defined accordingly to the FO angle (subsection 2.1.1) [27].

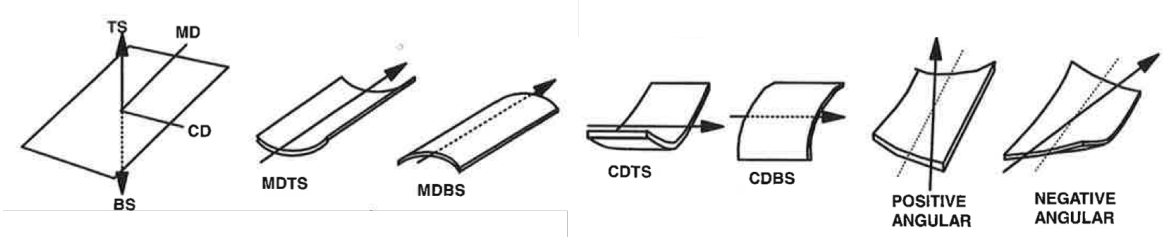

Figure 11. Illustration of curl occurring in CD, MD and diagonal direction [27].

Carlsson et al. [28] developed a mathematical equation to describe the contribution of MD, CD and diagonal curl to the overall curl w in z-direction:

$$w(x,y) = \frac{1}{2}K_x\ x^2 + \frac{1}{2}K_y\ y^2 + \frac{1}{2}K_{xy}\ x\ y \qquad [1/\mathrm{m}] \tag{2.2}$$

The variables x and y in Equation 2.2 represent the coordinates on the specimen in machine and cross direction, respectively. The K - values are the three representative curl-components for MD (K_x),CD (K_y) and diagonal curl (K_{xy}). They have the unit of a curvature [1/m] [29].
Owing to its origin, curl can be basically categorized in four types [27]:

- structural (reversible) curl: as a result of paper two-sidedness
- viscoelastic curl: due to an one-sided exposition to moisture or heat
- irreversible curl: caused by a release of dried-in strains
- roll set curl: mechanically induced by moving paper over edges or small diameter rolls

2.2.1 Structural curl

Structural curl is a consequence of an unbalanced hygroexpansion on top and bottom side of the sheet. Swelling and shrinkage variations over sheet thickness are caused by inhomogeneities in the paper structure. This two-sidedness due to filler, fines and fiber orientation differences was discussed in section 2.1. An uneven shrinkage or swelling in z-direction during liquid uptake or drying induces a bending moment and subsequently a curl formation [23, 27, 29]

If fibers are not aligned with the same angle on top and bottom side of the sheet as illustrated in Figure 12a, paper curls diagonally. Uesaka [27] derived a quantitative model for K_{xy} given in the following equation:

$$K_{xy} = \frac{3\,(\alpha_{TS} - \alpha_{BS})\,(\beta_{MD} + \beta_{CD})}{t} \qquad [1/\mathrm{m}] \tag{2.3}$$

Variation in FO angle ($\alpha_{TS} - \alpha_{BS}$), hygroexpansivity β in MD as well as in CD and sheet caliper t contribute to the extent of diagonal curl.

A simplified mathematical relation for the CD curl component K_y was given by Hirn and Bauer [29]:

$$K_y = \frac{2\beta_{CD}\,(A_{TS} - A_{BS})}{t} \qquad [1/\mathrm{m}] \tag{2.4}$$

Here the decisive factors are the hygroexpansivity β in CD and the FO anisotropy A on top and bottom side and the sheet thickness t.

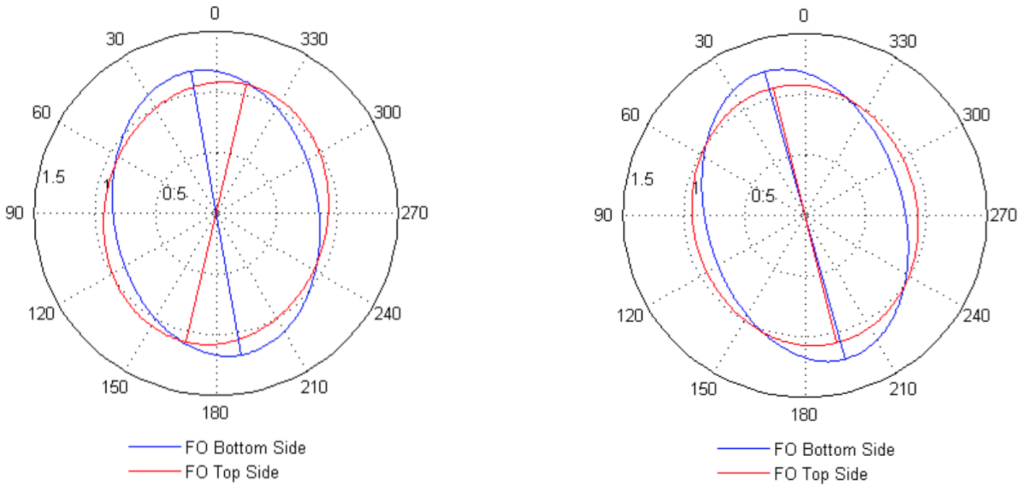

(a) Two-sidedness for FO anisotropy and angle provoke both a CD and diagonal curl.

(b) FO two-sidedness with concurrent FO angle resulting in a strong CD curl.

Figure 12. FO two-sidedness leading to a structural curl [29].

2.2.2 Viscoelastic curl

This curl type is generally independent of a structural two-sidedness. It is caused by an inhomogeneous moisture application or drying. If only one side of paper is wetted or dried, an irreversible viscoelastic deformation is induced on the opposite side. Dynamics for moistening case are visualized in Figure 13. An unconstrained paper specimen with a symmetrical moisture content of 5% is subjected to Top Side (TS) water application. Thus, TS of paper swells stronger than Bottom Side (BS) creating strains and stresses on both sides. BS counteracts the expansion undergoing an irreversible viscous stretching. However, due to swelling, a curl towards BS results. After an evaporation and resulting shrinkage of the TS to its initial dimensions, the paper curls back. The stretched BS shrinks less than the TS. Reaching the uniform moisture distribution again, a curl towards TS remains [25, 27].

Regarding one-sided drying, the heated side shrinks inducing an irreversible compression on the other side. This leads to a subsequent curl towards the not dried side.

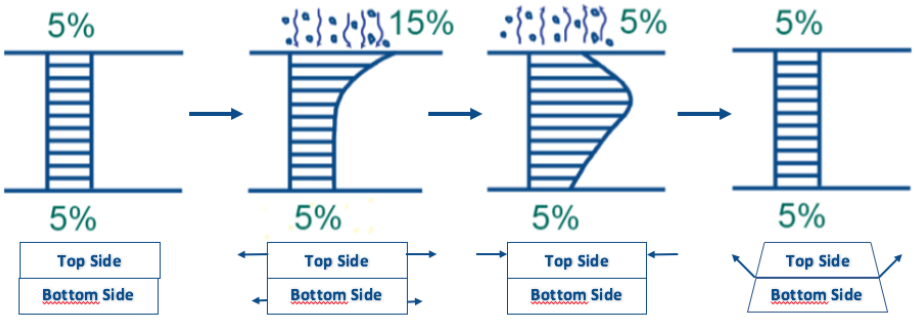

Figure 13. Sketch of viscoelastic curl illustrating moisture distribution and corresponding expansion of a paper sheet due to one-sided wetting and drying. Adapted according to [25, 27, 30].

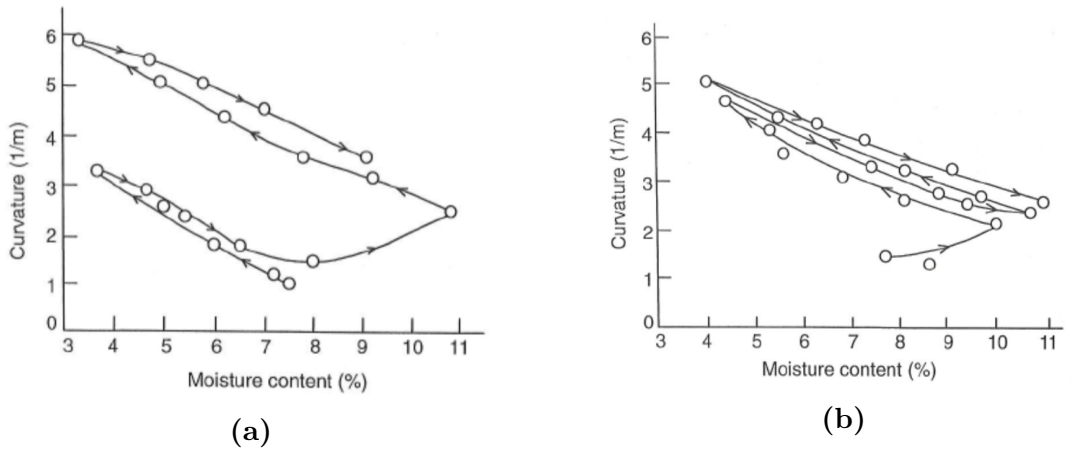

Figure 14. Dried-in strains are released upon wetting starting with **(a)** drying or **(b)** wetting. The initial curvature values are not reached again. The curl is irreversible [27].

In theory, curl formations may be compensated using appropriate process sequences. A curl adjustment is frequently done in paper mills by differential drying in multi-cylinder dryers, i.e. by compensating curl with defined heating curl to the other side. This also may control or prevent an irreversible curl [27].

It can be basically stated that paper always curls towards the side moisture is removed last. Nevertheless, curl mechanisms mostly interact making this assumption not universally applicable.

2.2.3 Irreversible curl

The irreversible curl is triggered by the release of dried-in strains due to an exposure to high relative humidity. During the manufacturing process, paper is hindered to shrink or curl due to the web tension and mechanical constraints. A one-sided drying has consequently no visible effect but creates inner tensions and strains. These strains are released upon wetting resulting in an asymmetric hygroexpansion and curl. Figure 14 illustrates how to trigger the irreversible curl. Paper is in both cases exposed to humidity cycles. The corresponding curl values in terms of curvature are shown in Fig. 14. After exceeding a critical moisture content of 8% in the first wetting cycle, paper undergoes an irreversible increase of curl. Further humidity changes only provoke a reversible curl which may be explained by structural reasons [27].

2.2.4 Roll set curl

This paper curl caused by viscoelastic stress relaxation arises when guiding paper over small diameter rolls or edges. It usually appears in MD and is sensitive to temperature and humidity rises which intensify the curvature. Mechanical de-curl elements are frequently installed, which are essentially rolls or edges where the paper is deformed in the opposite direction of the curl in order to remove the permanent deformation [27].

2.3 Basics on inkjet printing

This section deals with the basic principles of inkjet printing and the used inks. Due to the fact that this work addresses the impact of paper properties on the curl behaviour neglecting the influence of the printing process itself, this general overview will not dig deep into details.

Inkjet printing enables the application of a wide range of materials on different substrates, a high degree of personalisation and on-demand printing. These major advantages make it one of the most promising technologies for printing and deposition of functional layers (e.g. conductive patterns, transistors or gas and humidity sensors) on e.g. paper [31]. The principle is based on tiny fluid droplets which are sprayed directly onto the surface of the substrate. It can be basically classified into two mechanisms with respect to generation of these droplets [32]:

- continuous inkjet printing
- drop-on-demand inkjet printing

2.3.1 Continuous inkjet printing

In the continuous system as illustrated in Figure 15a, ink droplets are constantly ejected out of the nozzle by dynamic deflection of a piezoelectric element. The single droplets are further electrically charged and subjected to a deflection field. Due to the digital image data droplets are either recirculated into a gutter or deposited on the paper. Typical drop size is between 4-10 pl with an ejection frequency of 0.1-1 MHz [32]. Continuous inkjet printing is mainly used in high-speed and high-volume applications (e.g. coding and marking of packages) [33]. However, it is limited by a lower print resolution of 300-600 dpi compared to the drop-on-demand technology with up to 2880 dpi [32].

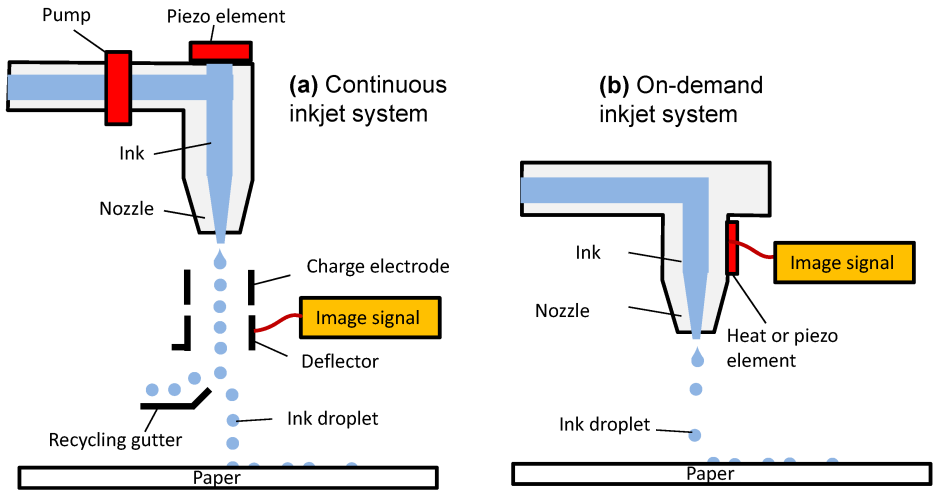

Figure 15. Principles of: **(a)** a continuous inkjet printer **(b)** a drop-on-demand inkjet printer [31].

2.3.2 Drop-on-demand inkjet printing

This type only generates a droplet when receiving a signal from the actuator, schematically shown in Figure 15b. The required ejection pulse is either generated by thermal, piezoelectric or electrostatic mechanisms. In the first case, local heating up to 300 ℃ leads to a vaporization of ink forming a bubble. The resulting pressure pulse pushes the ink through the nozzle and the ink chamber cools down again. Thermal inkjet is mostly used in home and office printers but also in industrial devices. It has some limitations due to heat build-up. For the piezoelectric jetting-element, durability of print heads is higher and there are hardly any limitations with respect to the jetted ink. Consequently, a lot of research and development has been done in this field pushing the technology into a leading position in industrial applications [32, 33]. The electrostatic principle as a third case is still of minor importance and requires conductive inks. Basically, an electrostatic field between an electrode and the nozzle attracts free charges within the ink. If the electrically induced pull exceeds the surface tension of the ink, a droplet is created. A big advantage of this technology is a high concentration of the printed material in the drops resulting in a high resolution with brilliant optical density. However, conductivity of fluids and high costs are serious drawbacks [33].

Due to the recently achieved development steps, piezoelectric drop-on-demand inkjet currently accomplishes high-speed and high-resolution requirements [32]. In fact, it also became the main printing technology at Océ.

2.3.3 Types of ink

Main components of all inkjet inks are colourants, carrier substances and additives. Carriers, responsible for jetting ability, amount to the major portion with 60-90%. Depending on the type of carrier used, inks are categorized into four main types: water-, or solvent-based, hot melt or UV curable [32, 33]. The dominant type used in professional colour printing is water-based. In Table 1 a generic formulation of this ink type is given indicating the respective purpose of each component.

Colourants are distinguished into dyes and pigments. Dyes are dissolved as molecular dispersion in the carrier and may penetrate into the pore system of the fibers forming molecular bonds. Thus, print quality depends on hydrophobicity of the paper and penetration dynamics. Dyes exhibit low light fastness (image permanence under exposure to light) while providing high chroma. The reduced water fastness of dyes is currently improved by fixing agents. In contrast to dye inks, inorganic or organic pigment inks show better light fastness but impaired colour purity. Pigment particles are homogeneously dispersed into the carrier seeking to avoid agglomeration or deposits. Print gloss, colour gamut and optical density depend on particle size distribution, porosity of the paper and possible surface pre-treatments.

Table 1. Overview of typical inkjet ink components [34].

Component	Purpose
Water	Primary solvent, carrier fluid
Colourants (0.5-10%): Pigments or Dyes	Produce colour
Co-solvents (5-50%)	Prevent nozzles from drying out
	Retain paper sheet flatness after printing
	Enhance ink film formation
Surfactants (0-2%)	Improve wetting of ink on media
	Reduce *"puddling"* of ink on print head
	Reduce resistor deposits
Polymeric binders (0-10%)	Improve durability of prints
	Improve gloss of prints
Biocides	Prevent growth of microorganisms
Chelating agents	React with free metals
Anti-corrosion additives	Prevent corrosion

Printing on plain papers may lead to pronounced penetration of pigments into the pores diminishing print quality [32, 34].

An important demand for inkjet inks is a suitable viscosity, low enough to enable a stable jetting of the droplets and concurrently high enough to ensure an appropriate spreading and penetration of ink on the substrate. Viscosity is commonly 1-30 mPa·s and typical surface tension values are 20-60 mN/m [32].

Interaction of ink and paper is a crucial factor regarding print quality and dimensional stability. The current work focuses on paper properties not taking into account the influence of ink parameters. Wetting and penetration of inks are quite complex phenomena, as discussed by Krainer [35]. If a substrate is wetted by a liquid highly depends on the relations of their corresponding surface energies. By determination of the resulting contact angle and its dynamic development, penetration and absorption of the liquid into paper or other materials may be predicted. Further important properties are viscosity of the ink as well as porosity of the substrate.

2.3.4 Océ-Technologies B.V.

Due to the fact that this master project was carried out in collaboration with Océ, some facts about the printing company are given here.

Océ with its headquarters located in Venlo, The Netherlands, was founded 1877 by Venlo chemist Lodewijk van der Grinten. He developed a revolutionary new colouring agent for margarine. In 1927, his grandson Louis van der Grinten invented a faster, ammonia-free and thus more eco-friendly blueprint process. It was named *O.C.* from the German *"ohne componenten"* or *"without components"* giving the company its name Océ. After the production of electro-photographic copiers followed by laser printers for wide- and cut-sheet format, Océ developed its own inkjet technology in the 1990s.

Nowadays, Océ produces a wide range of high-end industrial inkjet devices covering the segments of wide-format, cut-sheet and sheet fed printing. In 2013, Océ became fully integrated into Canon reinforcing their leading market position in printing. As a global player, Océ has research and manufacturing centres in Europe, Canada and South East Asia with approximately 3900 employees worldwide.

3 Materials and Methods

In this chapter the experimental methods of the thesis are described. It is divided into two parts. The first part covers the production of laboratory handsheets with defined paper components and properties. In the second part these papers were tested regarding their mechanical properties and performance on the test setups at Océ Venlo. The test trials at Océ comprised curl measurements, hydroexpansion tests and stiffness reduction due to printing.

3.1 Production of handsheets with defined properties

It was decided to investigate the influence of various paper constituents on the curl behaviour via handsheets. This basic laboratory scale approach enables full control of paper properties even though it is hardly comparable to an industrial papermaking process. In spite of this restriction, the bottom-up approach was considered suitable in order to identify the effects of single paper components on the deformation phenomenon. After a couple of pre-trials to evaluate the range of possible test points, an experimental design for handsheet production was developed. Table 2 represents the experimental design consisting in six independent trials. Every trial include three levels of the investigated paper property. In case of the *Furnish*-trial, an additional fourth test point was defined. Bleached Eucalyptus kraft pulp manufactured at Santa Fe, Chile was used for the entire handsheet fabrication. Except for the *Fiber orientation*-study (trial 6), all sheets were produced on a Rapid-Köthen-Sheetformer (Figure 16) according to ISO 5269-2. The target grammage for the entire paper series was 80 g/m^2.

Figure 16. Production of handsheets for five out of six trials was entirely realised on a Rapid-Köthen-Sheetformer.

Table 2. Experimental design for handsheet production. Line 1 represents the *zero point*.

	Refining	Furnish	Fillers	Fines	Sizing	Fiber orientation
1	1000 rev PFI	0% BCTMP	0% PCC	0%	0% AKD	Rapid Köthen SF
2	500 rev PFI	10% BCTMP	10% PCC	5%	0,05% AKD	DSF: 750 m/min
3	0 rev PFI	20% BCTMP	20% PCC	15%	0,1% AKD	DSF: 1000 m/min
4		40% BCTMP				

To evaluate the density influence on curl, sheets for trial 1 to 5 were further wet pressed on a hydraulic press at three levels:

not pressed - 0 bar

medium pressed - 75 bar

strongly pressed - 150 bar

The *zero point* for these trials was defined to have equal properties. It is line 1 in Table 2, i.e. 1000 rev PFI, 0% BCTMP, 0% PCC,etc. In this way, an overall comparison among the various trials is possible. Definition and realisation of the zero point are explained in subsection 3.1.1

With the objective to produce oriented sheets a Dynamic Sheet Former (DSF) was used in that trial. Pressure levels were reduced to 0, 4 and 8 bar respectively due to restrictions of the available laboratory roll press. A detailed description of the production procedure will be given in 3.1.6.

3.1.1 Trial 1: Refining

Beating pulp leads to a higher bonding capacity of fibers due to fibrillation and flexibilisation [10]. The effect of its corresponding rise in density and stiffness on paper curl was addressed within this trial. The impact of density is further emphasized by wet pressing.

Zero point. As seen in Table 2, all test groups start with an equal initial point. Dried Eucalyptus pulp was placed in deionised water overnight for swelling. Swollen fibers have a reduced refining resistance and thus require less energy to achieve a comparable outcome [10]. After 10 minutes of disintegration and a filtration step, pulp was refined with 1000 revolutions in a laboratory PFI mill according to ISO 5264-2. In each refining run 30 g of bone-dry pulp can be treated corresponding to eleven handsheets of 2.4 g bone-dry. Converted to 2.54 g air-dry with a sheet-area of 0.0317 m^2 this amounts to a grammage of 80 g/m^2.

The used PFI mill is shown in Figure 17. Following beating, the pulp was disintegrated with tap water for 3 minutes before starting the sheet forming on the Rapid Köthen Sheetformer according to ISO 5269-2. Here the automatic operating mode with fresh water was chosen performing the ensuing sequence:

filling	-	7l fresh water
agitation	-	5 s
calming	-	5 s
gravitational dewatering	-	until sheet is formed upon the screen plate
dewatering by vacuum pump	-	10 s

After couching the formed sheet, papers intended to be wet pressed were transferred to a hydraulic press. In between two carrier boards and two press felt sheets were pressed for 90 seconds, either applying 75 bar or 150 bar respectively. Figure 18 illustrates the ongoing pressing procedure at 75 bar. Both, not pressed and pressed papers, were subsequently dried in the Rapid Köthen drying unit at approximately 93 ℃. Once finished, the sheets were stored at least 1 to 2 days under standard conditions (23 ± 1 ℃; 50 ± 2% relative humidity). Afterwards, mechanical properties of the papers were measured in the same climate room. Details on the testing routines are given in section 3.2.

Variation of level of refining. The additional test points within this trial were 500 rev PFI and 0 rev PFI. Manufacture of the corresponding sheets was performed equally to the zero point apart from the refining step. As a common way to evaluate the refining process, the freeness of pulp is measured. It is quantified in terms of °SR in accordance with ISO 5267-1. The higher °SR the higher the drainage resistance indicating an intense beating. For 1000 rev PFI a value of 22 °SR was obtained. Values of 18.5 °SR for 500 rev and 17 °SR for 0 rev show a slight, but present increase of freeness with more intense refining.

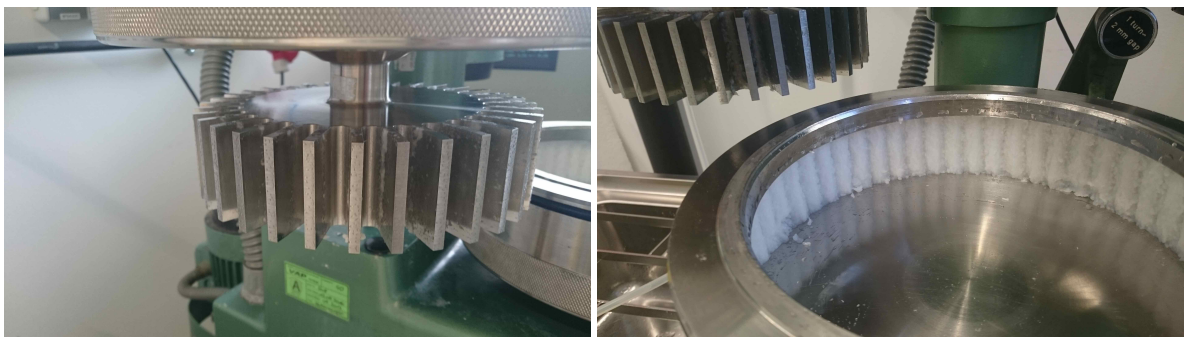

(a) **(b)**

Figure 17. Santa Fe Eucalyptus pulp refined in a PFI laboratory mill with **(a)** beating body and **(b)** beater box. The zero point was defined as 1000 revolutions in the PFI mill.

Figure 18. Hydraulic press used to variate paper density on three levels: 1) not pressed 2) pressed with 75 bar 3) pressed with 150 bar.

Industrial relevance. Industrial refining is mainly realised by using disc, conical or cylindrical refiner in which fibers are treated between the bars of rotor and stator. Beating in a PFI mill lead to milder impacts and less fiber cutting than industrial scale refiners complicating a straight-forward correlation between both methods. One argue, that milder impacts enhance fiber swelling due to delamination of the inner fiber structure and thus more accessible regions for water molecules [36]. However, studies were conducted showing no significant increase of the inner surface of the fiber due to beating [37].

Depending on the energy input, freeness in °SR typically increases from about 15-18 for unbeaten chemical hardwood pulp to 20-25 for refining in the PFI. Regarding industrial refining, the obtained SR is up to 10-15 points higher due to external fibrillation and fines creation.

3.1.2 Trial 2: Furnish - BCTMP

The second trial dealt with a combination of two pulp sources. On the one hand, similar to all the other trials, bleached Eucalyptus kraft pulp from Chile was used. On the other hand, Aspen Bleached Chemo Thermo Mechanical Pulp (BCTMP), produced at Tembec, Canada was added to the furnish. Due to the lignin and hemicellulose content, a perceptible reduction on the magnitude of curl was expected for BCTMP containing sheets. Three various fractions of Aspen BCTMP to Eucalyptus kraft pulp were made. The zero point served again as reference (compare Table 2).

BCTMP was provided by the industrial partner Mondi with a Freeness of 37 °SR. Thus, this pulp was not refined but only disintegrated for an extended duration of 30 minutes. Together with a prolonged swelling for two days, these measures were necessary to ensure a complete disintegration of the extremely rigid pulp. After refining the Eucalyptus kraft pulp, three portions of 10 wt%, 20 wt% and 40 wt% of Aspen BCTMP were mixed to the final furnish. The mixture was subsequently disintegrated for 3 minutes before forming sheets according to the routine of trial 1.

It is worth mentioning that refining within the *BCTMP*-trial was not working properly due to a misalignment of the refining gap in the PFI mill. Unfortunately, this was detected belatedly and the trial could not be repeated due to time issues. Regardless of this shortcoming, the refining influence was detected to be of minor importance compared to the effect of adding BCTMP to the stock.

Industrial relevance. Bleached or unbleached CTMP is commonly used in wood-containing printing papers, e.g. Super Calandered (SC) and Light Weight Coated (LWC), providing good opacity, printability and bulk. The drawbacks are limited strength properties and a low durability compared to wood-free papers. However, CTMP achieves better values than other mechanical pulp sources. A conventional SC paper typically contains 50-75% mechanical pulp, 5-25% chemical pulp and 10-35% fillers. Base paper of LWC grades is produced of a mixture of 50-70% mechanical pulp, 30-50% chemical pulp and 4-10% fillers [15].

3.1.3 Trial 3: Fillers - PCC

Usage of fillers in the pulp has a major impact on the inner sheet structure as explained in 2.1.2. Filled papers are expected to be less stiff and less prone to hygroexpansion due to inhibited inter-fiber bondings and hence lower stress transfer capacity. Additionally, an inhomogeneous distribution of particles in z-direction may provoke a structural curl appearance. Evaluation and quantification of that theory was the declared objective of this trial.

A scalenohedric PCC (Omya Syncarb) Slurry at 35% solids content was the selected filler material. According do industrial practice [10], target ratios of fillers to pulp were 10/90 and 20/80 respectively. Pre-trials had shown good retention values without applying any retention aid. This was highly favoured in order to eliminate any potential side effect of additional chemicals. PCC slurry was agitated until a homogeneous dispersion was obtained. In the pre-trials a concentrating of PCC in sheets had been observed when operating the sheetformer in white water recirculation mode. Thus, the production was carried out with fresh water. The essential amount of PCC dosage to achieve the target filler content of 10% and 20% respectively was established previously. Right before filling pulp into the forming column, PCC was mixed to the furnish and agitated for 30 seconds using a magnetic stirrer. Pressing and drying was accomplished identical to the other trials.

Determination of the accomplished filler content was done by ashing two specimens at 575°C according to ISO 1762. The ash content of all papers taking into account the ignition loss of 0.96% is given in Table 3. It demonstrates, that all sheets were close to the desired value of PCC content.

Table 3. Ash content of filler-sheets.

Sheet specification	Ash content [%]	Standard deviation
10% PCC 0 bar	10.9	0.65
10% PCC 75 bar	10.11	0.43
10% PCC 150 bar	10.23	0.23
20% PCC 0 bar	21.62	0.96
20% PCC 75 bar	20.61	0.56
20% PCC 150 bar	22.62	0.08

Industrial relevance. The effect of adding fillers to the paper furnish was discussed in 2.1.2. Diminished strength properties are accepted in favour of optical and economical reasons. Regarding wood-free uncoated paper grades, a total mineral content (mostly GCC or PCC) of 8-28% is common. By adding 2-3 coating layers, the amount rises up to 40-55% [12].

3.1.4 Trial 4: Fines

Comparable to fillers, addition of fines may lead to a certain two-sidedness regarding sheet structure and corresponding strength and liquid penetration properties. A closer insight into the effect of fines was given in 2.1.2. In order to study the contribution of fines towards paper curl, a trial adding secondary fines to the sheets was performed.

First, a fraction of fines out of Santa Fe Eucalyptus kraft pulp was created by extensive beating in a laboratory jokro mill according to ISO 5264-3. It consists of six beater boxes with a freely movable beating body inside. These boxes can be anchored in a cylindrical plate which rotates when the mill is running. The induced rotation of the inner solid beating bodies leads to a heavy physical stress of the fibers and increased creation of fibrillar material. Figure 19a shows the jokro mill with the screwed in boxes. An open box with pulp after refining is illustrated in Fig. 19b.

(a) **(b)**

Figure 19. Secondary fines of Santa Fe Eucalyptus kraft pulp were created by beating the pulp in a **(a)** jokro mill for one hour. The beating body of this device is freely movable within the **(b)** beater box.

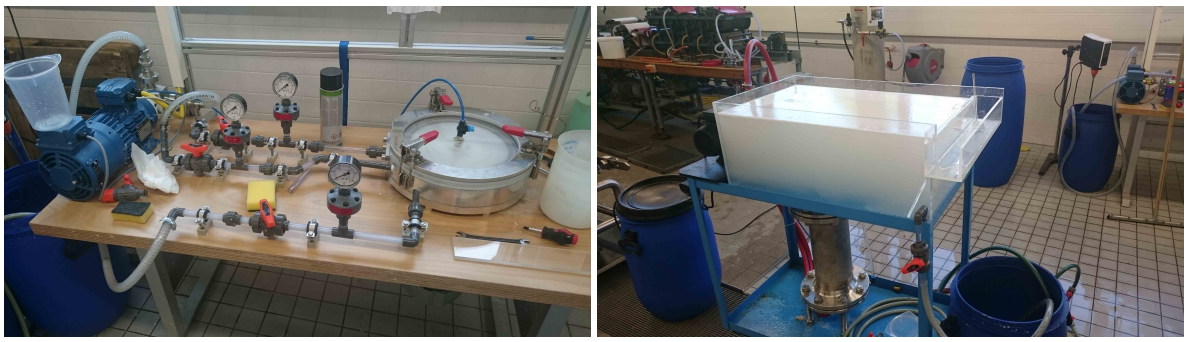

(a) **(b)**

Figure 20. Produced fines were separated by a **(a)** lab sorter followed by a **(b)** flotation to reach a higher consistency of the fine fraction.

Analogous to the PFI refining, the pulp was soaked overnight in deionised water before disintegrating it for 10 minutes. The pulp was afterwards beaten at a consistency of 16.6% for one hour. Subsequent to beating, fines separation by means of a laboratory pressure screen [38] and a final flotation were performed. The pressure screen, with a mesh size of the perforated screen of 100 μm, is shown in Figure 20a. Due to the low consistency of approximately 0.1%, the fine fraction (accept) of the separation was kept in a storage drum for 2 days to sediment. The remaining water excess was pumped out and fines were floated in the device shown in 20b. The coarse fraction (reject) of the separation was not used in the following sheet production.

In the second step of this trial, sheets with additional fines content were formed. Therefore, Santa Fe pulp was conventionally prepared by 1000 revolutions in the PFI mill. Fines were mixed to the agitated storage container of disintegrated pulp as a percentage of 5 and 15 wt% of pulp, respectively. Sheet forming itself was done on a Rapid Köthen Sheetformer equipped with a white water recirculation system. For sheet forming, a screen with a finer mesh size of 200 (74 μm openings) was used. All the other trials were carried out using a standard screen with 120 mesh (125 μm openings). According to the investigations of Giner Tovar [39], the amount of fines retained increase with the number of handsheets produced due to the recycling of white water. After 5 to 7 sheets, the retention values level out and reach a steady-state. Thus, the subsequently produced sheets were containing 5% (15% respectively) additional fines. It is worth mentioning, that drainage time was occasionally extended due to an increasing flow resistance of the furnish containing fines. Similar to the preceding trials, sheets were wet pressed and dried in the Rapid Köthen drying station.

Industrial relevance. Primary and secondary fines contents of the furnish are related to the used pulp source and the intensity of refining. The effective retention on the papermachine is realised by adding anionic trash catchers attaching the fines to fiber surfaces. These retention aids were not used in the laboratory why handsheets most likely contain less fines than industrial papers.

3.1.5 Trial 5: Sizing - AKD

Hydrophobic treatment of papers by using sizing agents is common practice. However, it is still not very widespread for HSI papers due to limited penetration and immobilisation of the ink leading to wicking issues (compare 2.1.3). Considering deformation and curl, less water uptake is favoured to reduce fiber swelling and hydroexpansion of the fiber network. Hence, in the fifth trial sheets with increasing water repellency were manufactured.

Commercially available AKD (Aquapel F320) was used at two dosage levels: 0.05% and 0.1% wax content with respect to basis weight. Like in the *PCC*-trial, no retention aid was added to exclude any undesired influences from additional chemicals. First, Eucalyptus kraft pulp was conventionally refined with 1000 revolutions in the PFI mill. Meanwhile, AKD was diluted with water to a solution of 0.1% wax content and permanently agitated. The sizing agent was subsequently mixed to the pulp furnish for one single handsheet and stirred for 30 seconds by a magnetic stirrer. In the following, sheets were formed, pressed and dried according to the routine explained in 3.1.1.

Measurement of degree of sizing by means of $\mathbf{Cobb_{60}}$. Efficiency of the internal sizing was investigated by $Cobb_{60}$ measurements in accordance with ISO 535. 50 ml of water were distributed on a specimen area of 50 cm^2. After 60 seconds, water absorbance in terms of g/m^2 was measured. As demonstrated in Figure 21, water instantly penetrated through non sized papers. However, sized papers achieved suitable values with a measurable variation between 0.05% and 0.1% AKD. The lower sized papers further showed differences on TS and BS as well as over the pressing range documented in Table 4. Two to three measurements per side and sample were conducted.

(a) **(b)**

Figure 21. Degree of sizing was measured by a $Cobb_{60}$ test. No representative value was achieved by testing unsized papers **(a)** due to an instant total penetration. In contrast, **(b)** sized papers showed an appropriate water repellency.

Table 4. $Cobb_{60}$ - values of sized handsheets.

Sheet specification	$Cobb_{60}$ $[g/m^2]$	Standard deviation
0.05% AKD 0 bar TS	34.95	1.88
0.05% AKD 0 bar BS	27.51	0.69
0.05% AKD 75 bar TS	51.95	7.35
0.05% AKD 75 bar BS	26.46	0.74
0.05% AKD 150 bar TS	54.58	0.98
0.05% AKD 150 bar BS	30.30	5.57
0.1% AKD 0 bar TS	22.12	0.23
0.1% AKD 0 bar BS	22.15	0.33
0.1% AKD 75 bar TS	23.63	0.53
0.1% AKD 75 bar BS	22.34	1.22
0.1% AKD 150 bar TS	22.69	3.33
0.1% AKD 150 bar BS	24.68	0.39

Industrial relevance. AKD is a commonly used sizing agent (compare 2.1.3). Paper of 80 g/m^2 with a dosage proportion of 0.1% AKD leading to a $Cobb_{60}$ value of 27 g/m^2 (St.dev=2) serves as an industrial reference.

3.1.6 Trial 6: Fiber orientation - DSF

Due to previously mentioned consequences of fiber orientation (compare 2.1.1) and the preferential swelling of fibers in transversal direction, highly anisotropic sheets may provoke severe dimensional stability issues in CD. FO two-sidedness is of particular importance with respect to induced drying or expanding stresses as explained in 2.2.1. Thus, the aim of this trial was to manufacture laboratory sheets with a preferred alignment of pulp fibers in machine direction.

This was realised by using a Dynamic Sheet Former equipment from Techpap located at the Sappi Gratkorn R&D department. The device shown in Figure 22 consists of two cylindrical jars. In the right one the prepared pulp suspension is agitated before it is sprayed onto the internal wire of the left-hand forming drum. The fiber suspension is applied by an up- and down sweeping nozzle and subsequently dewatered by centrifugal forces of the rotating drum (see Figure 23). Deposition of fibers as shown in the following, occurs essentially even. However, a range of various jet-to-wire ratios can be adjusted in order to achieve a desired anisotropy. Estimation of the obtained anisotropy was carried out by a L&W TSO Tester, an ultrasonic measurement device to determine the ratio of Tensile Stiffness Index (TSI) in MD to CD. The TSI is defined as ratio between the modulus of elasticity $[MPa]$ and the density $[kg/m^3]$. Substantially, by measuring the ultrasonic velocity v $[m/s]$ in a certain direction, the TSI can be calculated by means of a dimensionless constant c for the used pulp and the following equation [40]:

$$TSI = c\, v^2 \qquad \left[\frac{kNm}{g}\right] \tag{3.1}$$

Newsprint paper for instance has a $\text{TSI}_{MD/CD}$ ratio of 3.5 - 5 compared to sack kraft paper of just 1.1 - 2.3. A copy paper for cut sheet printing obtains a range of 1.4 - 2.2 [40].

(a) **(b)**

Figure 22. A Dynamic Sheet Former located at Sappi Gratkorn was used to produce oriented sheets. In **(a)** the entire device together with a laboratory roll press in the background is shown. **(b)** provides a close-up of the rotational forming wire and the traversing application nozzle.

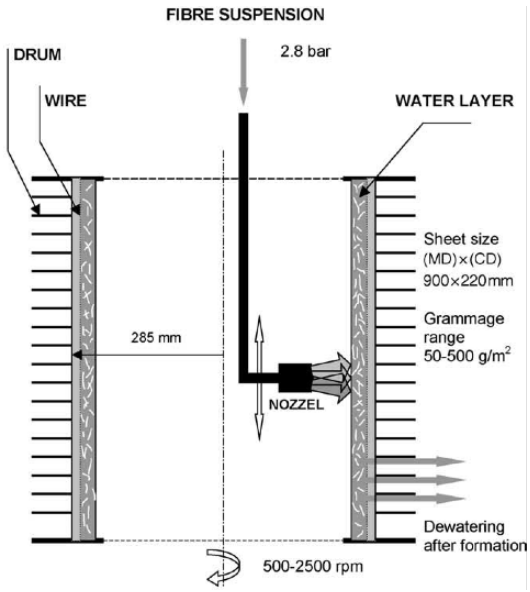

Figure 23. Illustration of the up- and down sweeping nozzle inside the forming section of a DSF and centrifugal dewatering of the fiber mat [41].

Before starting the forming procedure, Santa Fe Eucalyptus kraft pulp was disintegrated in a Valley Beater for 30 minutes and afterwards beaten for 10 minutes according to ISO 5264-1. Usual refining in a PFI mill was not efficiently applicable due to the high amount of pulp required. The freeness after beating was 19.5 °SR, representing a value between 500 rev and 1000 rev in the PFI mill (compare 3.1.1). Runs on the DSF were conducted with 750 and 1000 m/min, respectively. Due to some troubles with stabilising sheet grammage to 80 g/m^2, it was decided to establish these two test points though the anisotropy difference detected by the TSO tester was rather low. At 1000 m/min a $TSI_{MD/CD}$ ratio of 1.9 was obtained compared to 1.7 at 750 m/min. Pressing of the rectangular sheets was carried out between two felts on a laboratory roll press applying 4 and 8 bar respectively. A third series of not pressed sheets was also produced. All papers were subsequently dried in a curved handsheet dryer. The sheet was clamped onto a curved heating plate by a stretched cotton felt restraining the paper from shrinkage. Thus, both drying mechanisms performed within the entire handsheet production belonged to restraint drying with all possible consequences regarding dried-in strains.

Handsheets of the *zero point* serving as reference were manufactured on a Rapid Köthen Sheetformer with the identical stock as used for oriented sheets. The applied pressure with the hydraulic press was accordingly adapted to 4 or 8 bar.

Investigating fiber orientation two-sidedness by sheet splitting. Using the sheet splitting method developed by Hirn and Bauer [29], the fiber orientation and especially anisotropy and FO-angle two-sidedness were examined. Therefore 6 samples with 3.6×7 cm^2 of DSF-sheets and 2 samples of Rapid Köthen sheets as reference were cut by a punch. All specimens belonged to the 4 bar pressed series.

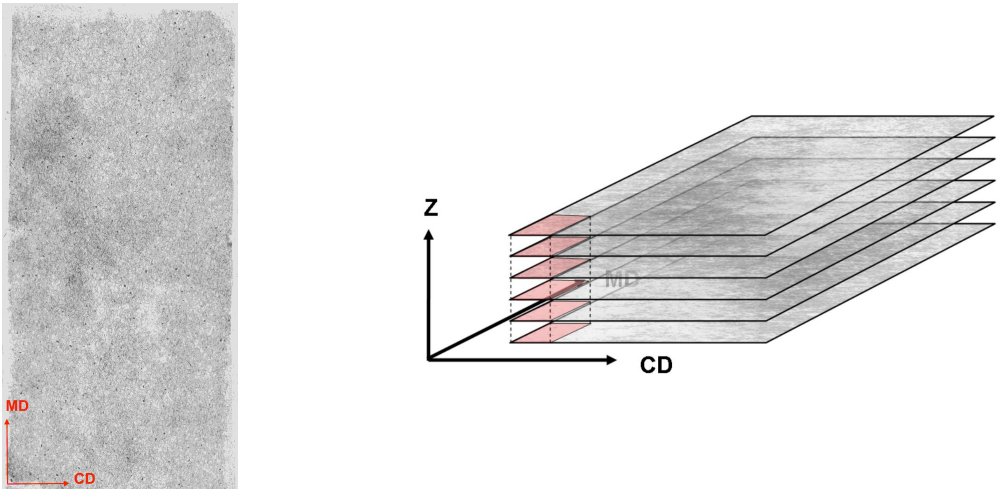

(a) Single layer of splitted sheet specimen with 3.6×7 cm^2. A coordinate system is defined by the sample edges to precisely localize the original position of single fibers within the sheet.

(b) Three dimensional model of the fiber orientation is obtained by stacking of individual FO data layers [29].

Figure 24. Sheet splitting method was carried out to determine fiber orientation over the z-direction.

To improve the contrast in the following image analysis, samples were dyed with a 0.1% Cartasol black solution for 24 hours. Subsequently, the dyed specimens were pressed between blotting paper for 2 days. By laminating the sheets with adhesive tapes in a commercial hot laminator, a splitting in two halves was enabled. The procedure was repeated several times until 25 to 30 thin layers with clearly perceptible single fibers were obtained. The image analysis started with scanning the layers at a high resolution and defining a coordinate system with MD and CD by the sample edges. In the next step, the corresponding FO-anisotropy and FO-angle of single layers was determined by a Matlab-routine. Finally, a three-dimensional model of the sheets was derived by assembling the individual layers by means of the previously defined coordinate system. A single layer and a sketch of the resulting stack is illustrated in Figure 24.

Distributions of FO-anisotropy and FO-angle over the z-direction are shown in Figure 25 and 26 respectively. Sheets manufactured on a DSF do not exhibit any FO two-sidedness. These results emphasize expectations that a DSF may produce a mainly layered sheet structure with homogeneous properties on TS and BS. It is presumed, that this characteristic is caused by the continuous spraying of the fiber suspension onto an already immobilised fiber mat. With regards to the theoretically isotropic sheets produced on a Rapid Köthen Sheetformer, FO-anisotropy was basically inhomogeneous over sheet thickness. Besides, relatively high values of up to 2 were obtained. Stochastic fluctuations can be explained by the sheet forming mechanism but the fairly intense anisotropy remains unclear. However, some FO-misalignment has also been observed in previous studies [11].

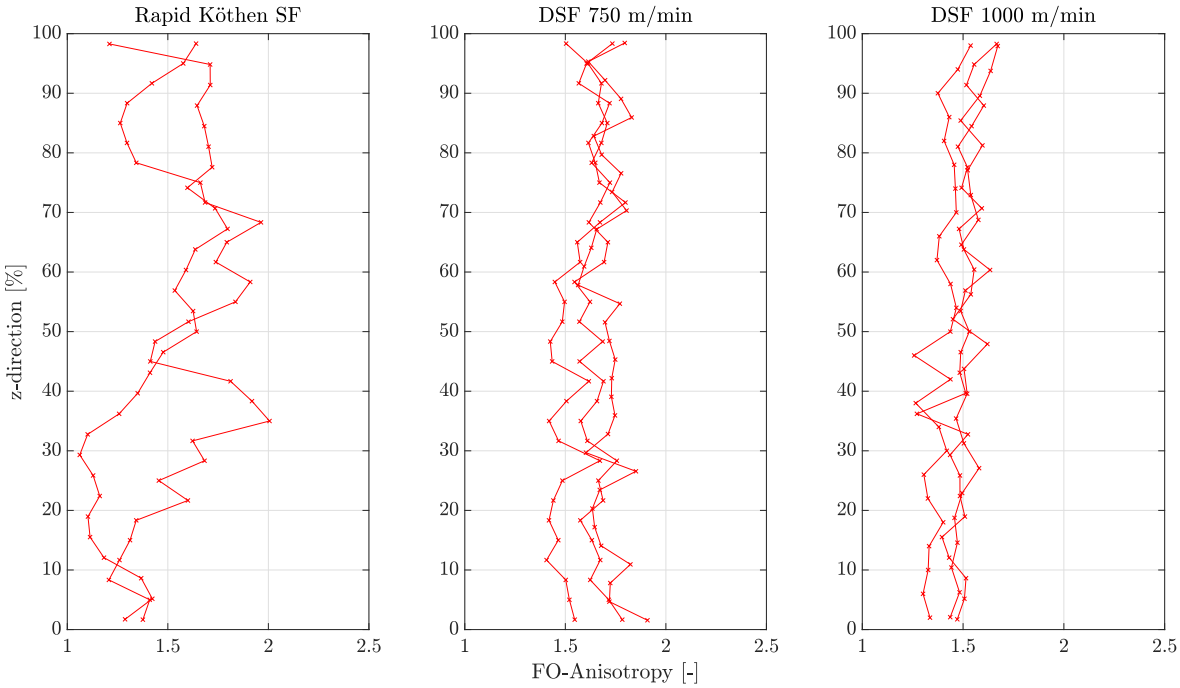

Figure 25. Anisotropy over z-direction of handsheets produced on a DSF was determined by sheet splitting [29] and compared to Rapid Köthen sheets. Dynamic sheets show a rather homogeneous anisotropy over sheet thickness. However, conventional handsheets have intense fluctuations.

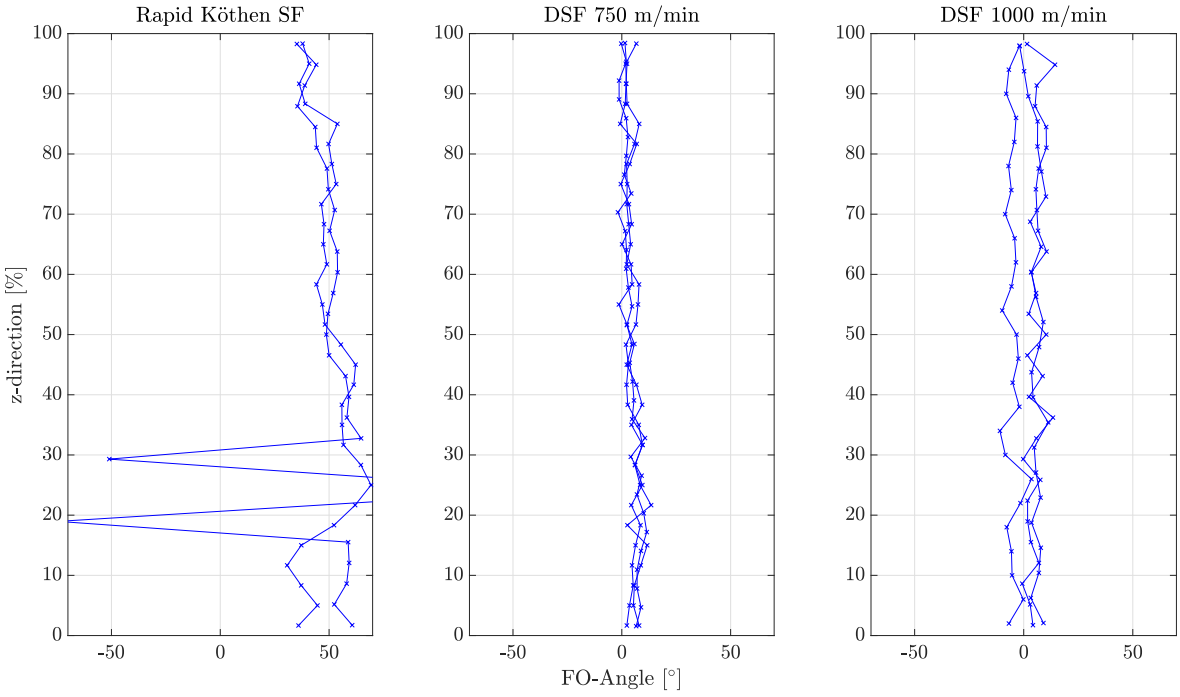

Figure 26. FO-angle over z-direction of handsheets produced on a DSF was determined by sheet splitting [29] and compared to Rapid Köthen sheets. Comparable to Figure 25, dynamic sheets show no two-sidedness regarding FO-angle.

3.2 Mechanical properties of the paper samples

Except for the *refining*-trial, the entire handsheet series was tested on mechanical properties regarding tensile strength and bending stiffness. For sheets of trial 1 which had been considered a pre-trial only bending stiffness values were measured. Before the tests, the sheets were climatised for a minimum of 24 hours in a climate room. The observed measurement standards are summarised in Table 5.

Density ρ of sheets was calculated by the ratio between grammage $[g/m^2]$ and thickness d $[\mu m]$:

$$\rho_{sheet} = \frac{grammage}{d} \qquad [g/cm^3] \tag{3.2}$$

Bending stiffness was determined by measuring bending resistance on a L&W Bending Tester. The force $[N]$ required to bend the free end of a rectangular specimen to a specified angle was subsequently transformed to a stiffness S^b value related to the width according to following equation:

$$S^b = \frac{60\ F\ l^2}{\pi\ \phi\ b} \qquad [Nmm] \tag{3.3}$$

in which: l = bending length $[mm]$, b = specimen width $[mm]$ and ϕ = bending angle [°] (here 15°).

By means of the area moment of inertia I $[mm^4]$, the modulus of elasticity E^b out of bending stiffness S^b was calculated:

$$E^b = \frac{S^b\ b}{I} \qquad [N/mm^2] \tag{3.4}$$

with $I = \frac{d^3\ b}{12}$.

Tensile strength measurements were carried out on a Tensile Tester supplied by Frank PTI. The clamp distance of specimens was 100 mm with a constant rate of elongation of 20 mm/min. Values for breaking force $[N]$, strain at break [%], tensile strength $[N/m]$, tensile strength index $[Nm/g]$ and modulus of elasticity $[N/mm^2]$ were established.

Table 5. Measurement standards.

Property	Standard	Optional settings
Grammage	ISO 536	-
Thickness	ISO 534	-
Tensile strength properties	ISO 1924-2	constant rate of elongation: 20 mm/min
Bending resistance	ISO 2493-1	bending angle: 15°; bending length: 10 mm

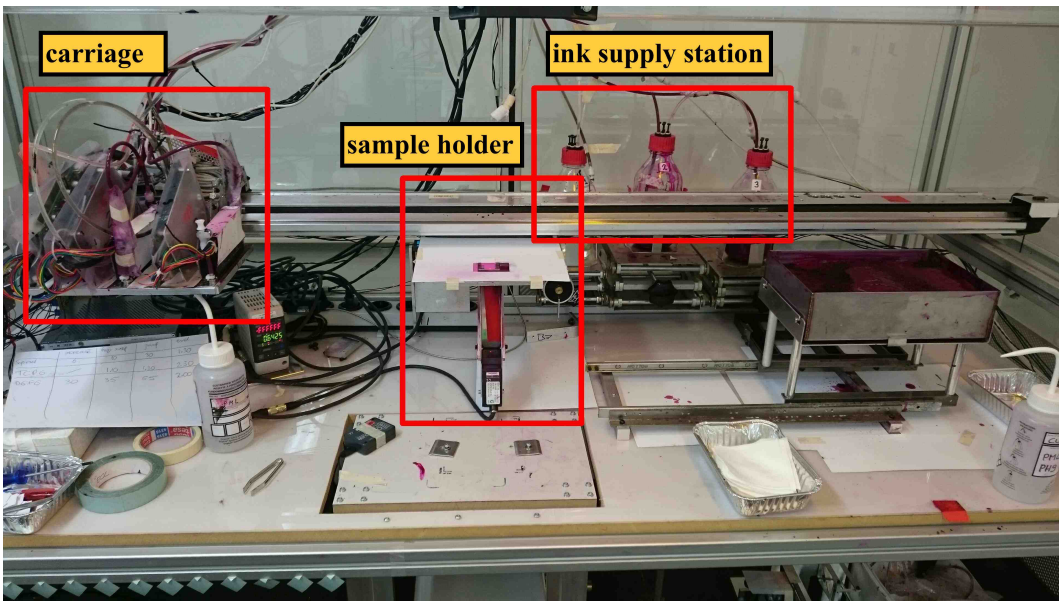

Figure 27. Pilot curl test setup.

3.3 Curl test setup

3.3.1 Description of the equipment for curl tests

A major part of experiments were carried out on a pilot curl test setup located at Océ Venlo. It was developed by Ern Clevers with the objective to investigate paper and ink related reasons for curl. Though it is a basic lab-scale apparatus, its core part consists of three industrial print heads as commonly installed in commercial printers. Figure 27 shows the main components of the setup:

- a carriage with three print heads, illustrated in detail in Figure 29b
  - one for possible primer application
  - two for inks
- a sample holder with a laser displacement sensor provided by Keyence to measure paper deflection after printing (sketch in Figure 28, close-up in Figure 29a) and during the subsequent free drying
- an ink supply station

One advantage of the setup is a small sample size of 1.7 x 5 cm, enabling a maximized number of tests with reduced paper consumption. Simultaneously it represents a severe drawback regarding industrial printing devices. Due to the dimensional gap, papers might perform differently in real-life machines. However, the chosen small-scale approach should provide a better understanding of isolated curl behaviour focussing on influences from the paper side. A further positive aspect is the amount of different inks (up to 6) printable on one single paper sheet. Thus, some production related variations of paper properties can be eliminated.

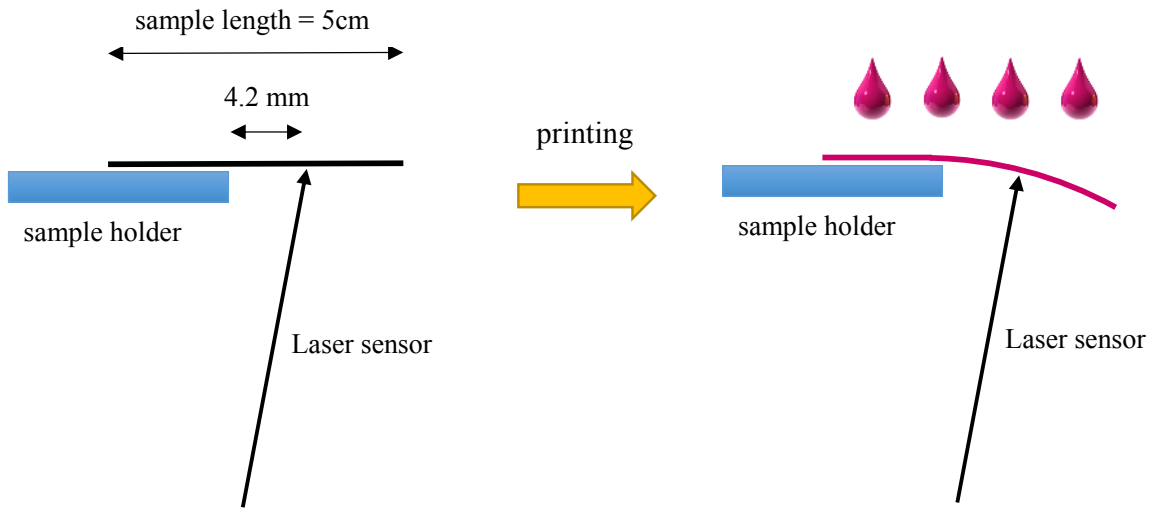

Figure 28. Samples with a length of approximately 5cm were attached to a sample holder by two sided tape. The laser displacement sensor measured the position of the sample at a 4.2mm distance from the sample holder. After printing, the sample curled downwards and the deflection at the same distance was measured by the laser sensor.

The setup was located in a climate chamber, in which papers for the subsequent sample preparation were stored as well. However, a variation of ± 5% in relative humidity and ± 1°C was observed. After the transport of the manufactured handsheets to Venlo, they were climatised for a minimum of 24 hours before carrying out any test.

Sample preparation. Samples were prepared out of three handsheets per specification, e.g. 1000 rev PFI 0 bar. Three stripes of 1.7 cm were cut off at the edges before specimens were taken from the center of the sheet as shown in Figure 30. The direction of stripes transverse to the wire marker on the sheets was defined as cross direction, whereas machine direction corresponded to samples perpendicular to the mark.

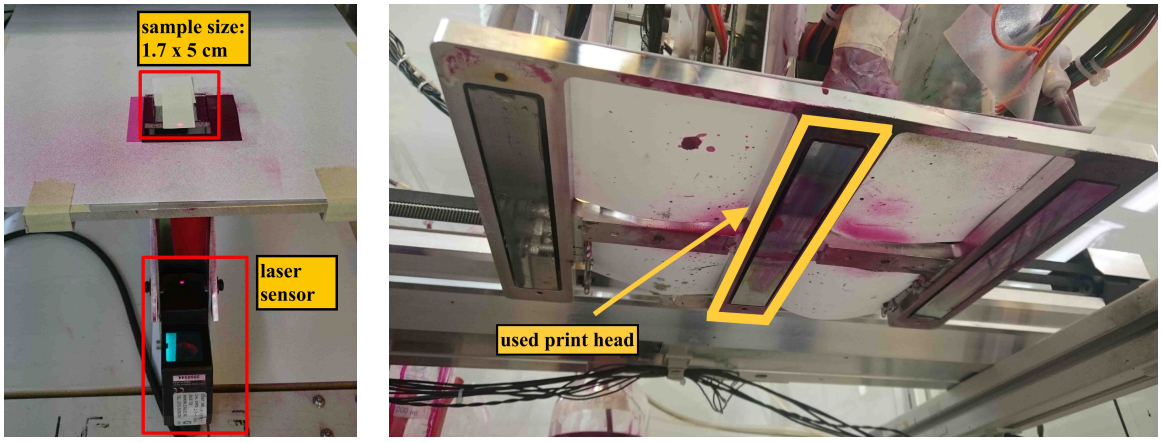

(a) **(b)**

Figure 29. Samples of 1.7 x 5 cm were placed by two sided tape onto a sample holder **(a)** with an attached laser displacement sensor. Printing was then realised by a carriage **(b)** with three print heads of which only the middle one (arrow) was used within this work.

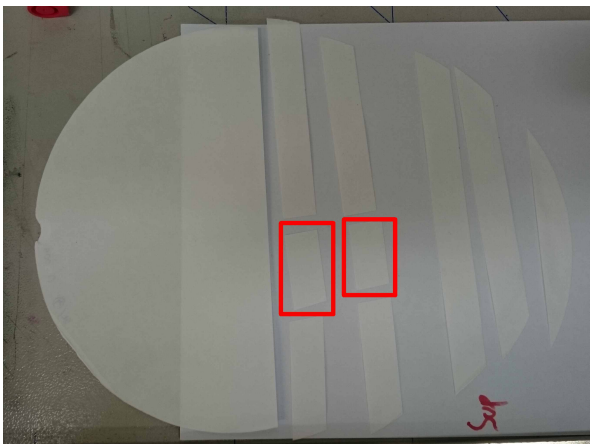

Figure 30. Specimens were taken from the center of the sheet after cutting off three stripes á 1.7 cm.

Of course, these are arbitrary definitions and do not represent any substantial fiber alignments. Nevertheless, samples in both directions were necessary to compare isotropic sheets with anisotropic dynamically formed sheets. Specimens of dynamic handsheets were equally located at the middle of the sheet. Here MD and CD coincide with conventional definitions.

In total, sixteen samples were prepared for conducting curl measurements. Eight were printed on top side and eight on bottom side respectively. Bottom side represents the sheet side towards the forming wire. In case of the *Fiber orientation*-trial, ten samples were aligned in CD and six samples in MD respectively.

3.3.2 Procedure of a single curl test

For all performed curl tests, a standard printing method was established. The three piezo electric print heads were able to generate three different drop sizes with adjustable ink coverage percentages. However, it was decided to conduct all tests with the same ink amount of 8.4 ml/m^2 representing a drop size of 13.7 pl. By the usage of just one print head for ink and a print frequency of 20 kHz, a resolution of 600 x 600 dpi was obtained. The effect of using various liquids was not investigated and thus no primer was applied. Only a water based ink with approximately 60% water content and a viscosity η of 5.3 mPa s was used.

Following the standard sample preparation, the specimen was fixed to the sample holder by using a double sided tape. Figure 28 shows a sketch of the fixed sample and the following curl due to printing. The tip of the sample standing out over the metallic table was kept freely moveable. It was not touched before printing and amounted to approximately 7 mm. During the entire printing process, the displacement of the freely moveable paper sample is recorded by a laser sensor spot, who measures the sample position in a distance of 4.2 mm to the edge of the table (Figure 31).

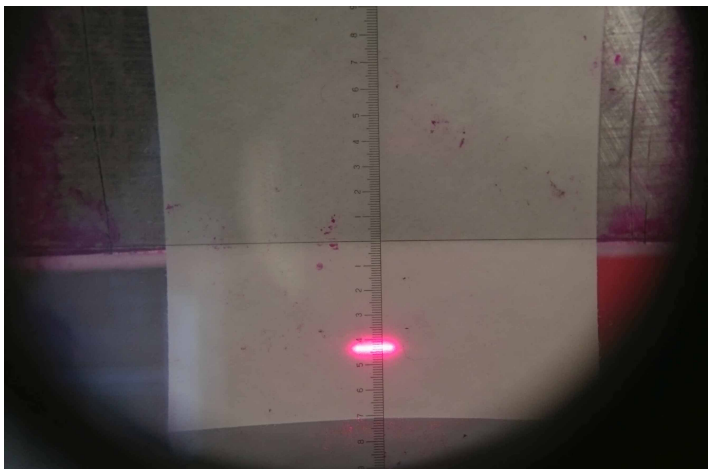

Figure 31. Arm length of the freely moveable sample part. The curl was measured at a distance of 4.2mm from the sample holder. The picture was taken through a measuring magnifier.

Previous to every single test run, the carriage was moved to its starting position on the right side of the carriage guidance. The used print head Nr. 2 was purged and cleaned by a moistened tissue. Recording of the sample displacement was started prior to the cleaning step in order to receive a stable signal of the initial position. In the following, the carriage was switched to the left side at a speed of 0.833 m/s and the sample was printed on the synchronized position. The specimen was then freely dried without applying vacuum or hot air. Curl radius was calculated automatically from the distance readings of the laser sensor using basic trigonometry. By means of a second laser sensor, a time synchronization of the actual point in time when the sample was printed, was done. This step made it possible to analyse time dependency of the curl phenomenon.

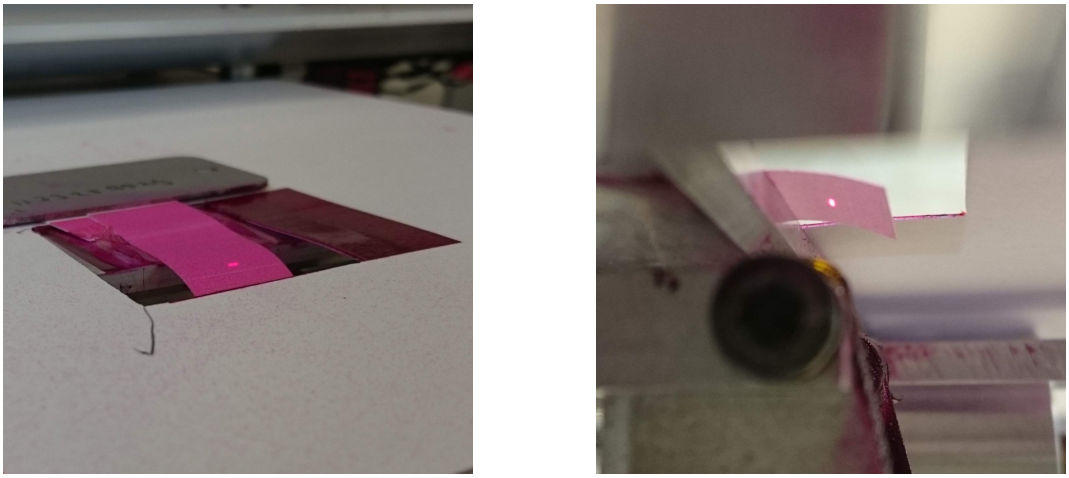

(a) **(b)**

Figure 32. Maximum curl shape seen from **(a)** top and **(b)** bottom. The sample is bending downwards.

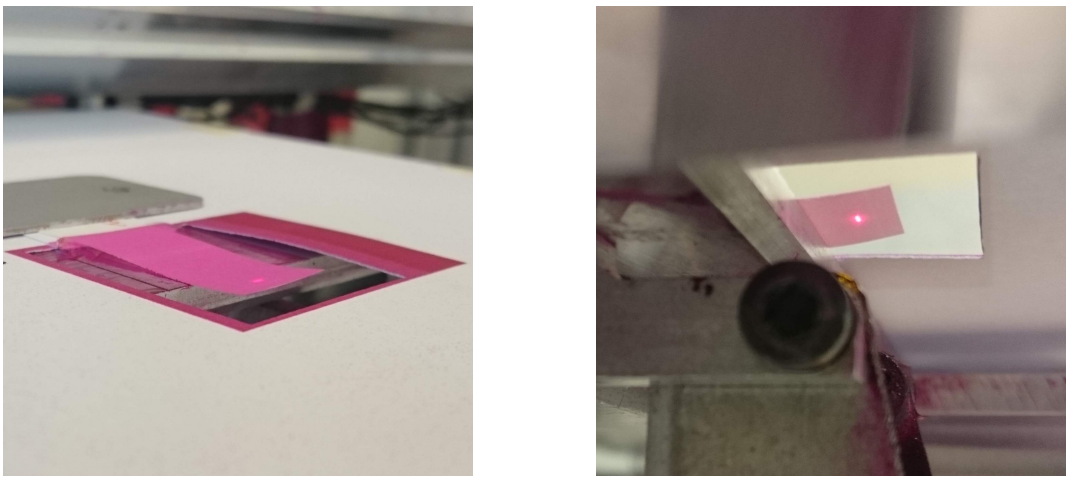

(a) **(b)**

Figure 33. End curl shape after drying, seen from **(a)** top and **(b)** bottom. The sample is bending upwards.

Instantly after applying ink, paper started to curl towards the non printed side. Within 1 to 9 seconds, the maximum deflection was reached before the curl radius decreased continuously until it stabilised after approximately 3 minutes. The two characteristic points of the curl behaviour are illustrated in Figure 32 and 33 respectively. It is clearly visible that the sample at first curled downwards and then ended up with a slight upwards curl to the printed side. According to previous trials gravitational effects due to inkload could be neglected.

Data storage was carried out for 4 minutes in total to obtain sufficient sample positions for post processing. Namely 30.000 data points were recorded at a frequency of 125 Hz. The ensuing analysis was realised by several MATLAB scripts as explained below.

3.3.3 Post processing method of the laser sensor data using a MATLAB-Fit

Data obtained from the laser sensor was imported into a MATLAB script for analysis. In the first step, the deflection values retrieved from the first laser sensor were synchronized with the time values of the second laser sensor. Thus, the starting point of the curl development could be determined. Then, maximum and final value of the curl is calculated. It is quantified by means of the curvature in terms of $1/R$ $[1/mm]$. A high curvature value represents a strong curl or minimum curl radius. A low curvature value in contrast refers to a soft curl, whereas a negative curvature in this context expresses a curl upwards to the printed side.

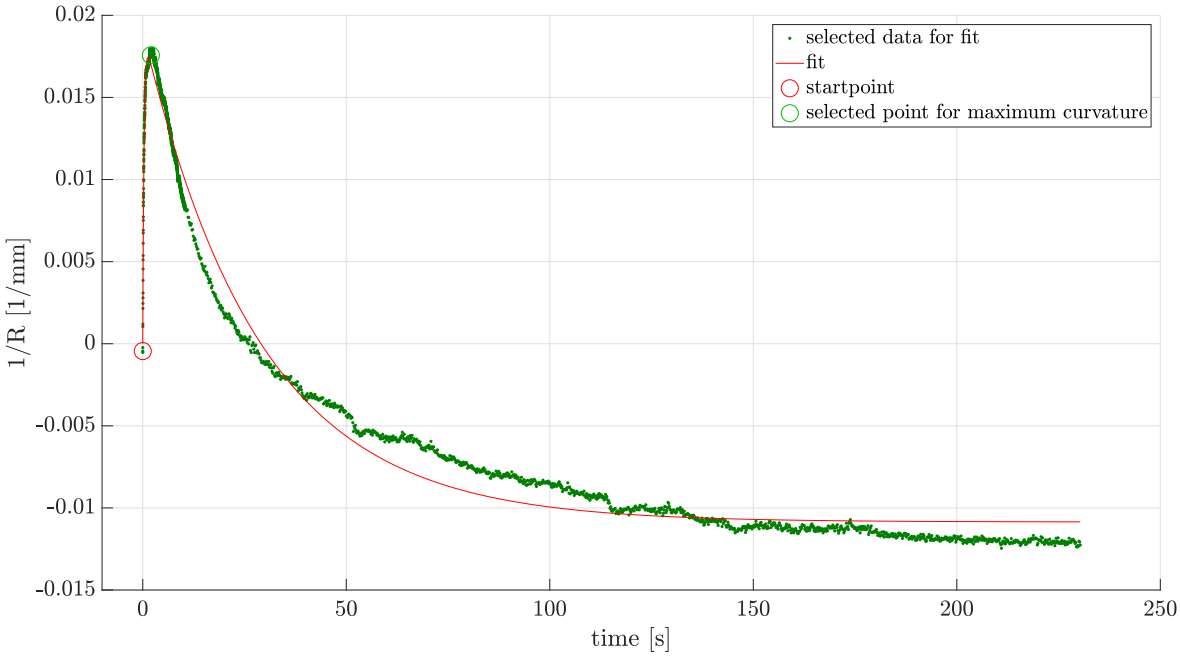

Figure 34. Example of typical curve representing the curl curvature 1/R over time. A combination of two exponential curves (red line) was fitted to the laser sensor data (green).

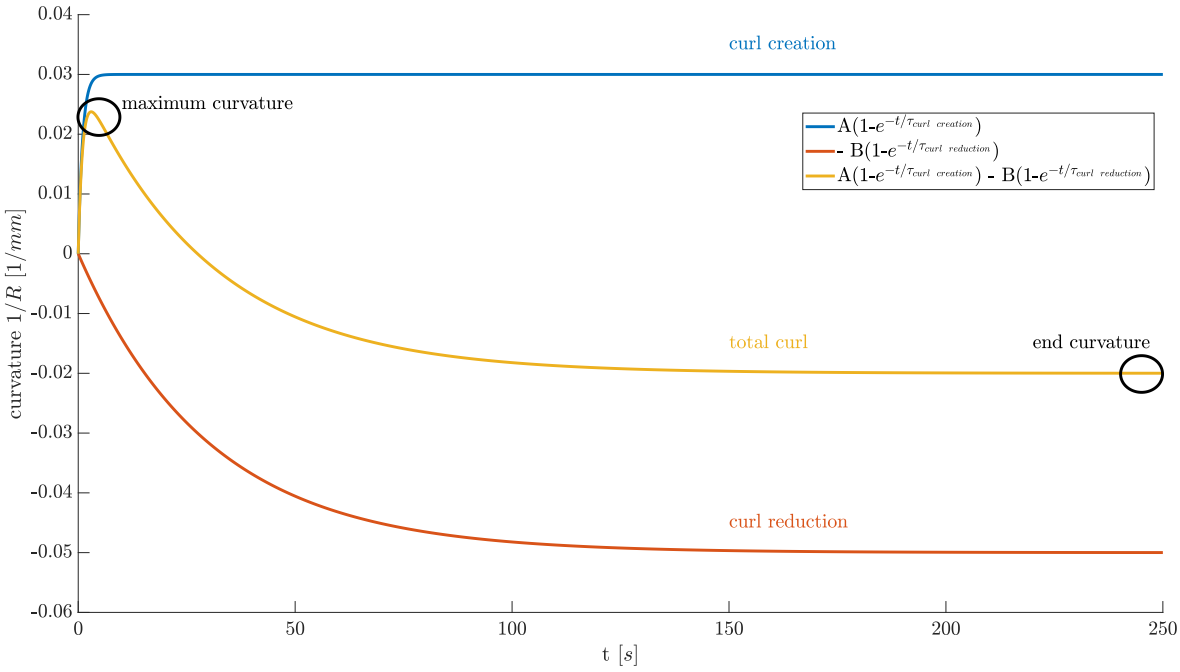

Figure 35. Deformation data from laser sensor were fitted by using a combination of two exponential curves.

In Figure 34, a characteristic curve of the curl behaviour is demonstrated. The development of curvature $[1/R]$ is plotted over time $[s]$. It is visible at first sight that curvature was rapidly increasing and reached its maximum point within a couple of seconds after ink appliance. The following decrease and creation of a back curl to the opposite side was one order of magnitude slower. With the objective to quantify the dynamic behaviour of the curl, it was discovered that a combination of two exponential curves lead to reasonably good fitting:

$$fit_{curl} = A(1 - e^{(-t/\tau_{curl\ creation})} - B(1 - e^{-t/\tau_{curl\ reduction}}) \qquad [1/mm] \qquad (3.5)$$

Figure 35 illustrates how these two curves contribute to the overall curvature graph.

A - amplitude of curl creation

$\tau_{curl\ creation}$ - time constant of curl creation

B - amplitude of curl reduction

$\tau_{curl\ reduction}$ - time constant of curl reduction

In the first 5 to 10 seconds the curl creation (blue line) represent the dominant part of the fit. Afterwards, the curl reduction (orange curve) determines the shape of the overall function (yellow line) which has a permanent offset amounting to $A - B$. As previously mentioned, the maximum and end curvature values can be found at the extreme and end point of the fit respectively. The achieved goodness of fit values were between 0.75 and 0.999.

It was decided to further use the original data obtained by the laser sensor regarding maximum and end curvature rather than the values from the fitted curve. In fact, the values for maximum curvature essentially coincide to a great extent. Fitting the end value of curvature did occasionally not lead to accurate results, though the offset was in the range of 0.005-0.01 1/mm.

The fit was used in further steps to describe the time dependency of the curl creation and reduction respectively in terms of $\tau_{curl\ creation}$ and $\tau_{curl\ reduction}$. The time constant τ in a $C(1-e^{-t/\tau})$ function represents the point in time at which 63.2% of the amplitude C of the corresponding function is achieved. A low $\tau_{curl\ creation}$ signifies a fast curl generation. A low $\tau_{curl\ reduction}$ indicates a fast curl decline.

Additionally to $\tau_{curl\ creation}$, another parameter for the speed of curl development was calculated. It is a linear function fitted to the curve in the range of the first milliseconds. In Figure 36 the curve of Figure 34 is zoomed in, focussing on the initial increase of curvature. By determining the slope of the linear fit, an initial curl creation rate in terms of $[1/mm\ s]$ could be defined. Selected data for this type of fit included all curvature values less than 40% of the maximum value.

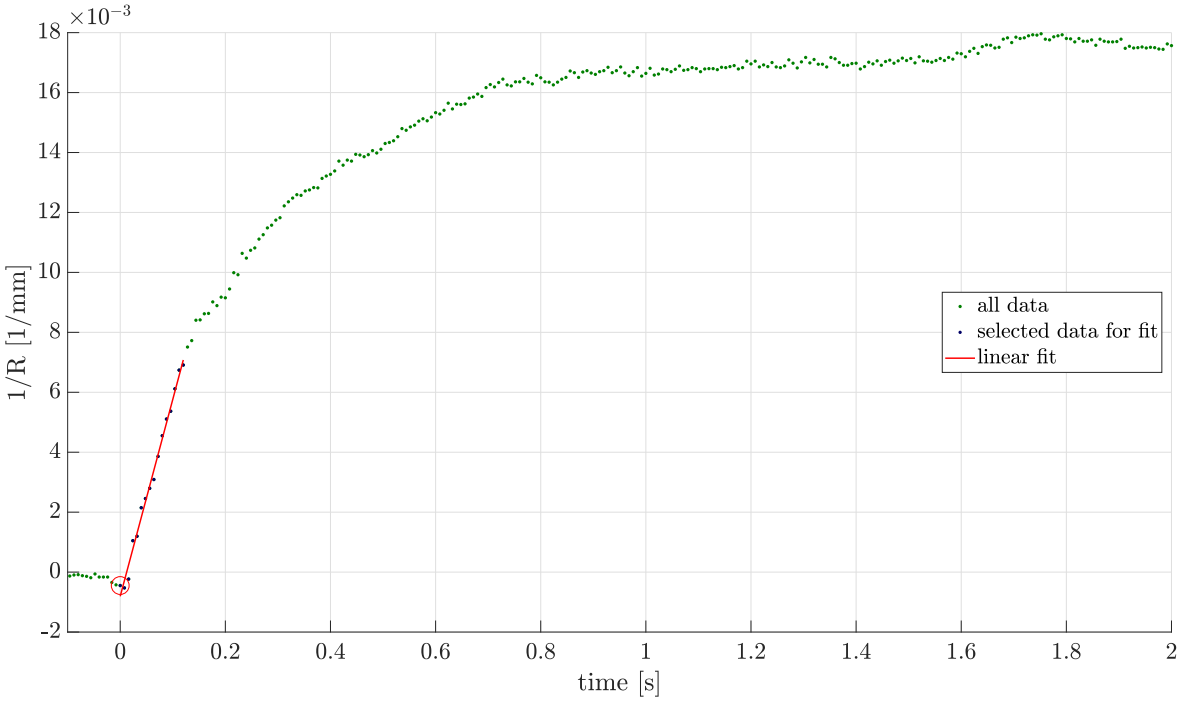

Figure 36. In order to obtain a more accurate value for the initial curl creation, a linear fitting for the first milliseconds was carried out.

3.3.4 Definition and chart of KPIs

A set of Key Performance Indicator (KPI)s was established to depict, compare and interpret the obtained curl data. All further used KPIs and their origin are listed in Table 6. The calculated or retrieved values for all handsheet trials were collected and arranged into a structure of a new MATLAB script. Subsequently a statistical analysis was performed to remove outliers by using the Median Absolute Deviation (MAD). Values more than three scaled MAD from the median were considered outliers and in the following replaced by the respective upper or lower threshold of the MAD interval. MAD represents a more robust measure to detect outliers than the standard deviation around the mean [42].

Means and a Confidence Interval (CI) of 95 % were calculated for the entire series of handsheet specifications (e.g. 1000 rev PFI 0 bar CD top side printed). These values were then plotted over sheet density $[g/cm^3]$ including specifications of one trial. Figure 37 shows one of these graphs in case of the *refining*-trial. Each marker represent the mean value for a certain pressure point. In this sense, as density increases with applied wet pressure, markers of 0, 75 and 150 bar are aligned along the x-axis.

Here no difference regarding orientation (CD or MD) or printed side (TS or BS) was made. There is a clear tendency towards a stronger maximum curl when increasing sheet density. The behaviour with respect to all trials is discussed in detail in chapter 4.

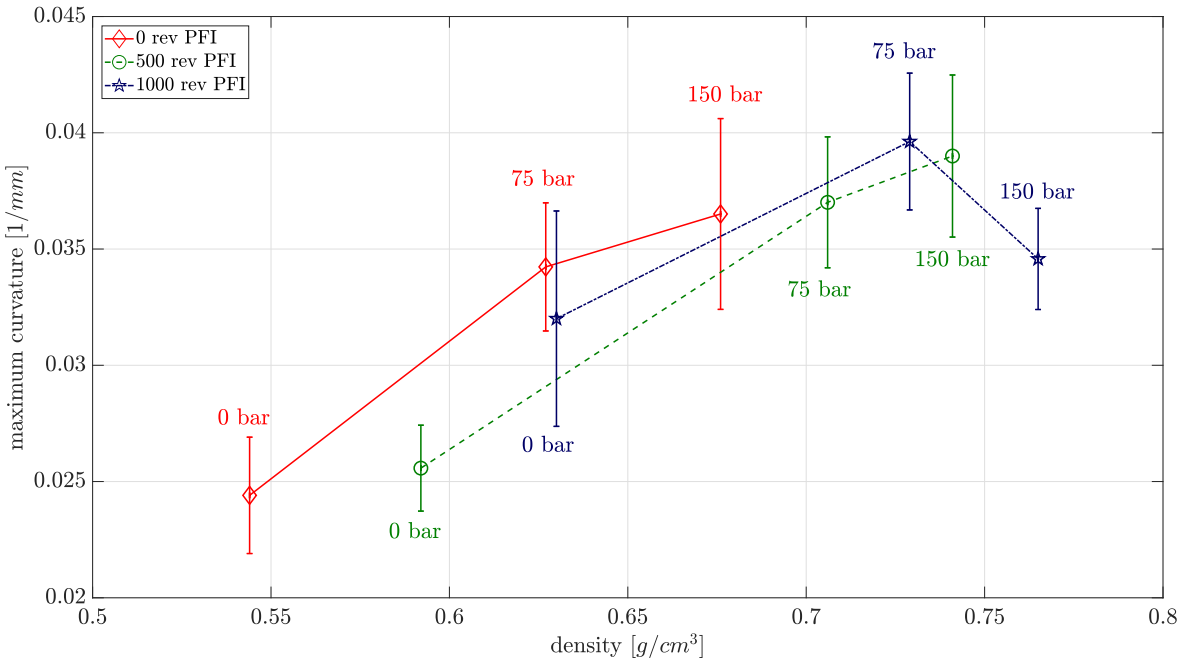

Figure 37. Every KPI (here maximum curvature) was plotted over sheet density to describe this influence. The errorbars represent a 95% CI.

Table 6. Definition of KPIs for curl tests.

KPI	description	origin
Maximum curvature $[1/mm]$	maximum = initial curl	laser sensor data
End curvature $[1/mm]$	curl at end of measurement	laser sensor data
$\tau_{curl\ creation}$ $[s]$	time constant of curl increase	exponential fit
$\tau_{curl\ reduction}$ $[s]$	time constant of curl decrease	exponential fit
initial curl creation rate $[1/mm\ s]$	initial slope of curl creation curve	linear fit

3.4 Development of a method to compare individual trials

Due to various density ranges achieved within the individual handsheet trials, a method was developed to exclude this parameter appropriately. This method is described by means of the *Refining* trial and is illustrated in Fig. 38-41.

The mean values of one KPI, e.g. maximum curvature, at four densities (0.6, 0.65, 0.7 & 0.75 g/cm^3) were calculated by a linear regression model as seen for the test point of 500 rev PFI in Figure 38. Also the 95% prediction intervals (black double arrows) for the mean values were determined. The average of the four mean values was considered the mean response of the respective KPI in a density interval of 0.6-0.75 g/cm^3. The corresponding CI was calculated by the average of the four prediction intervals. In Figure 39 the mean response with the CI of the maximum curvature for the *Refining* trial is plotted. The first yellow framed bar represents the defined *zero point* that was used for the following normalisation explained in Figure 40.

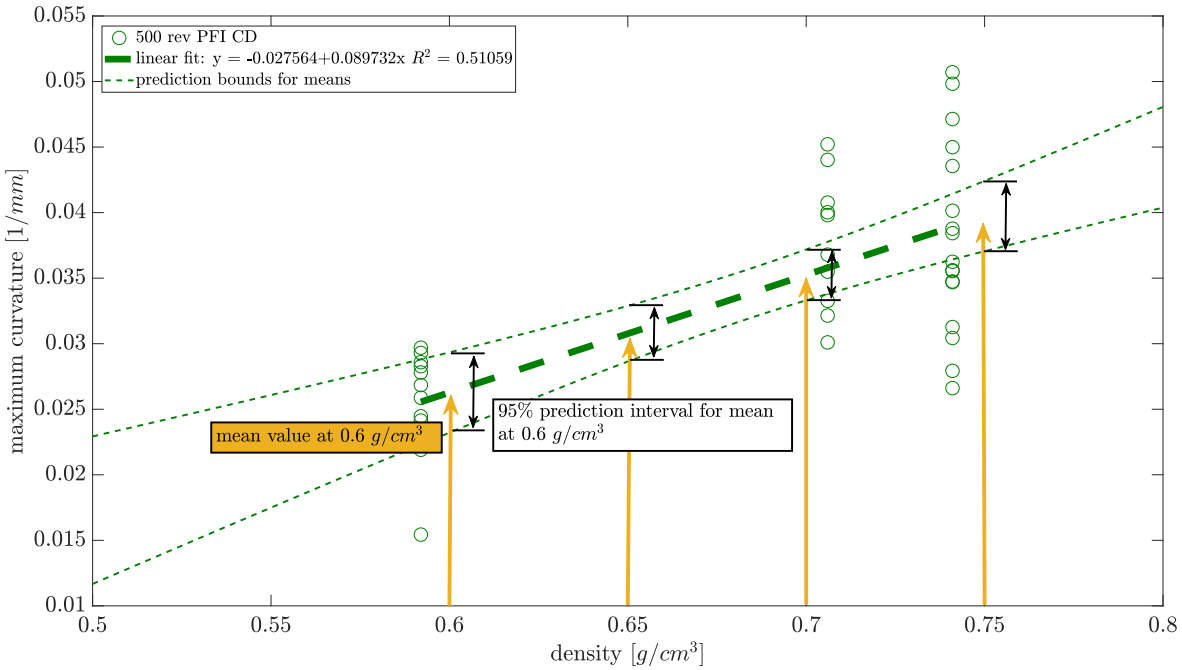

Figure 38. Calculation of mean response of a variable. In order to eliminate the influence of density for each trial, the response was calculated at densities 0.6, 0.65, 0.7 & 0.75 using a linear regression model. The average of these four fitted values is the mean response of the KPI. The average of the corresponding 95% prediction interval at the four density values is the confidence interval for the calculated mean response.

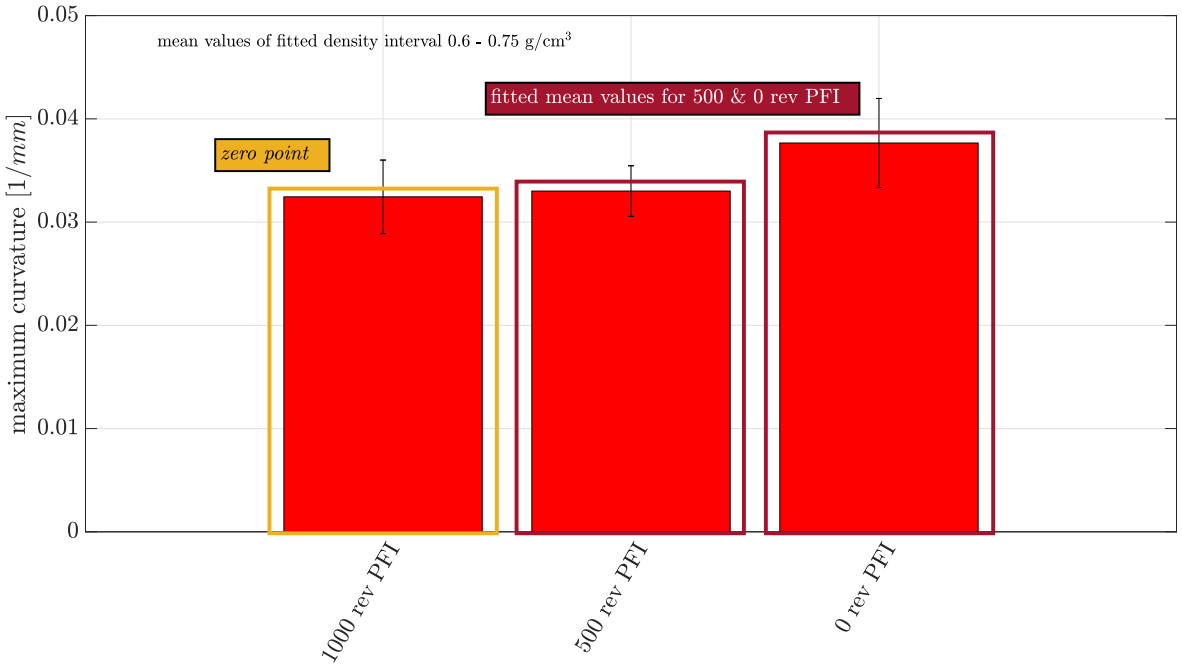

Figure 39. Mean response of maximum curvature for *refining* trial. 1000 rev PFI was defined the *zero point* for this trial and the entire handsheet series.

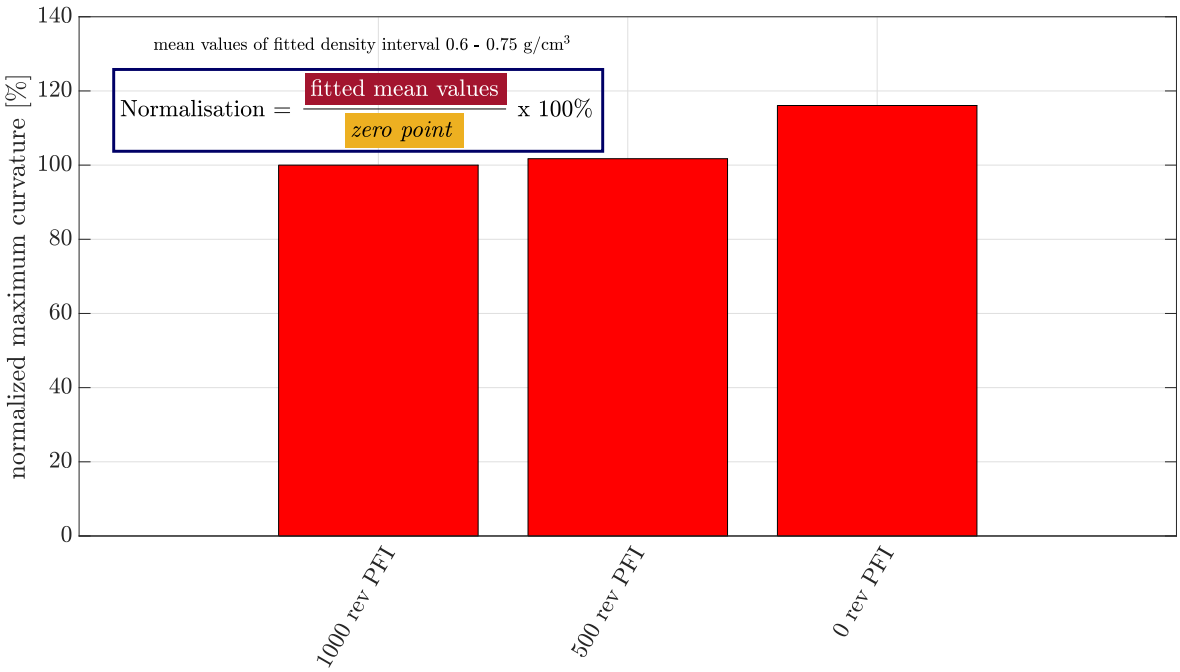

Figure 40. Normalisation of mean response relative to the *zero point*. The fitted mean values of the maximum curvature in Figure 39 were divided by the *zero point* to visualise the change in value referring to the *zero point* when e.g. the refining degree decreases.

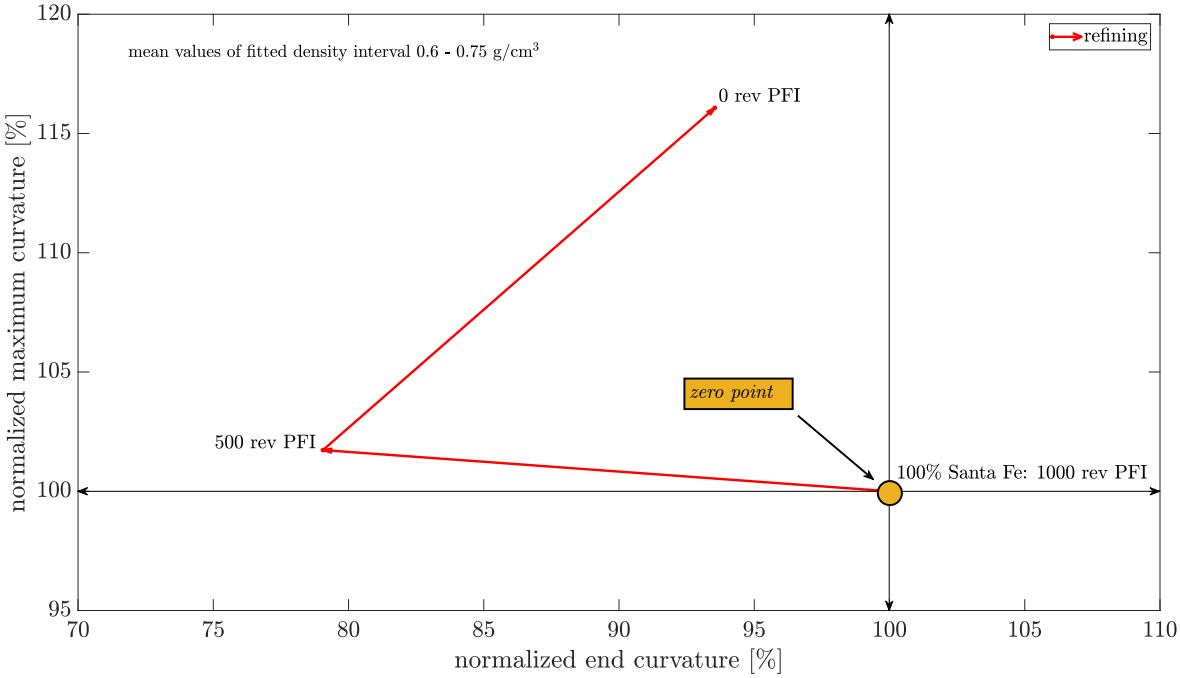

Figure 41. Comparison of normalised values for two KPIs. This arrow plot shows the development of maximum and end curvature with decreasing refining degree starting from the *zero point* (= 1000 rev PFI) at 100%. The normalised mean values for maximum and end curvature are obtained by the method visualised in Fig. 38-40.

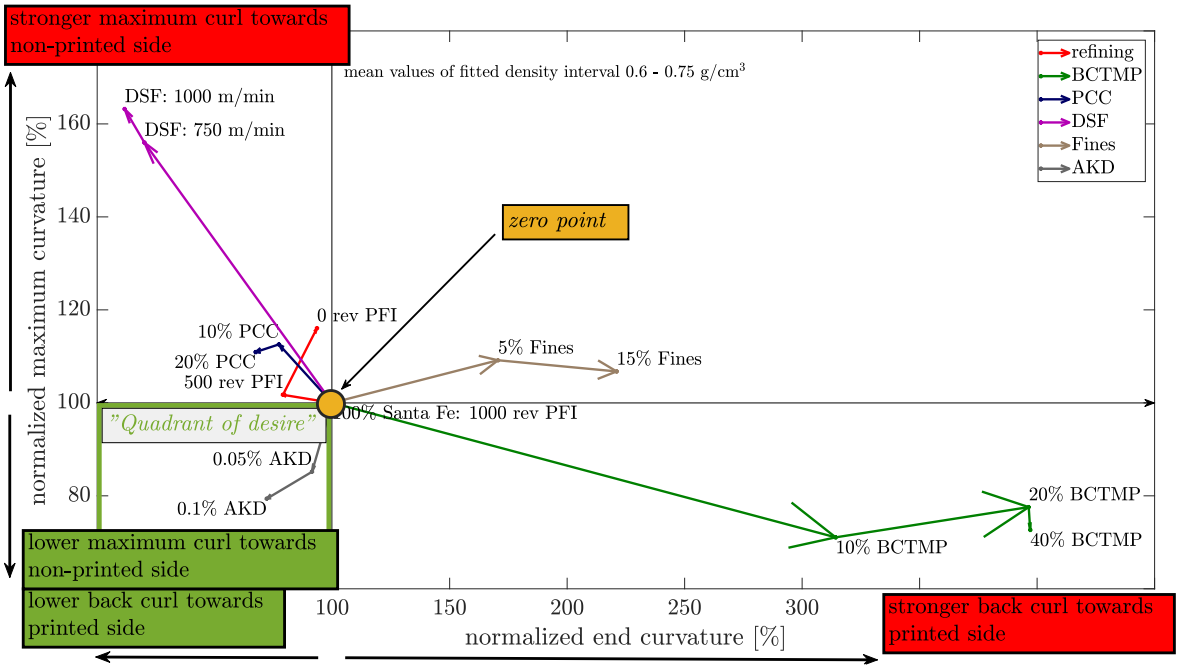

Figure 42. Explanation of summary plots. Here maximum and end curvature for all six trials are compared according to the method explained in Fig. 38-41. The *zero point* (= 1000 rev PFI, 100% chemical pulp & no additives) is defined in the first line of Table 2.

In the normalisation step all fitted mean values were divided by the *zero point* leading to a percentage value related to this *zero point*.

In the last step regarding visualisation of obtained results, the normalised mean values of two KPIs were compared to each other in an arrow plot (Figure 41). Starting from the *zero point*, the influence of a decreasing refining degree of the sheets regarding both respective KPIs is shown.

Applying the method explained in Fig.38-41, the performance of all six trials regarding e.g. maximum vs end curvature is compared in one plot as shown in Figure 42. The *zero point* is located at the intersection of the corresponding 100% values for each KPI plotted on one axis. As described in 3.1.1 and defined in the first line of Table 2, this initial test point was manufactured equally with an adaption of wet pressing respecting the *Fiber orientation* trial.

Proceeding from the *zero point*, the effect of varying a defined paper constituent on two compared KPIs is clearly visible. As indicated in the plot, the green framed *"Quadrant of desire"* for this pair of KPIs is located in the south-west corner signifying both a lower maximum curvature and end curvature. Each specification point is labelled to achieve a superior readability. It is remarked that regarding the *Fiber orientation*-trial only samples in CD were considered when creating this summary plots.

It has to be further mentioned that the density range of some test points (e.g. 0 rev PFI) did sometimes not entirely overlap with the chosen range of 0.6-0.75 g/cm^3.

For instance, only data points between 0.54 and 0.67 g/cm^3 were available for the 0 rev PFI specification. In this case the CI for the fitted mean response of a KPI increases. However, the applied method was considered suitable to evaluate the variation of defined properties leaving aside the density influence. The sometimes appearing wide confidence intervals of the fitted mean values should be taken into account.

For the isolated discussion of individual trials in section 4.1 - 4.6, the considered density range for fitting was adapted according to the sheet densities of the respective trial. For instance, in case of the *Fiber orientation*-trial the mean response of KPIs was calculated in a minimized density range between 0.6-0.63 g/cm^3. Thus, no extrapolation was necessary and more accurate results could be obtained.

3.5 Description of the Hydroexpansion device

All produced handsheets were additionally tested on their wet expansion behaviour by means of submerging them into liquid. When a paper sample is soaked in water, its dimensional change is termed hydroexpansion. Within the conducted trials at Océ, ink was the predominately used fluid in order to permit a straight-forward correlation with the curl experiment if applicable. This wet expansion measurement was performed on a simple test device demonstrated in Figure 43. A paper sample of 1.7 cm width and approximately 8 cm length was clamped to two metallic sample holders by tiny magnets. The specimen was taken from the centre of the sheet, comparable to 3.3.1. As illustrated in the sketch of Figure 44, one sample holder was freely movable in x-direction and preloaded by a small weight of 1.72 g. The sample was subsequently submerged into a little container filled with ink or water. Due to the liquid uptake into the fiber network and the applied pretension, the right sample holder moved in horizontal direction.

(a) **(b)**

Figure 43. Hydroexpansion in ink was investigated on a simple setup. A paper specimen was clamped onto two sample holders **(a)**, one of them preloaded with a tiny weight of 1.72 g. The sample was then immersed into ink **(b)** recording the expansion by a laser sensor.

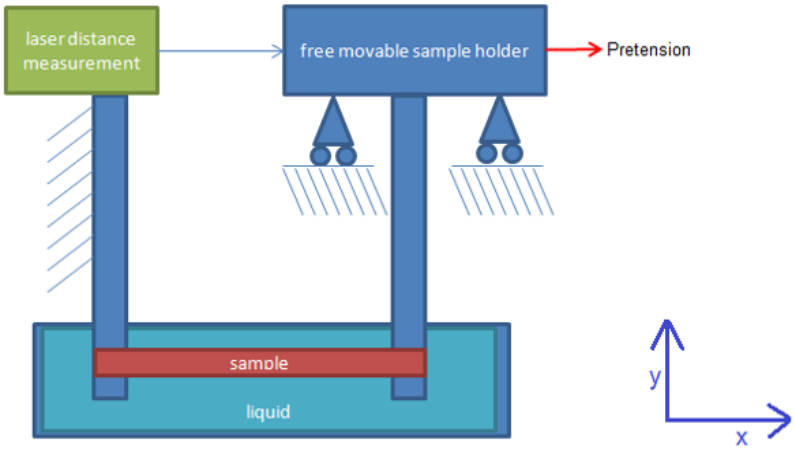

Figure 44. Sketch of hydroexpansion measurement by Ern Clevers.

This expansion was constantly recorded by a laser distance sensor for a period of 20 minutes. Similar to the curl tests, 30.000 data points were recorded, but with a reduced sample frequency of 25 Hz. Prior to immersing, the exact length of the specimen was determined by the laser sensor measuring the distance for approximately 30 seconds. The initial dimension was later used to calculate the strain.

Measurement, preparation and cleaning of the setup was more time consuming than for curl tests. Additionally, curl and hydroexpansion tests could not be performed simultaneously due to a shortage of laser sensors. Consequently, only two tests per test point were performed. In the trials in which deionised water was used, the container was refilled after each testing run to prevent any contamination of the liquid by paper components. In case of ink, the testing fluid was replaced after six measurements. Due to the complex composition of various substances in the ink, impurities were considered less significant. The majority of tests was conducted with ink. Only the AKD sized papers were additionally tested for wet expansion using deionised water.

3.5.1 Post processing of hydroexpansion tests

Analysis of the investigated wet expansion was done by means of a MATLAB script. First, the expansion was quantified in terms of percentage change in length of the sample. The respective strain ε_{hydro} at a defined point in time t was calculated according to:

$$\varepsilon_{hydro} = \frac{length_t - length_{t_0}}{length_{t_0}} \qquad [\%] \tag{3.6}$$

$Length_{t_0}$ represents the sample length before submerging it into water.

The obtained ε_{hydro}-values were plotted over time and then fitted by using two exponential curves. Figure 45 illustrates the inferior goodness of fit obtained by using only one exponential curve. Thus, the preferred fit type was as follows:

$$fit_{hydro} = A(1 - \exp(-t/\tau_{hydroexpansion})) + B(1 - \exp(-t/\tau_2)) \qquad [1/mm] \tag{3.7}$$

Goodness of fit values for fitting with two curves were in the range of 0.85 - 0.96.

Comparable to the curl experiments, KPIs were defined to describe the performance of paper samples regarding wet expansion. The end strain was calculated by Equation 3.6 with $t = t_{end}$. In order to describe the time dependency of the expansion by one single parameter, it was decided to use time constant $\tau_{hydroexpansion}$ of the dominating part of the fit. Due to the fact that the amplitude A is higher than B, the first part of the fit is considered the dominating part.

However, due to a possible loss of information about the real behaviour, a linear fitting similar to the curl tests was considered appropriate. This method is demonstrated in Figure 46. By calculating the slope of the fit at the very first seconds, a gradient termed *initial strain development rate* was received. Strain values ε_{hydro} of less than 40% of the end strain were taken into account for fitting.

The relevant KPIs used to evaluate the hydroexpansion results are listed in Table 7. Charts of KPIs comparing hydroexpansion tests of all handsheet trials were created similar to the method presented in 3.4

Table 7. Definition of KPIs for hydroexpansion tests.

KPI	description	origin
end strain [%]	wet expansion at the end of measurement	laser sensor data
$\tau_{hydroexpansion}$ $[s]$	time constant of dominating part of the fit	exponential fit
initial strain rate $[\%/s]$	initial slope of expansion curve	linear fit

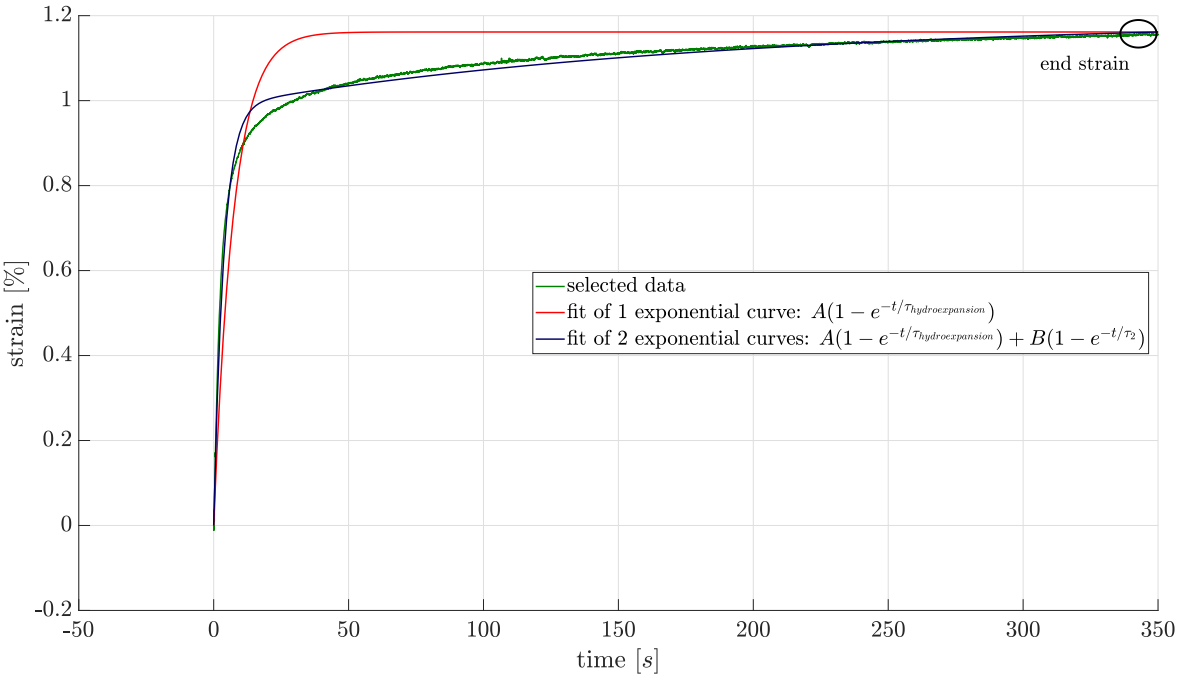

Figure 45. The strain ε obtained during hydroexpansion measurements was fitted by using two exponential curves. The value at the end of the test was termed end strain.

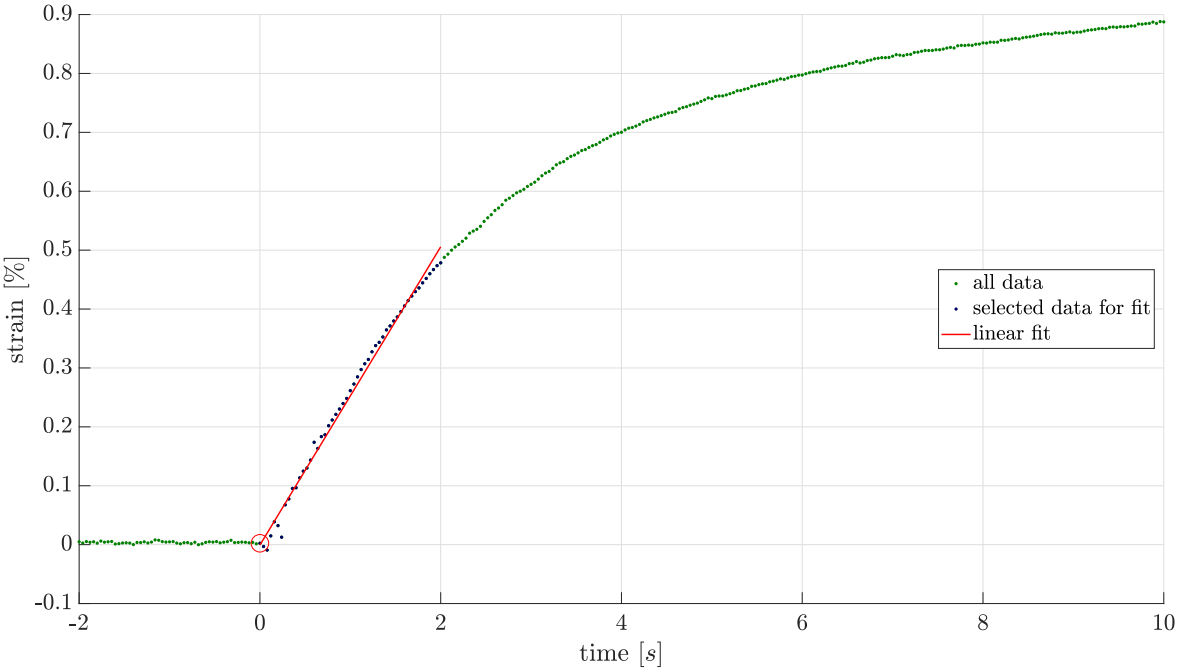

Figure 46. Wet strain is plotted over the first seconds of submerging a specimen into liquid. To obtain a gradient of the expansion, values $< 40\%$ of the end strain were fitted linearly .

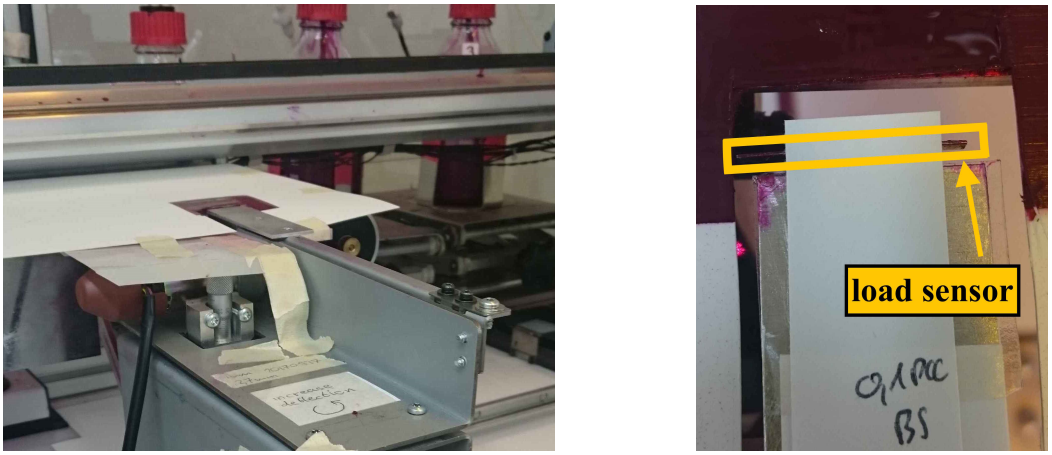

(a) **(b)**

Figure 47. The stiffness reduction setup **(a)** can be placed in the curl test setup to print ink on the sample attached to the sample holder **(b)**.

3.6 Description of the stiffness reduction test setup

As third experimental part of the investigations on liquid-paper interactions, a stiffness reduction measurement during printing was conducted. Main objective of this investigation was to detect any correlations with the results of curl tests. However, due to lack of time only a reduced number of tests could be performed. The setup used within these stiffness reduction tests is shown in Figure 47a. It replaced the sample holder of the curl tests at the same position in order to enable an equal printing as in case of curl tests. A paper sample was attached to a metallic beam by two sided tape. This beam was constantly moved with an adjusted frequency by an actuator illustrated in 48 and Figure 49b. The tip of the specimen was deflected by a load sensor located in a distance of 2.7 mm from the edge of the beam (Figure 47b). Preload was adjusted by a deflector shown in Figure 49a. The load signal varied periodically due to the actuator movement.

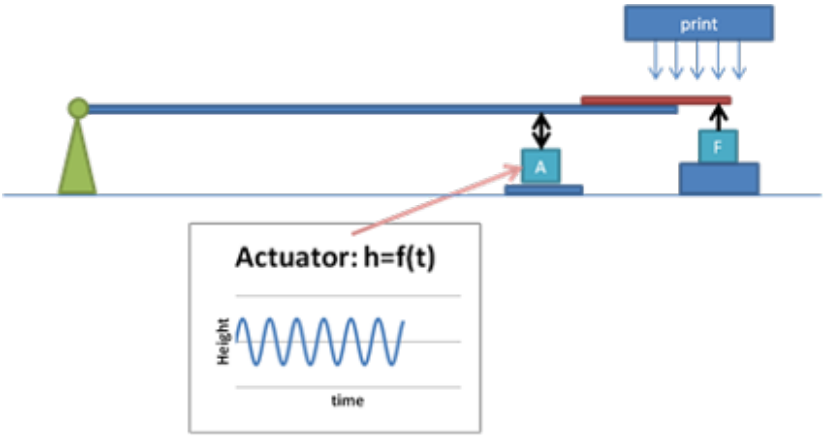

Figure 48. Sketch of the stiffness reduction setup by Ern Clevers.

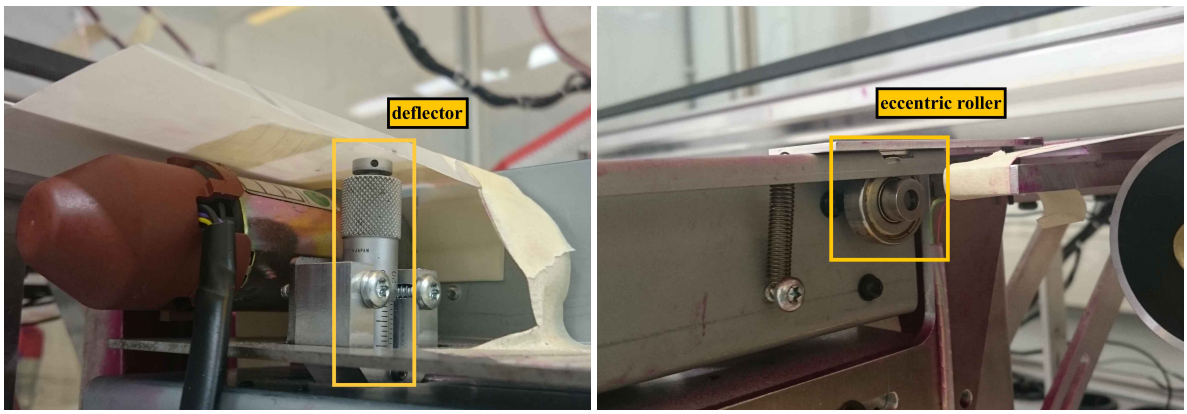

(a) **(b)**

Figure 49. The initial deflection of the sample is adjusted by a screw **(a)**. The actuator signal is transmitted by an eccentric roller **(b)**.

By placing the measurement device at the position of the curl test sample holder, printing of the specimen was enabled. After applying a pre-load of 5-6 g and starting the record of the load signal, the sample was printed with equal settings as in 3.3.2. Due to the ink application, a sudden reduction in stiffness in terms of a drop of the applied deflection force was observed. A stabilized load signal was achieved again after a couple of seconds. Therefore the total testing time for one sample was approximately 30 seconds. Two samples of each handsheet specification (e.g. 0.1% PCC 0 bar) were printed on BS and two samples were printed on TS respectively.

It is worth mentioning that absolute stiffness values could not be derived with this setup. However, the relative change in load signal could be related to a loss in stiffness.

3.6.1 Post processing of stiffness reduction measurements

The data recorded by the load sensor was post processed in a MATLAB file. Similar to the previously described methods, an exponential curve was fitted to the raw data. In Figure 50, the mean values of the force variation is plotted over time. At $t = 0$ ink was applied and the occurring drop in force was fitted by an exponential function:

$$fit_{stiffness\ reduction} = A(1 - \exp(-t/\tau_{stiffness\ reduction})) + force_{initial} \quad [mN/10] \quad (3.8)$$

For the majority of samples fitting was acceptable with goodness of fit values between 0.5 and 0.88. Nevertheless, inferior values of under 0.3 were obtained occasionally. Bad fitting performance is partly explained by less oriented point clouds after the force drop caused by noise of the highly sensitive load sensor.

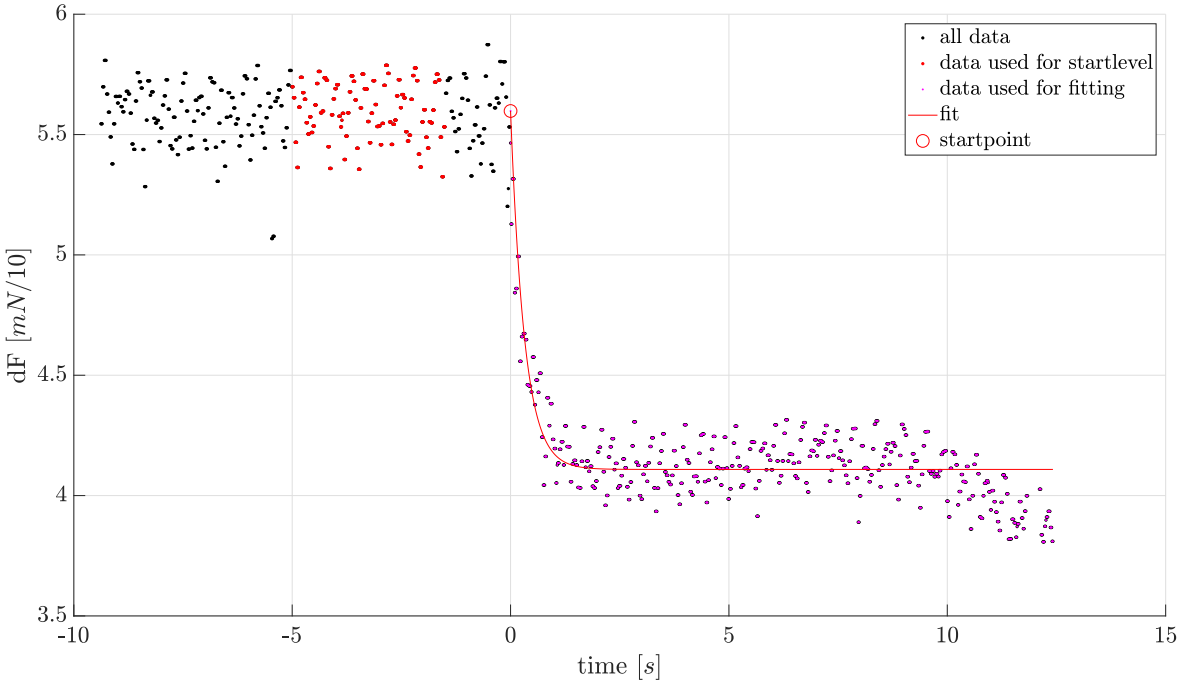

Figure 50. Fit for stiffness reduction test.

Results of theses measurements were evaluated by means of two KPIs.

First, the extent of stiffness reduction was defined by a *stiffness reduction factor* [%]. It was calculated by the ratio between the minimum force detected by the load sensor to the initial force:

$$stiffness\ reduction\ factor = \frac{F_{min}}{F_{initial}} \qquad [\%] \tag{3.9}$$

Second, $\tau_{stiffness\ reduction}$ $[s]$ of Equation 3.8 was used to describe the time dependency of the stiffness loss. Table 8 lists the KPIs for this measurements. Comparison of various handsheet trials was done according to 3.4.

Table 8. Definition of KPIs for stiffness reduction tests.

KPI	description	origin
stiffness reduction factor [%]	ratio of loss of stiffness	load sensor data
$\tau_{stiffness\ reduction}$ $[s]$	time constant of stiffness reduction curve	exponential fit

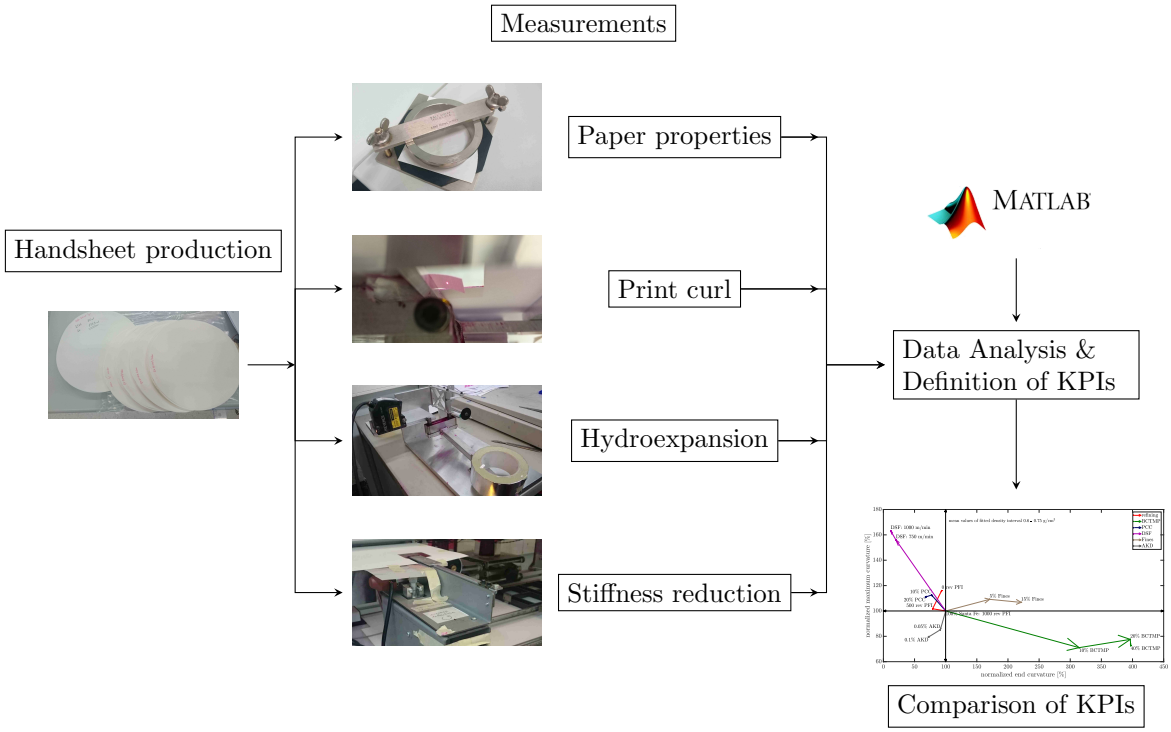

Figure 51. Flowchart of experimental implementation.

The flowchart in Figure 51 illustrates the experimental implementation of the thesis.

4 Results and Discussion

The practical part of this work consisted of two main work packages. On the one hand, a series of handsheets with specific characteristics was manufactured. On the other hand, this sheets were subsequently tested on three test setups located at Océ Venlo. The results regarding mechanical properties of all papers and their performance in curl, hydroexpansion and stiffness reduction measurements are depicted and discussed in this chapter. In the beginning, individual trials are evaluated in an isolated manner before analysing them collectively. The primary focus is on curl results with the latter intention to draw conclusions and correlations with wet expansion and stiffness loss.

Selected mechanical properties of the produced handsheets are collected in tables using the following abbreviations. The given values represent mean values with corresponding standard deviations.

Abbreviations for tables

ρ - mean density $[g/cm^3]$

d - thickness $[\mu m]$

bw - basis weight $[g/m^2]$

S^b - bending stiffness $[Nmm]$

E^b - modulus of elasticity calculated from bending stiffness $[N/mm^2]$

TI - tensile strength index $[Nm/g]$

E^t - modulus of elasticity derived from tensile tester $[N/mm^2]$

4.1 Results for trial 1: Refining

In the first handsheet trial, three levels of refining were compared to each other. The mechanical properties of the total nine specifications are listed in Table 9. No tensile test was performed here and thus no data on Tensile Strenght Index (TI) nor E^t is available. It is clearly visible that even this low intensity of refining leads to a remarkable increase in density and modulus of elasticity. Wet pressing additionally intensifies these effects.

4.1.1 Maximum, end curl and curl rate

Regarding the magnitude of the initial curl after printing in the test setup, the various beating levels show comparable results as already depicted in Figure 37. Mean values

Table 9. Mechanical properties of papers of trial 1: Refining.

Specification	ρ $[g/cm^3]$	d $[\mu m]$	bw $[g/m^2]$	S^b $[Nmm]$	E^b $[N/mm^2]$
0 rev PFI_{0bar}	0.544	156±1	84.8±0.4	0.408±0.011	1291±34
0 rev PFI_{75bar}	0.627	135±2	84.7±0.4	0.295±0.017	1435±82
0 rev PFI_{150bar}	0.676	126±2	85.4±0.1	0.295±0.020	1750±121
500 rev PFI_{0bar}	0.592	146±2	86.4±0.2	0.516±0.024	1990±93
500 rev PFI_{75bar}	0.705	124±2	87.3±0.5	0.401±0.010	2537±61
500 rev PFI_{150bar}	0.741	118±2	87.7±0.3	0.361±0.010	2613±74
1000 rev PFI_{0bar}	0.630	135±1	84.9±0.4	0.510±0.008	2508±41
1000 rev PFI_{75bar}	0.729	117±1	84.9±0.3	0.388±0.002	2931±15
1000 rev PFI_{150bar}	0.765	111±1	84.8±0.8	0.359±0.026	3165±231

for samples of beaten pulp tend to be slightly lower but no unambiguous trend can be observed. If splitting up the values for top side printed and bottom side printed, there is no systematic two-sidedness (Figure 52). The displayed values represent mean values calculated on the basis of 8 measurements per point (e.g. 500 rev PFI 0 bar).

However, it is obvious that a denser sheet implicates a more severe maximum curvature towards non-printed side. A direct correlation with correspondingly inferior bending stiffness is assumed. This assumption is emphasized by Figure 53a, plotting the maximum curvature over bending stiffness. Lowest curl values for each degree of refining are obtained with stiffer samples. The overall minimum, though, does not correspond to the stiffest paper, but to the thickest as illustrated in Figure 53b. Despite the extended CI's, the determining factor in this trial respecting the maximum curvature seems to be sheet thickness.

Due to the facts that density is directly derived from thickness and basis weight is in a comparable range, both Figure 37 and 53b display equal trends. The graphs are just mirrored around the vertical axis.

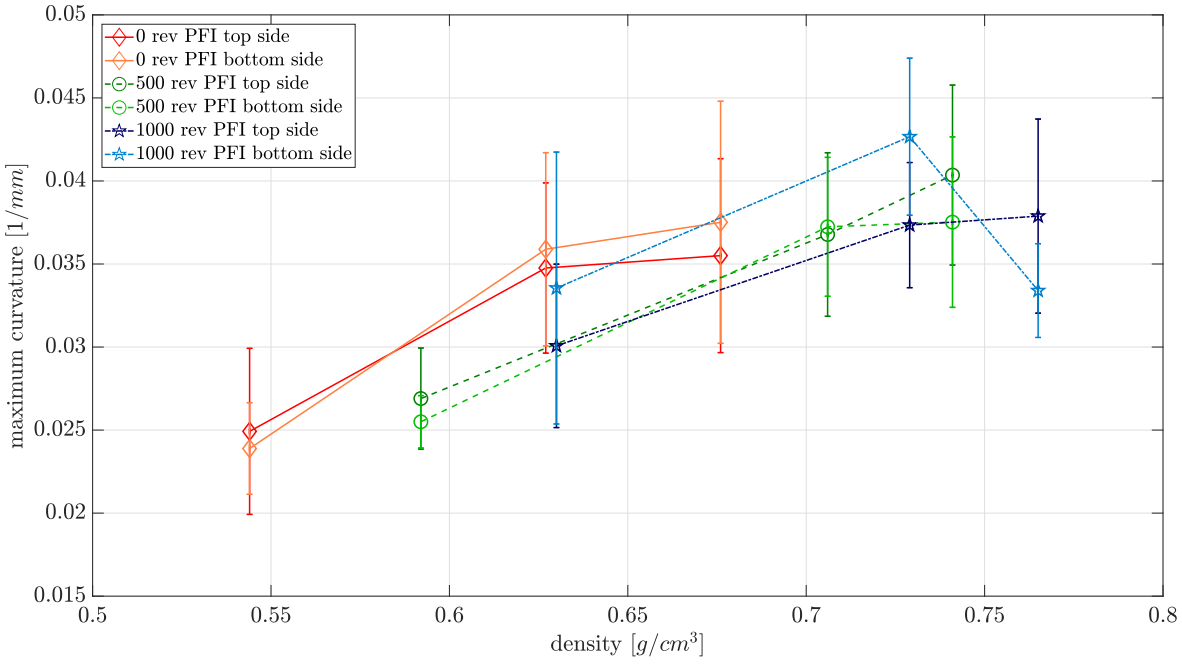

Figure 52. Maximum curvature over density for *Refining* trial.

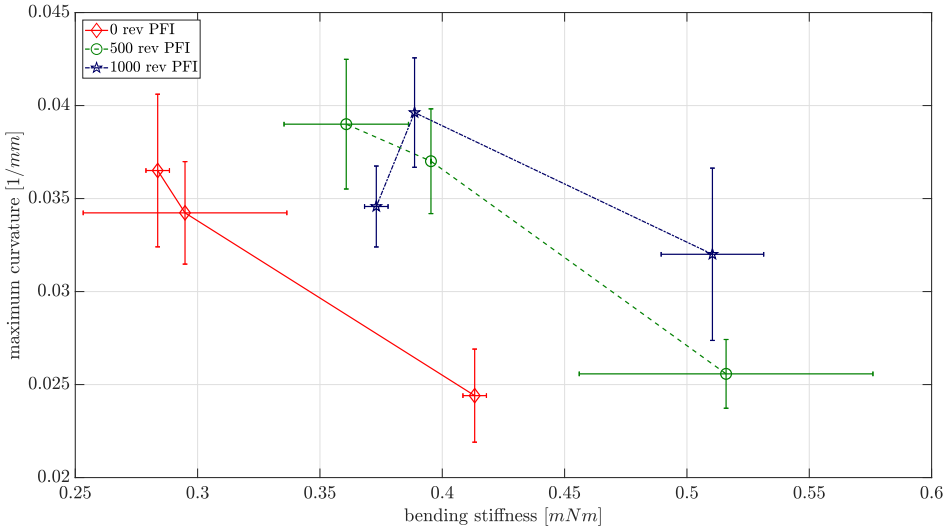

(a) Maximum curvature vs bending stiffness.

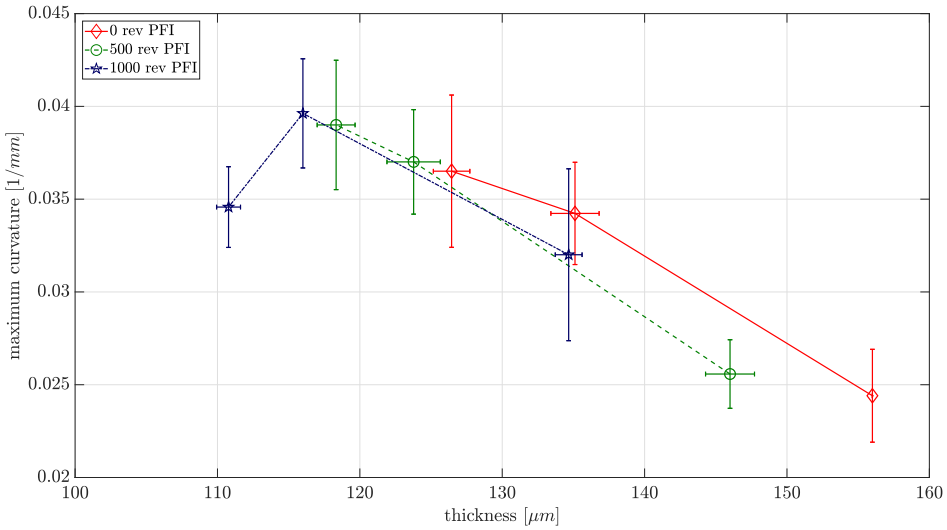

(b) Maximum curvature vs thickness.

Figure 53. Influence of bending stiffness and sheet thickness on the maximum curvature for the *Refining* trial.

The significant increase of modulus of elasticity is responsible for a noticeable higher bending stiffness of papers though sheet thickness simultaneously diminishes.

The higher density is reported to increase *hygro*expansion, but this effect is stronger in freely dried sheets than in restraint dried sheets [24]. However, the *hydro*expansion results discussed in section 4.7 show a decrease at higher degrees of refining.

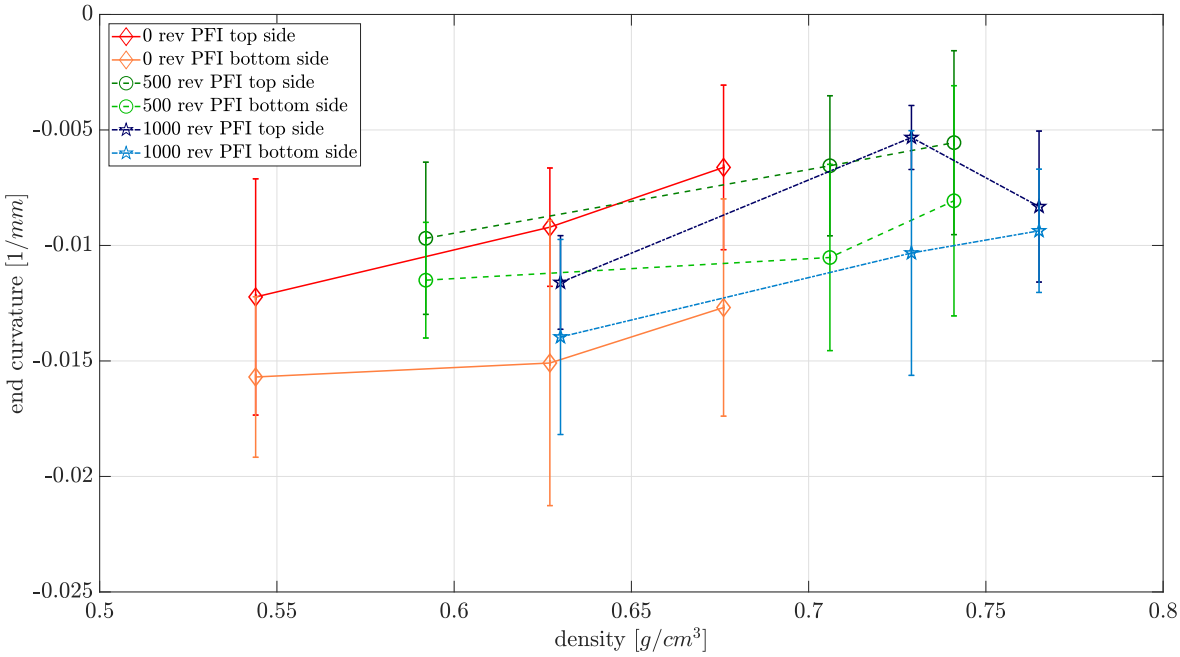

Figure 54. End curvature over density for *Refining* trial.

In contrast to the maximum curvature, the curl at the end of the measurement termed *end curvature* points to the opposite, the printed side. It develops during evaporation at ambient air and is measured approximately 3.5 minutes after applying ink. Figure 54 illustrates the end curvature over density, again split up for the two print modes. Here, a more negative value on the y-axis indicates a stronger end curvature towards printed side. To put it another way, a value close to 0 signifies a desired negligible curl.
In this trial, end curl reduces with higher density although the thickness influence seems to be less significant than in case of the maximum curl. The average end curvature is lower when printed on TS even if the confidence intervals overlap. Nevertheless, gaps between TS and BS printed tend to be more distinctive and systematic than in Figure 52. This occurring two-sidedness may be caused by an inhomogeneous distribution of (primary) fines. It is known, that sheets produced on the Rapid-Köthen Sheetformer exhibit a higher amount of fine material on the wire side (BS). Hence, top and bottom side might show differences in penetration speed, absorption and swelling behaviour.

According to this theory one would assume an increasing variation with higher levels of beating, due to the additional fines creation. In fact, neither larger gaps are observed nor refining has a detectable influence on the extent of end curvature. Actually, all specifications are in similar ranges. The discussion respecting fines are continued in section 4.4.

When looking at the initial curl creation rate in Figure 55, denser sheets deform quicker than voluminous papers. At equal density levels higher degrees of refining slow down the curl formation speed. Regarding TS and BS printed, the 0 rev PFI specimens show certain differences but with considerable deviations.

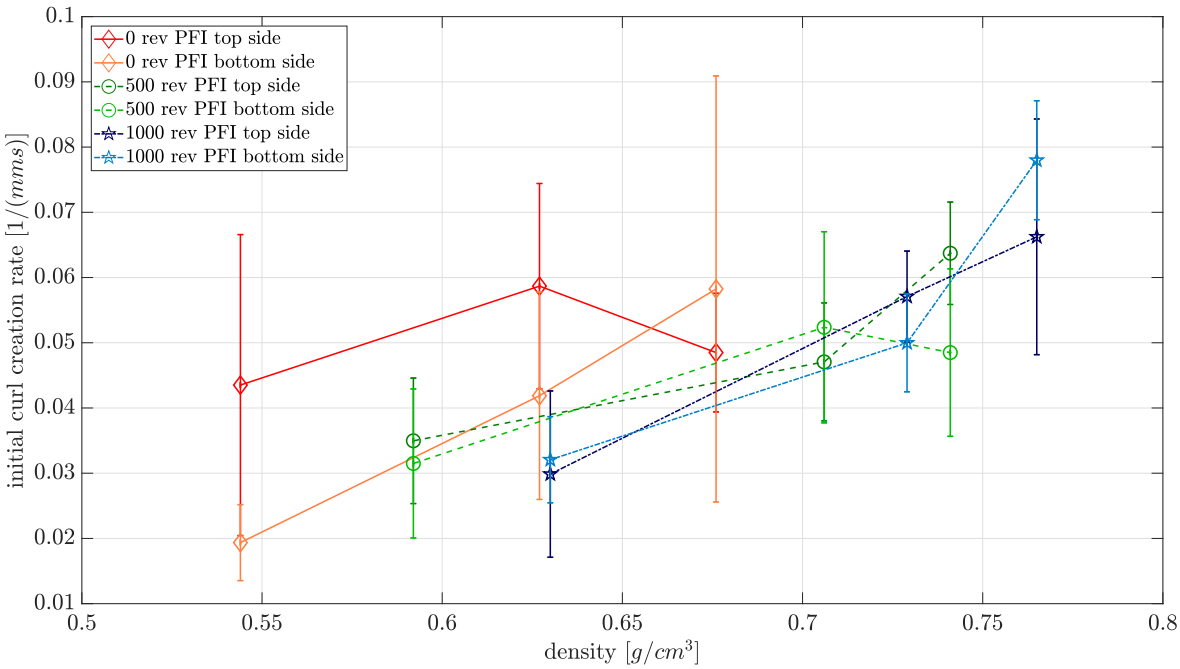

Figure 55. Initial curl rate over density for *Refining* trial.

Conclusion of *refining* trial

To conclude the observations of trial 1, it can be stated that a sheet specification with a more severe initial curl display a lower final curl to the other side. Additionally, results coincide with the viscoelastic curl theory (compare 2.2.2) that a curl towards the printed side remains after drying. Beating has a positive effect on the modulus of elasticity and reduces sheet thickness. Both parameters are related to an increased fiber flexibility and thus superior bonding capacity. An enhanced fiber-fiber bonding may restrict a severe paper deformation due to the hindered free swelling of fibers within the network. On the other hand, this lead to a build-up of internal stresses what may contribute to a stronger deformation. In the results of the curl tests, a tendency towards slower deformation and equal maximum curvature values at higher refining degrees is visible.

Although it is argued that refining generally increases fiber swelling due to internal fibrillation [36], this was not seen in other studies [37]. Also the hydroexpansion tests conducted within this work did not show any enhanced swelling but rather a lower expansion with higher degrees of refining.

Regarding strength and stiffness properties, the desired improvement was achieved, which may counteract the deformation. However, variation of levels of refining is not essentially high which impedes a plain conclusion of the overall effect of refining on curl.

4.2 Results for trial 2: BCTMP

In trial 2, four ratios of two different pulp sources were investigated upon their liquid-paper interactions. Eucalyptus kraft pulp was mixed with fractions of Aspen BCTMP. The determined mechanical properties are given in Table 10. Adding BCTMP to the furnish results in a slightly higher bending stiffness of the sheet, though thickness of wet pressed sheets even diminishes compared to pure kraft papers. Figure 56 displays the rise in modulus of elasticity concurrently with a progressively denser sheet. The slight difference between values shown in the graph and in the table is explained by the detection and replacement of outliers before plotting.

Table 10. Mechanical properties of papers of trial 2: BCTMP.

Specification	ρ $[g/cm^3]$	d $[\mu m]$	bw $[g/m^2]$	S^b $[Nmm]$	E^b $[N/mm^2]$	TI $[Nm/g]$	E^t $[N/mm^2]$
$0\%BCTMP_{0bar}$	0.562	145±2	81.5±0.1	0.434±0.039	1708±153	31.2±1.2	4783±631
$0\%BCTMP_{75bar}$	0.641	128±1	81.8±0.2	0.320±0.019	1845±111	32.2±5.1	6365±1324
$0\%BCTMP_{150bar}$	0.687	120±2	82.5±0.5	0.276±0.015	1909±106	45.0±2.9	5350±624
$10\%BCTMP_{0bar}$	0.557	145±3	80.6±0.4	0.393±0.012	1554±49	30.8±0.9	4455±539
$10\%BCTMP_{75bar}$	0.663	123±2	81.8±0.3	0.323±0.014	2062±92	37.0±1.2	4972±317
$10\%BCTMP_{150bar}$	0.716	117±2	83.8±0.5	0.287±0.017	2145±127	44.2±1.2	5705±635
$20\%BCTMP_{0bar}$	0.555	147±2	81.7±0.4	0.432±0.023	1626±86	30.3±0.9	4538±385
$20\%BCTMP_{75bar}$	0.661	124±1	81.8±0.2	0.326±0.007	2068±46	38.9±1.6	5056±549
$20\%BCTMP_{150bar}$	0.713	115±3	82.0±0.4	0.299±0.023	2357±184	45.3±1.9	5424±413
$40\%BCTMP_{0bar}$	0.542	147±2	79.7±0.6	0.390±0.017	1473±63	33.6±0.7	4510±270
$40\%BCTMP_{75bar}$	0.639	125±2	80.0±0.4	0.326±0.014	1994±88	41.1±1.0	5412±342
$40\%BCTMP_{150bar}$	0.691	116±1	80.2±0.4	0.289±0.016	2208±122	45.2±1.3	5656±760

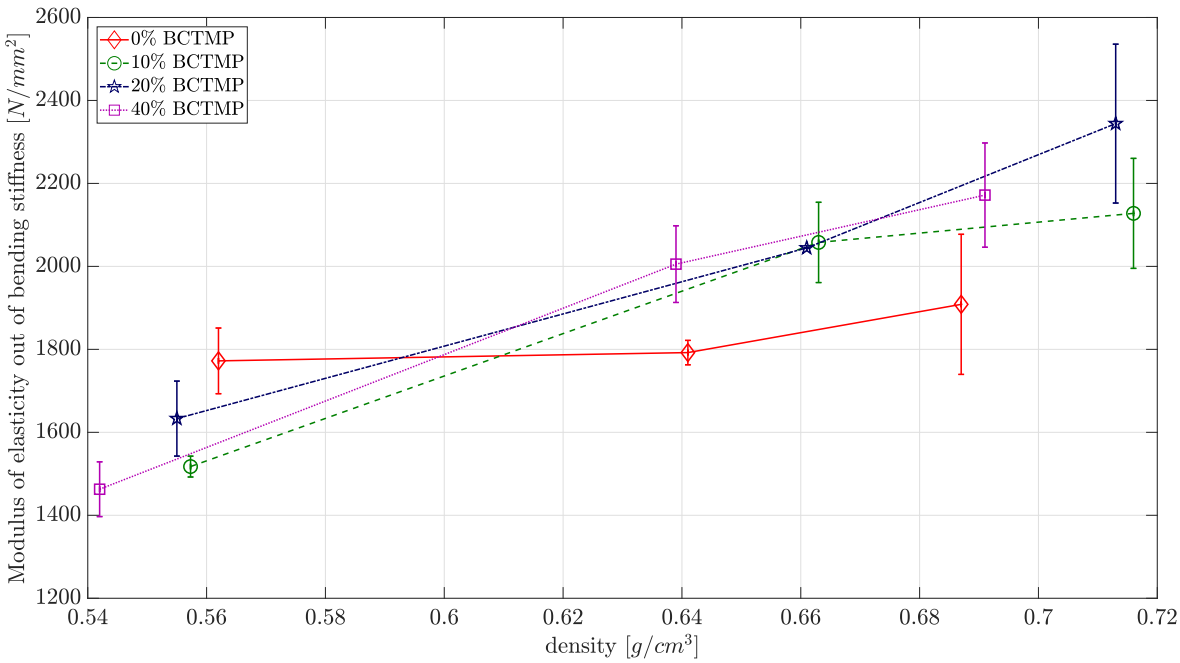

Figure 56. Modulus of elasticity over density for *BCTMP* trial.

In case of the wood-free paper, there is no significant increase in the modulus of elasticity observable. Thus, bending stiffness of the respective sheets declines further if thickness decreases. Despite the little higher stiffness values, the effect was expected to be more significant.

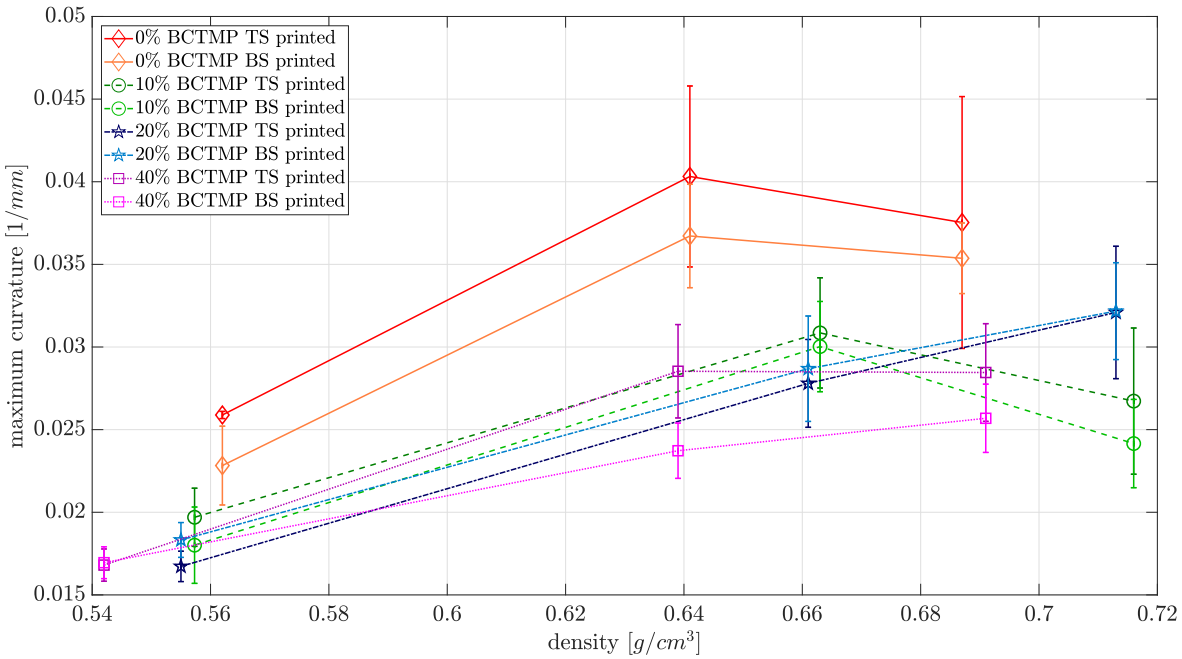

Figure 57. Maximum curvature over density for *BCTMP* trial.

It is remarkable that only the not pressed sheets show the anticipated density reduction. The remaining pressure points exhibit denser sheets if containing mechanical pulp. Particularly, the 10% and 20% fractions lead to thinner papers than the 0% and 40% BCTMP sheets.

4.2.1 Maximum, end curl and curl rate

It is clearly visible in Figure 57 that the mechanical pulp fractions inhibit an equally high maximum curl as samples out of 100% kraft pulp. The astonishing point here is the lacking difference between the actual BCTMP/Kraft pulp ratios. As long as sheets contain a small amount of mechanical pulp, the initial curl height decreases. Regarding higher densities, the behaviour resembles the observations of trial 1 detecting elevated maximum curl when printing on denser sheets. Even if the error bars overlap, there is a slight two-sidedness observable. On average, little higher maximum curvature values are reached if printed on TS.

In case of the end curvature in Figure 58, the TS printed samples tend to lead to a stronger end curl, though only the 40% BCTMP test point show unambiguous results. It is remarkable that the end curl of BCTMP sheets remains fairly constant with increasing density but is considerable compared to the pure chemical pulp sheets. Similar to the maximum curl, the absolute extent of back curl towards printed side seems to be only slightly depending on the effective BCTMP content. Mean values of the 10% fractions tend to be a bit lower but overall trends are valid for all mix ratios.

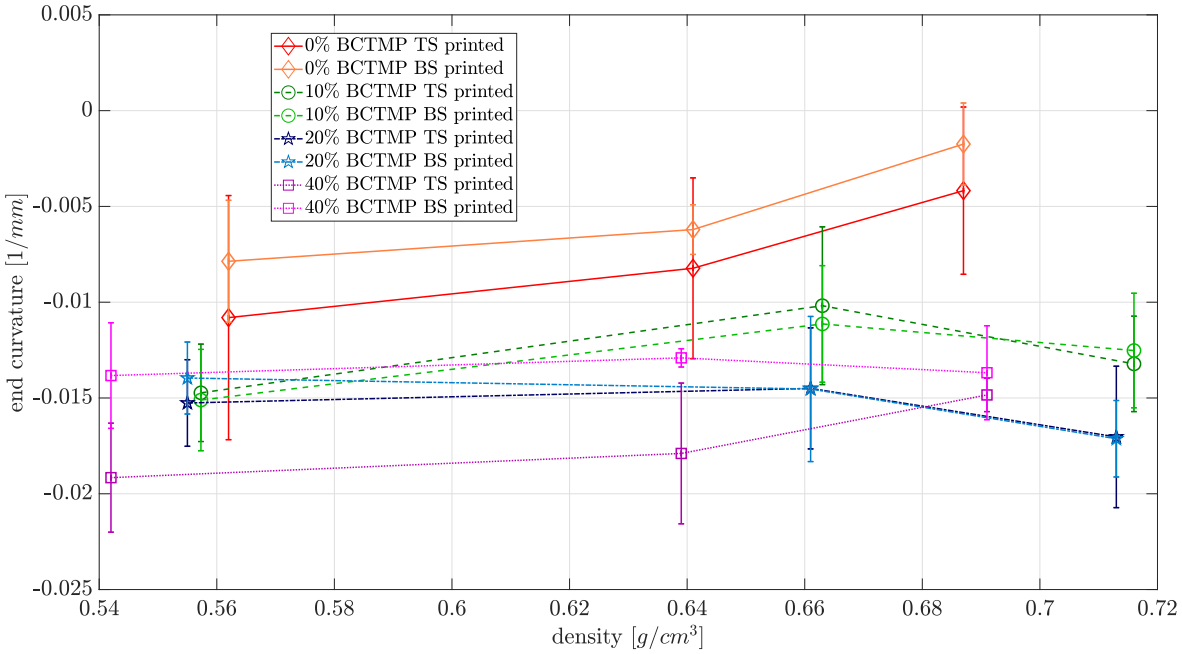

Figure 58. End curvature over density for *BCTMP* trial.

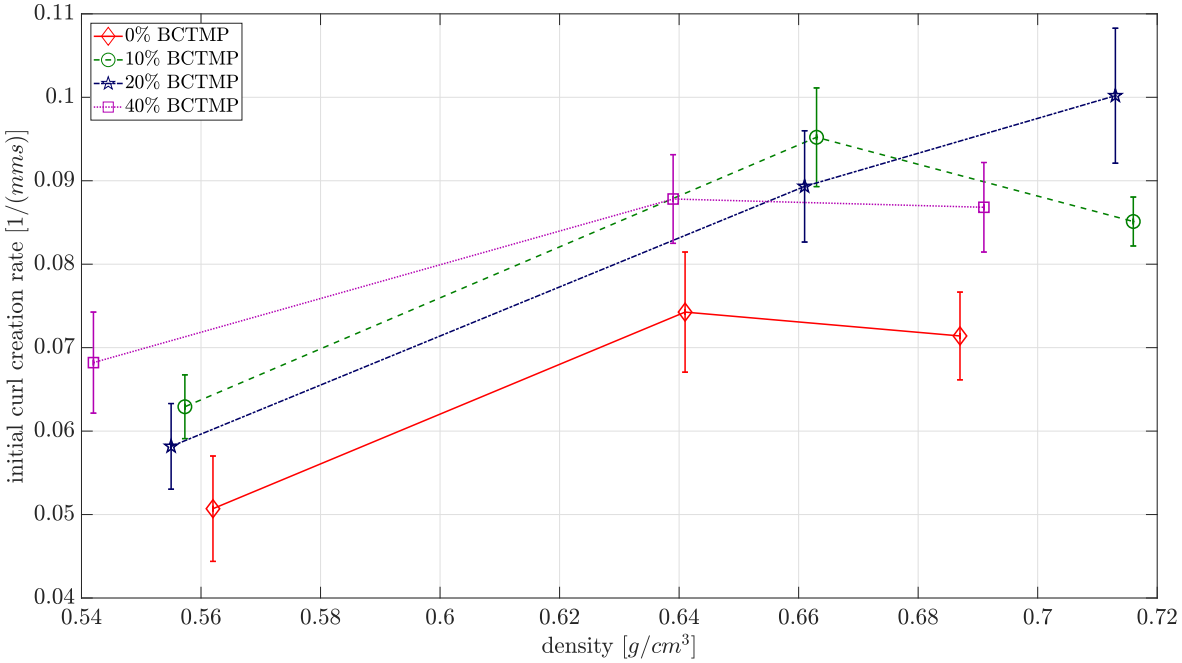

Figure 59. Initial curl creation rate over density for *BCTMP* trial.

Analogous results are obtained for the initial curl creation rate in Figure 59. The BCTMP sheets do not differ significantly among each other, whereas they all show a faster curl development. Equivalent correlations were found for the time constant $\tau_{curl\ creation}$. Two-sidedness was not considered in this case due to negligible variations.

Conclusion of *BCTMP* trial

It is worth mentioning that refining of this trial was not conducted properly resulting in reduced stiffness and strength properties as well as more voluminous sheets. Nevertheless, the mean curvature values of the 1000 rev PFI sheets and the corresponding 0% BCTMP samples are in a comparable range of 0.025 to 0.042 1/mm for maximum curvature and -0.013 to -0.003 1/mm for end curvature.

Although BCTMP fractions induce a significant increase in curl creation rate of the respective sheets, simultaneously a lower initial (maximum) curl is observed. On the other hand, the ensuing backwards (end) curl turns out more severe than for wood-free paper. The percentage of BCTMP seems to be irrelevant regarding both mechanical properties and deformation behaviour. To improve stiffness values a reasonable content would be 20% BCTMP.

A crucial point is the fact that not pressed sheets at densities between 0.54-0.56 g/cm^3 already show the same trends regarding maximum curvature and end curvature, though the values of modulus of elasticity and bending stiffness are comparable or even lower for BCTMP sheets compared to pure chemical pulp sheets. Thus, the influence of the modulus of elasticity is not the decisive factor for the curl development.

Swelling of mechanical pulp is restricted by the hydrophobic lignin network and the more intact fiber wall structure [43, 44]. Additionally, due to missing information about the drying history of the BCTMP, hornification can not be excluded as a possible influence. The irreversible crosslinking of pulp fibres by a hydrogen bonding formation during water removal decreases the prospective swelling ability [10].

As further shown, sheets with BCTMP content expand on average to a higher extent when submerging into ink than papers out of kraft pulp. Though it is not very significant considering the CIs, a lower swelling is not detected there.

4.3 Results for trial 3: PCC

Within trial 3, handsheets with filler content at two levels were manufactured and subsequently tested on the pilot test setups at Océ Venlo. Mechanical properties were additionally measured and are collected in Table 11. Density, tensile and stiffness properties diminish due to reduced interfiber bondings and the spacing effect of the calcium carbonate particles. The influence on the modulus of elasticity calculated out of bending stiffness is depicted in Figure 60. Sheets with 20% filler content only achieve half of the value obtained by papers without PCC. This remarkable decline leads to a significant lower bending stiffness regardless of a slight increase in sheet thickness.

Table 11. Mechanical properties of papers of trial 3: PCC.

Specification	ρ $[g/cm^3]$	d $[\mu m]$	bw $[g/m^2]$	S^b $[Nmm]$	E^b $[N/mm^2]$	TI $[Nm/g]$	E^t $[N/mm^2]$
0% PCC_{0bar}	0.614	131±2	80.6±1.2	0.461±0.032	2447±169	43.1±3.0	5170±550
0% PCC_{75bar}	0.719	112±2	80.9±0.4	0.351±0.012	2962±104	52.6±1.2	6143±611
0% PCC_{150bar}	0.769	105±1	80.6±0.2	0.299±0.020	3112±210	64.4±1.7	6697±485
10% PCC_{0bar}	0.576	138±1	79.5±0.6	0.371±0.010	1691±46	28.2±1.9	4320±291
10% PCC_{75bar}	0.690	114±2	78.6±1.1	0.250±0.028	2032±228	31.1±3.8	5950±1903
10% PCC_{150bar}	0.737	108±1	79.6±0.7	0.251±0.011	2398±101	37.3±5.6	6432±1524
20% PCC_{0bar}	0.553	145±3	79.9±0.5	0.304±0.010	1210±41	18.2±0.8	3423±935
20% PCC_{75bar}	0.676	115±6	77.8±1.8	0.194±0.025	1529±194	22.1±0.5	3815±222
20% PCC_{150bar}	0.719	107±5	76.7±3.6	0.154±0.025	1516±249	23.1±1.9	4370±557

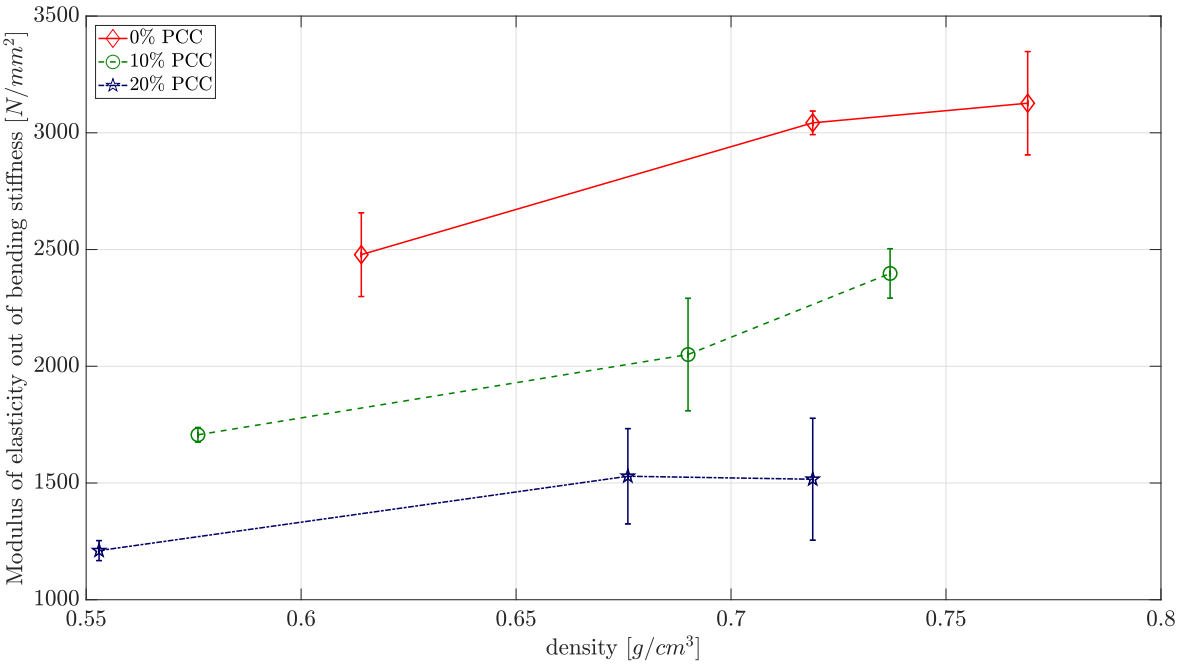

Figure 60. Modulus of elasticity over density for *PCC* trial.

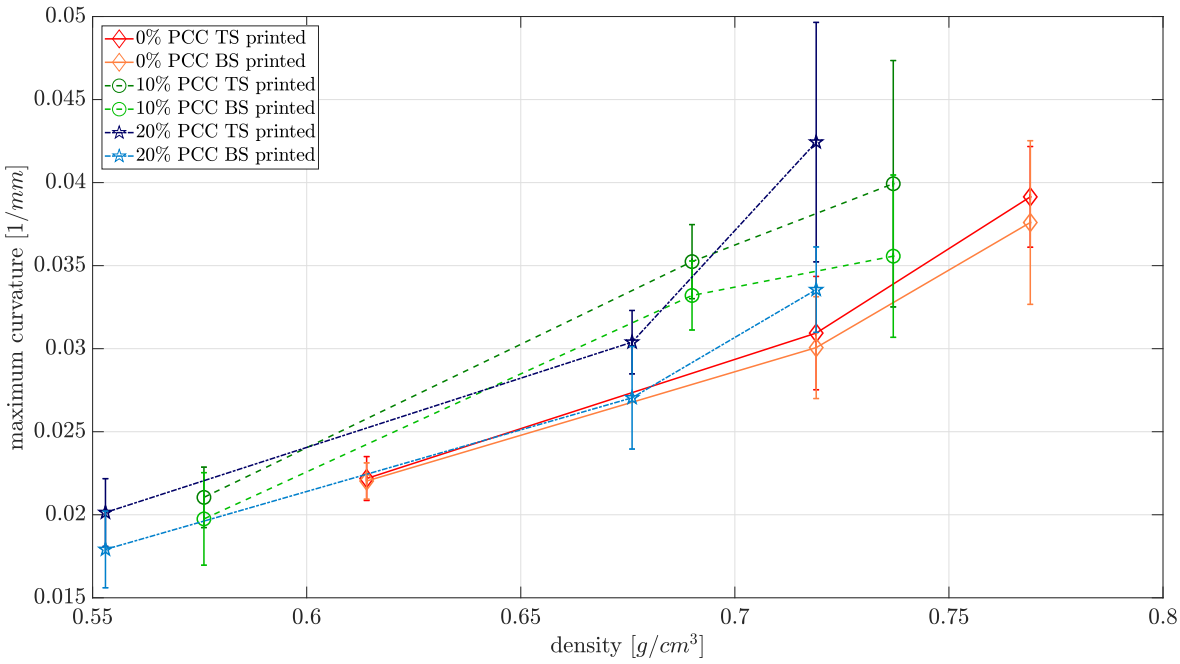

Figure 61. Maximum curvature over density for *PCC* trial.

4.3.1 Maximum, end curl and curl rate

Due to literature addressing structural curl, a distinctive two-sidedness in curvature values for filled papers was expected. Actually, the average difference between TS and BS printed is increasing with higher PCC content, shown in Figure 61. Though confidence intervals overlap, the tendency is more significant than in previous trials. The gap further spreads apart in stronger pressed sheets. If printed on BS, maximum curvature values are similar to the zero point with one exception, the 75 bar pressed 10% PCC sheets. However, printing on TS provokes an augmented maximum curl towards non-printed side.

Focusing on the chart of end curl over density in Figure 62, similar relations are detectable. First, the back curl of BS printed samples is less severe compared to TS print mode. Even the error bars do not overlap in case of sheets which are not pressed. Curiously, here the zero point exhibits an intensive end curvature which is higher than observed in previous trials. Mechanical properties, however, are comparable to the 1000 rev PFI specification of trial 1.

The initial curl creation rate for the current trial is shown in Figure 63. Analogous to the diagrams with respective curvature values, a certain two-sidedness is also seen in this plot. TS printed samples of filled papers display a higher initial speed of curl formation. Elevated PCC contents seem to slow down the curl development, although equal values are reached at higher densities if printed on TS.

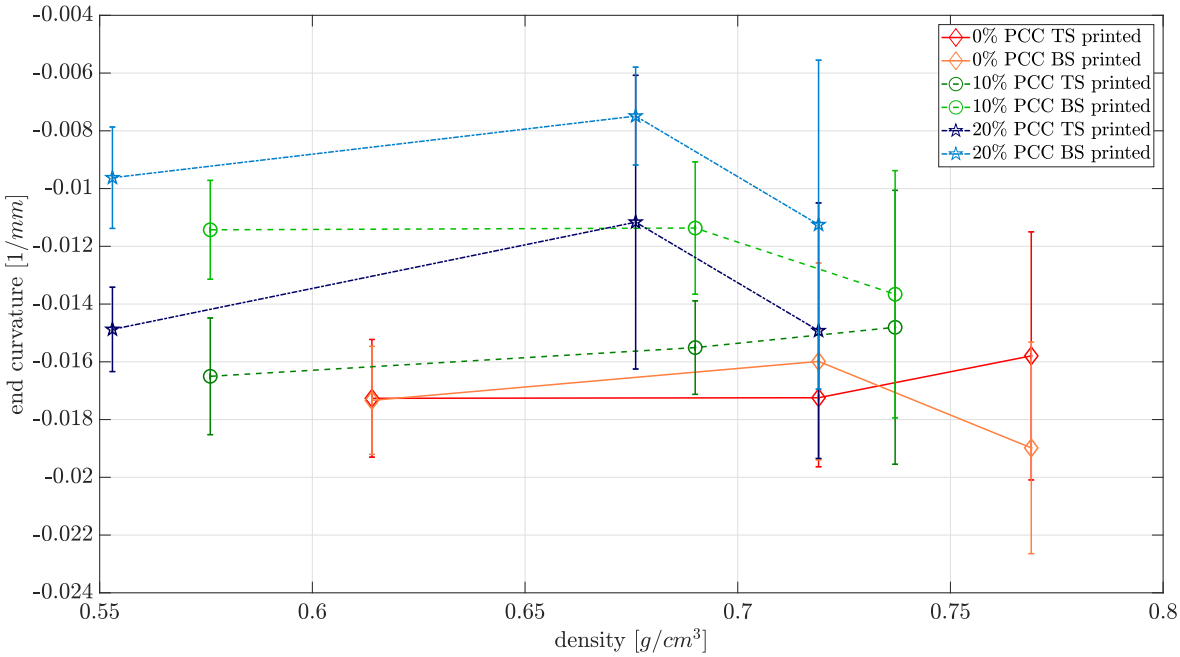

Figure 62. End curvature over density for *PCC* trial.

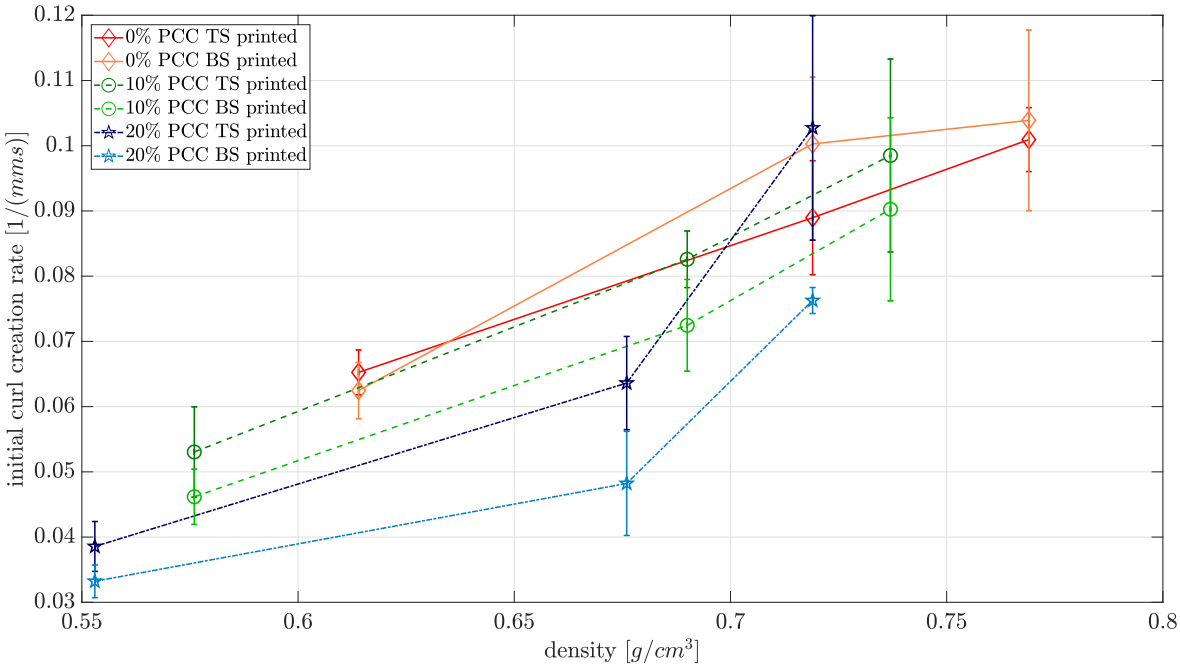

Figure 63. Initial curl creation rate over density for *PCC* trial.

Conclusion of *PCC* trial

Filler and fine material tend to arrange on the wire side (BS) of handsheets. A consequently closer structure is obtained due to filling up of free voids among the fibers. On the other hand, interfiber bondings are impaired by fillers. If liquid is now applied onto BS, penetration into the network may be slower than if printed on TS. Penetration depth and liquid uptake might be lower because of more water being evaporated. Assuming this, the resistance counteracting a curl formation on the not wetted side is relatively higher due to a lower filler amount and thus stiffer structure. As a consequence, a minor initial curl develops and the end curvature declines likewise because of a lower overexpansion of the non-printed side (compare curl theory 2.2). In contrast, if printing on TS penetration speed is comparable to non filled papers and the maximum curvature reaches even higher levels. This may be explained by the overall diminishing sheet stiffness. A stronger maximum curl consequently provokes a subsequent stronger back curl. However, the plain paper shows a more critical end curl than the top side printed filled papers. It is assumed, that the moment triggering back curl for PCC sheets is weaker as a result of the reduced stiffness properties on the not wetted filler containing side.

In Figure 64 the rough assumption of the filler impact on curl is depicted graphically.

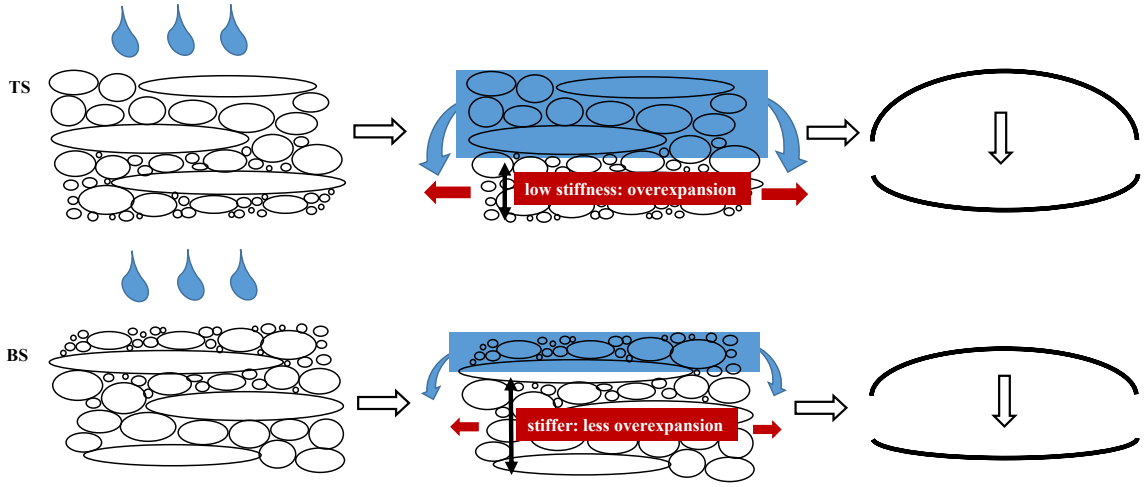

Figure 64. Assumption of filler influence on curl.

4.4 Results for trial 4: Fines

In the fourth trial, sheets with an additional amount of secondary fines were manufactured. Table 12 includes the measured mechanical properties of sheets for the respective zero point, 5% fines addition and 15% fines addition to the furnish. Corresponding to literature [13], an increasing fines content results in denser sheets with improved stiffness and strength properties, discussed in 2.1.2. The development regarding modulus of elasticity is shown in Figure 65. By adding 15 wt% secondary fines relative pulp weight to the furnish, the modulus of elasticity gains about 600 N/mm^2 on average. Already 5% fines have a positive outcome regarding enhancement of the modulus of elasticity. However, bending stiffness declines due to a decrease in sheet thickness. Giner Tovar et al. [39] received similar results.

Table 12. Mechanical properties of papers of trial 4: Fines.

Specification	ρ $[g/cm^3]$	d $[\mu m]$	bw $[g/m^2]$	S^b $[Nmm]$	E^b $[N/mm^2]$	TI $[Nm/g]$	E^t $[N/mm^2]$
0% $Fines_{0bar}$	0.618	130±2	80.5±0.5	0.438±0.021	2385±113	51.5±1.4	5278±384
0% $Fines_{75bar}$	0.720	111±1	79.7±0.7	0.334±0.011	2957±99	56.9±3.0	5928±500
0% $Fines_{150bar}$	0.756	108±4	81.4±0.3	0.316±0.021	3034±202	60.2±3.4	6493±522
5% $Fines_{0bar}$	0.661	122±4	80.4±2.0	0.432±0.025	2887±169	54.9±4.9	5438±661
5% $Fines_{75bar}$	0.762	106±2	81.1±0.7	0.356±0.017	3548±167	61.0±5.0	6438±817
5% $Fines_{150bar}$	0.787	102±1	80.3±0.2	0.275±0.018	3099±208	62.9±3.2	6524±484
15% $Fines_{0bar}$	0.688	116±5	80.0±0.2	0.411±0.031	3146±237	61.4±6.4	5823±420
15% $Fines_{75bar}$	0.766	105±6	80.5±0.4	0.369±0.065	3817±672	69.2±9.3	6212±747
15% $Fines_{150bar}$	0.813	98±3	79.5±1.1	0.303±0.011	3902±136	79.3±4.9	7675±610

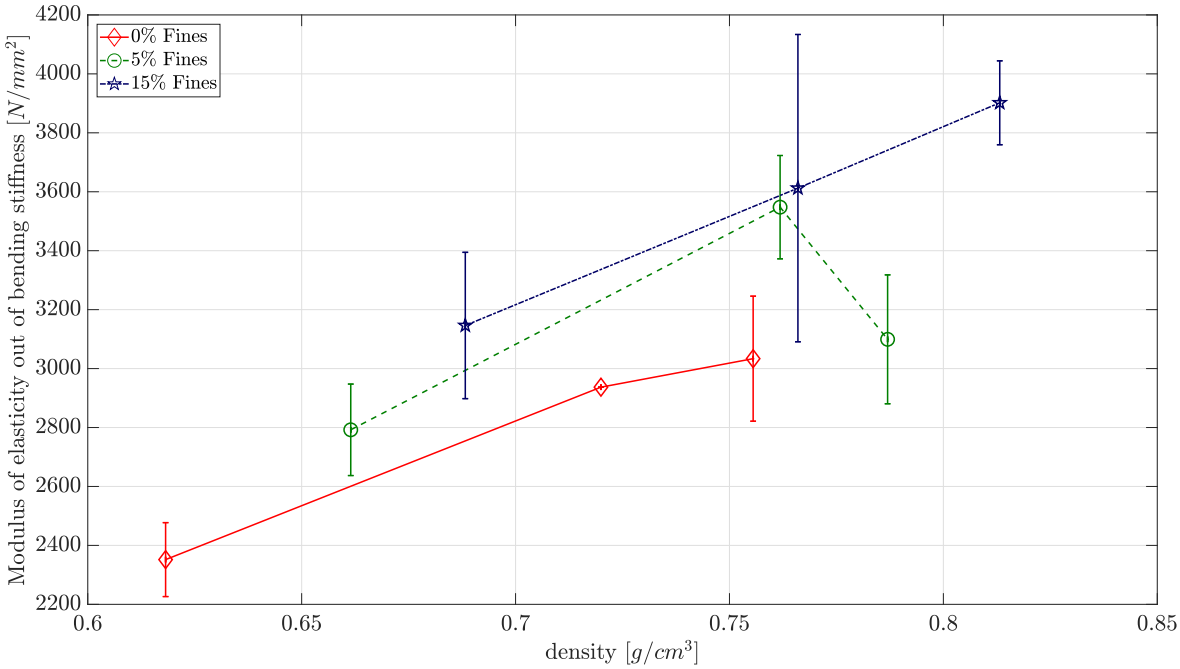

Figure 65. Modulus of elasticity over density for *Fines* trial.

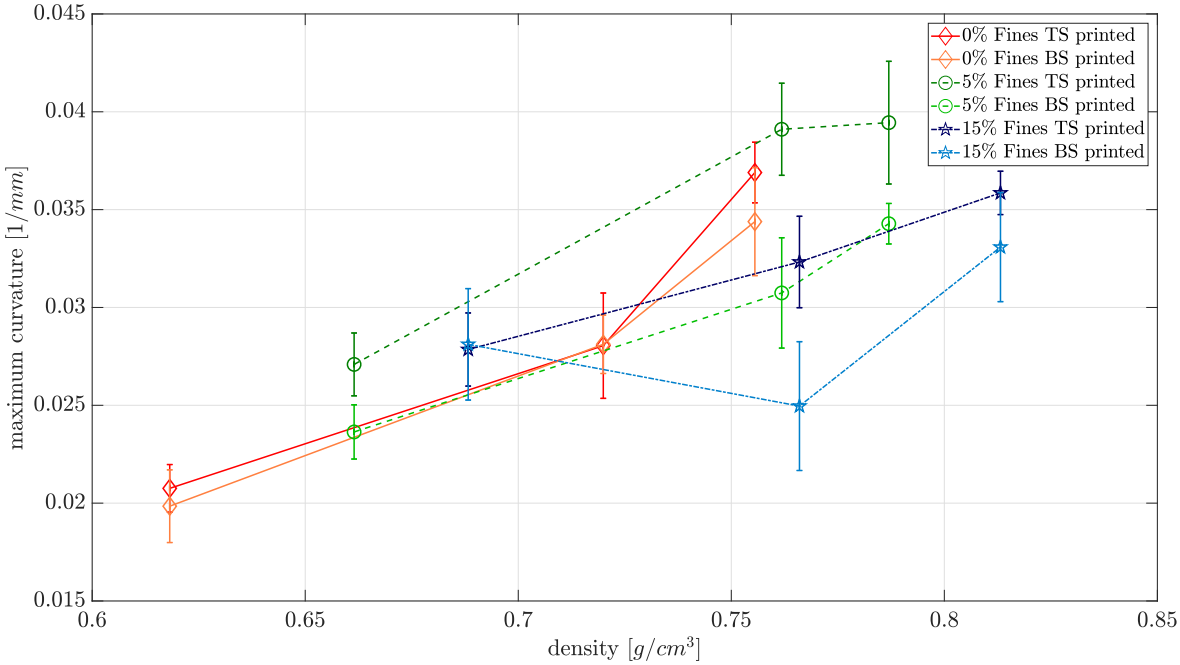

Figure 66. Maximum curvature over density for *Fines* trial.

4.4.1 Maximum, end curl and curl rate

According to the *PCC* trial in 4.3, a noticeable two-sidedness was anticipated when testing sheets with additional fines content on the curl setup. The observations regarding maximum curvature in Figure 66 essentially coincide with that expectations. Mean values at every density level except of the not pressed 15% fines sheets show a distinctive variation of achieved curl heights. In contrast, conventional handsheets deform almost equally, irrelevant if printed on TS or BS. Top side printed samples of 5% fines sheets obtain higher values than the zero point, whereas the 15% fines fraction show a slightly different behaviour. The increase of curvature provoked by a higher density is lower than for 0% and 5% fines. Consequently, their average values, both for TS and BS printing mode, at densities over 0.75 g/cm^3 are beneath the previously mentioned specimens.

In case of end curvature, sheets with elevated fines content induce a considerable back curl at nearly similar absolute values as for the maximum curvature. Although CI of the 15% fines fractions are occasionally extraordinary high, a mean value under -0.02 1/mm was not detected in any other trial before. In addition, here BS printed specimens lead to a stronger curl towards non-printed side which is contrary to the observations of the *PCC* trial. As seen previously, density contribution is minor compared to the maximum curl development.

Results for the initial curl creation rate in Figure 68 reflect a decelerating curl formation with a progressive fines content, although the second values of the zero point (75 bar pressed) deviate somehow. The variation regarding 15% fines sheets is expanded which complicates a statistically significant conclusion.

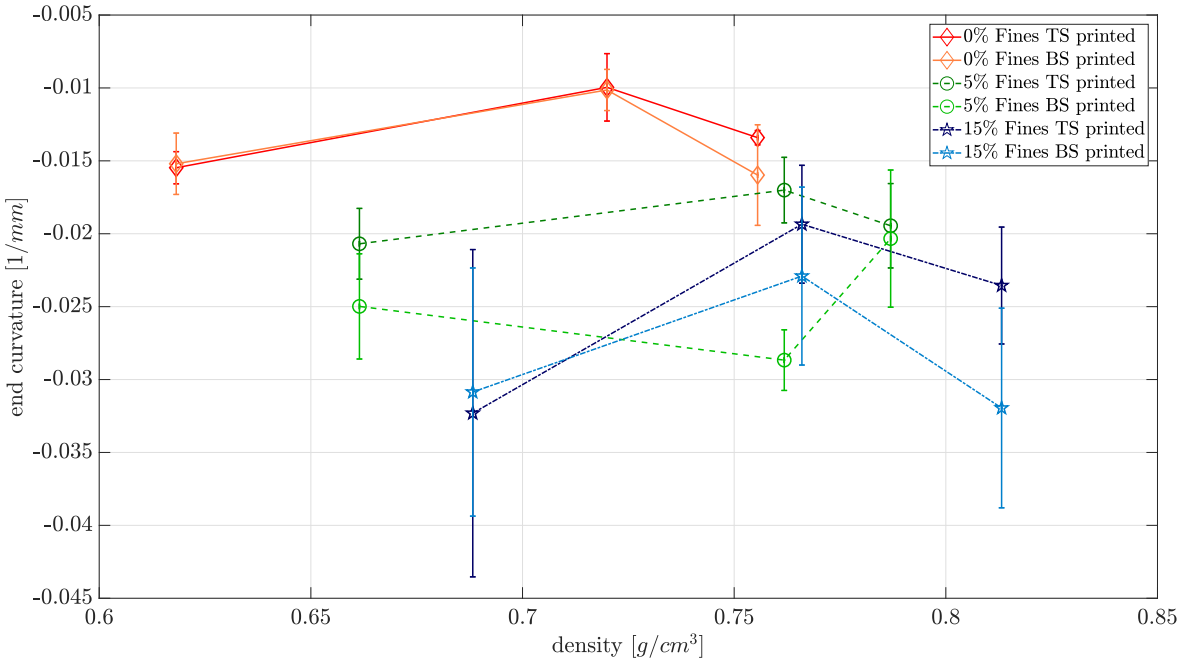

Figure 67. End curvature over density for *Fines* trial.

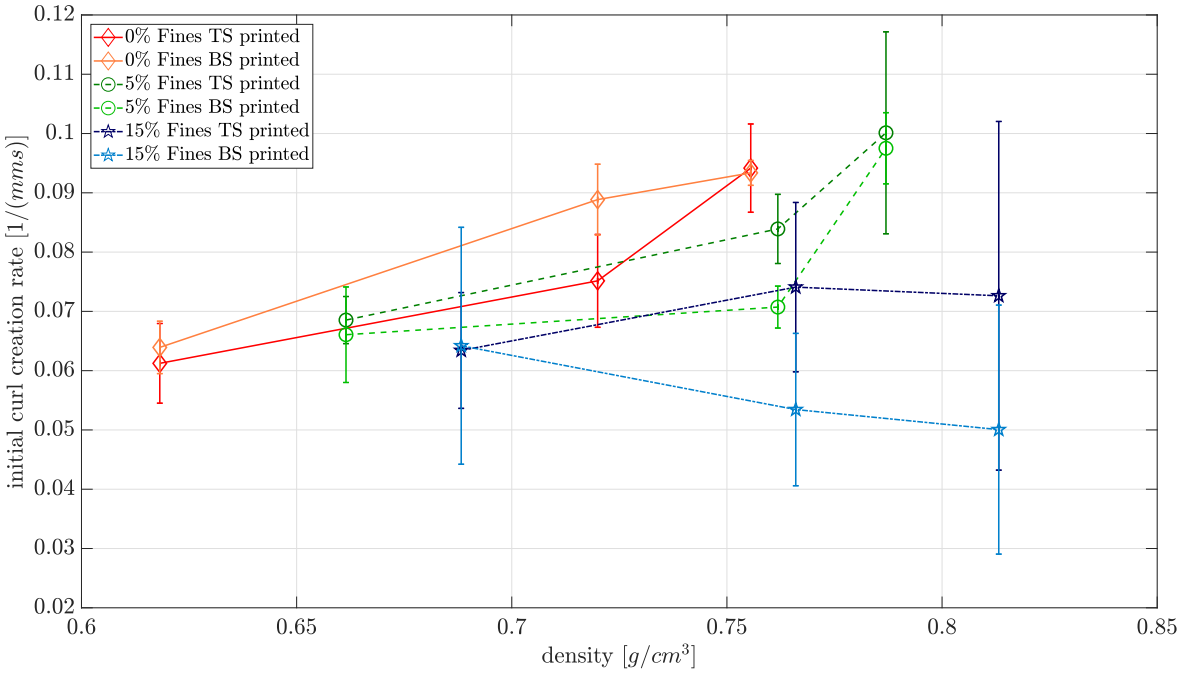

Figure 68. Initial curl creation rate over density for *Fines* trial.

Conclusion of *Fines* trial

As discussed in 2.1.2 and shown in Table 12, addition of fine material yields a denser sheet with simultaneous improvements in strength and stiffness properties. Fibrillar secondary fines have a much higher swelling capacity than fibers due to an outstanding surface area with high surface charges [45]. It is assumed, that relatively more fines are located on the BS of the sheets as a result of the drainage flow entraining the fine material until it is trapped within the fiber mat. Due to a lower porosity of the sheets, liquid penetration might be slower, especially if printed on BS. The mentioned higher swelling capacity of fines is not necessarily leading to an extended deformation. Enhanced fiber-fiber bondings and the consequently hindered penetration into the fiber bonding regions might also reduce the overall swelling of the network. The maximum curvature if printed on TS is subsequently higher due to a less compact network compared to the BS and minor hindering effects of swelling.

However, a higher swelling on the printed side induce a serious overexpansion on the not wetted side according to Uesaka [27]. Subsequent to the evaporation of liquid, a considerable back curl towards printed side occurs as consequence of the irreversible stretching of the corresponding side. This theory would explain the findings of a more severe end curvature.

Another possible explanation for the curl could be an irreversible shrinkage after drying of the printed side. Due to minor changes regarding dimensions and stiffness on the not wetted side, a final curl towards the printed side develops.

To conclude this trial, it is conceivable that multiple effects contribute to the obtained outcomes and further investigations are inevitable. These may also include studies on an unbalanced release of dried-in strains generated during the restrained sheet drying process. If dried-in strains are set free due to wetting or high relative humidity, paper is able to shrink to a higher extent. One side of the sheet might be more compressed after drying than the opposite side resulting in a curl towards the side with a higher release of dried-in strains.

Various studies including the recent work of Harter [1] have shown, that dried-in strains are already released upon an increase of relative humidity. The arising question is if one-sided wetting provokes an inhomogeneous release over the z-direction.

4.5 Results for trial 5: Sizing

The main objective of this trial was to study the influence of an improved water repellency on the curl formation. Two degrees of sizing were investigated, using the non sized zero point as reference. $Cobb_{60}$ values between 27 and 52 g/m^2 were measured for sheets with a sizing amount of 0.05% AKD. For 0.1% AKD values of 22 to 24 g/m^2 were obtained. The lower sized papers showed a more effective hydrophobisation on the bottom side, whereas high sized sheets did not show significant variations.

The respective mechanical properties of the manufactured handsheets are listed in Table 13. It is unambiguously seen that sizing do not deteriorate paper strength or stiffness. Sheets of equal pressing levels show comparable properties.

Table 13. Mechanical properties of papers of trial 5: Sizing.

Specification	ρ $[g/cm^3]$	d $[\mu m]$	bw $[g/m^2]$	S^b $[Nmm]$	E^b $[N/mm^2]$	TI $[Nm/g]$	E^t $[N/mm^2]$
$0\%AKD_{0bar}$	0.620	131±3	80.9±0.4	0.438±0.030	2367±162	48.4±2.7	5655±386
$0\%AKD_{75bar}$	0.728	110±2	80.2±0.6	0.336±0.019	3009±167	58.2±3.1	6126±381
$0\%AKD_{150bar}$	0.769	105±3	80.4±0.3	0.289±0.019	3035±198	67.7±2.4	6997±644
$0.05\%AKD_{0bar}$	0.620	131±2	81.1±0.2	0.452±0.028	2416±151	45.8±3.7	5402±539
$0.05\%AKD_{75bar}$	0.724	111±4	80.7±0.6	0.345±0.017	2989±149	55.5±2.9	6263±504
$0.05\%AKD_{150bar}$	0.774	105±1	81.2±0.2	0.313±0.015	3254±160	62.6±4.0	6663±848
$0.1\%AKD_{0bar}$	0.612	132±1	81.0±0.3	0.446±0.005	2308±28	48.2±2.4	5743±514
$0.1\%AKD_{75bar}$	0.737	109±2	80.1±0.6	0.338±0.021	3157±196	54.4±3.8	6749±822
$0.1\%AKD_{150bar}$	0.786	102±2	80.4±0.4	0.311±0.014	3482±160	59.5±5.0	6944±590

4.5.1 Maximum, end curl and curl rate

The curves in Figure 69 demonstrate a clear tendency of a lower maximum curvature for sized papers compared to sheets without a previous hydrophobisation. Within the individual specifications, some points show a measurable variation among TS and BS printed. In case of the lower sized sheets, this is explainable by the different $Cobb_{60}$ values on the corresponding sides. However, high sized papers with 0.1% AKD do not show any $Cobb_{60}$ two-sidedness (compare Table 4), though it would be expected considering the two-sidedness detected in Figure 69-71.

An overall trend towards a slightly lower end curvature for sized papers is detectable in Figure 70. Similar to previous trials, sheet density plays no role regarding this KPI.

According to the expectations, a remarkably diminished curl rate for AKD sized papers is found in Figure 71. High sized sheets only reach about half of the value obtained by the conventional handsheets. It is straightforward that the sizing inhibits a fast liquid uptake into the paper structure and thus contributes to a reduced curl formation regarding both maximum and end curl.

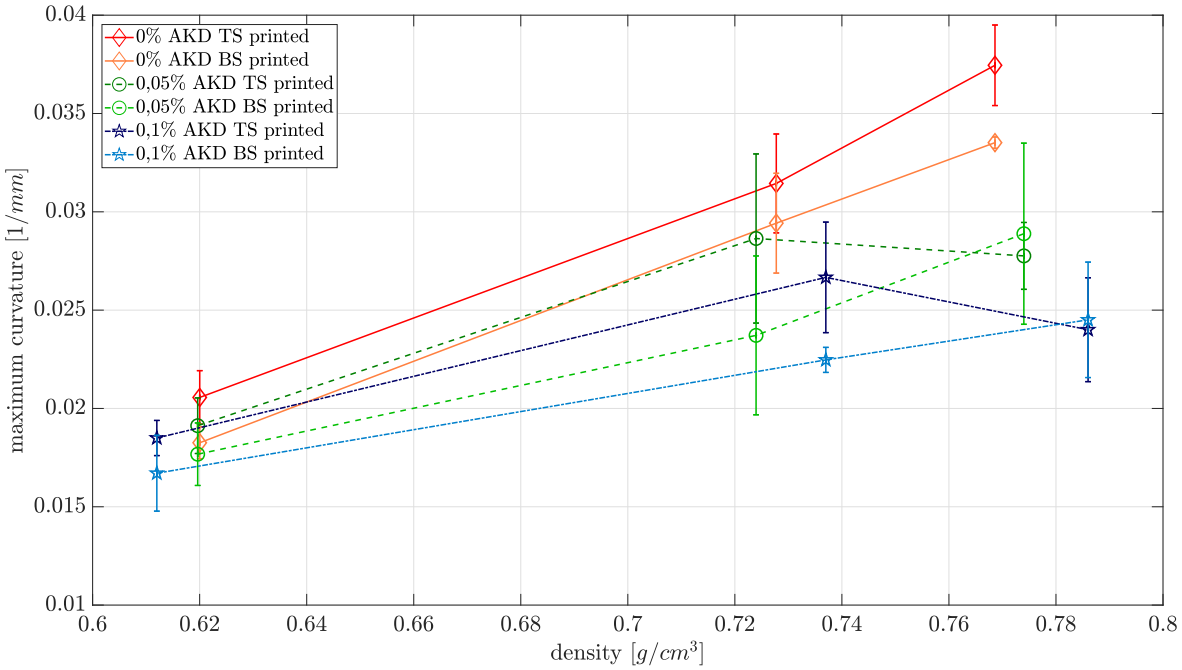

Figure 69. Maximum curvature over density for *Sizing* trial.

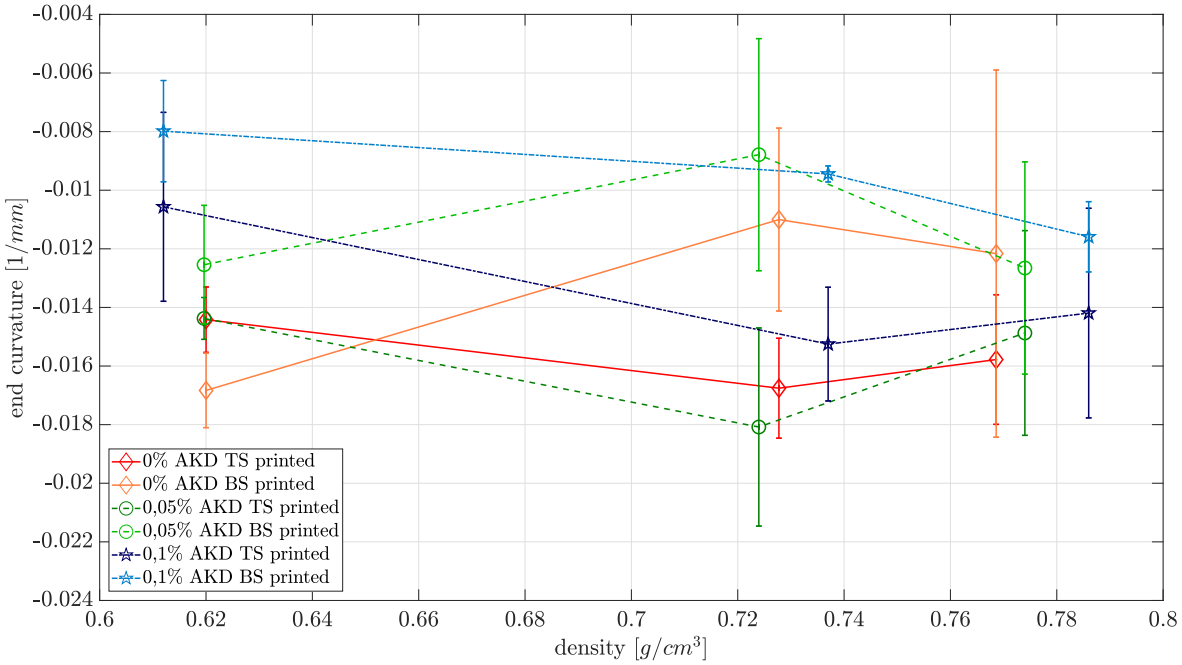

Figure 70. End curvature over density for *Sizing* trial.

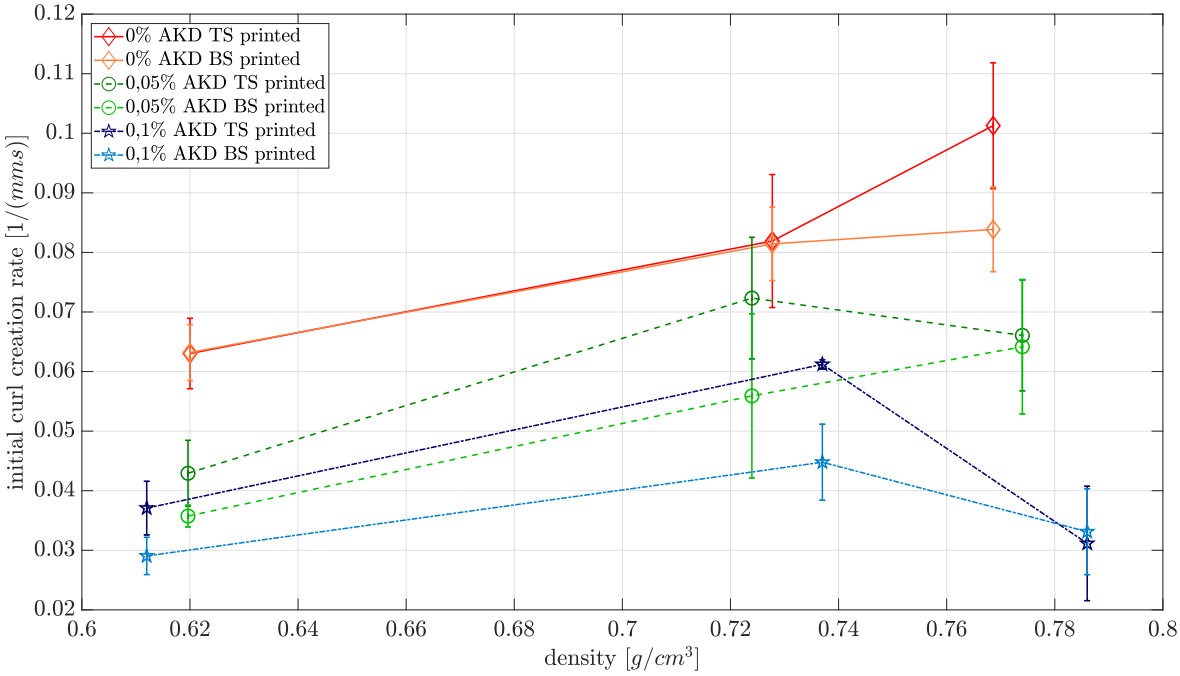

Figure 71. Initial curl creation rate over density for *Sizing* trial.

4.5.2 Hydroexpansion in ink vs deionised water

Within the current work, wet expansion was usually investigated by submerging paper samples into the identical ink as used in the curl test setup. The AKD sized papers were additionally exposed to deionised water. Figure 72 shows the final strain after 20 minutes of submerging into the respective liquid. The bars represent mean values of a fitted density interval between 0.62 and 0.72 g/cm^3. Fitting method was explained in 3.4. It has to be mentioned that the fit in this case is based on six values, two for each pressure point (e.g. 0.1% AKD 75 bar). Variations over density are quite low and thus also the CIs, considering the few test points.

Hydroexpansion of samples is reduced with higher degrees of sizing. It is further shown, that the AKD sized samples expand to a lower extent in water than in ink. Regarding the speed of this dimensional change illustrated in Figure 73, unsized papers expand to one order of magnitude faster in deionised water compared to ink. This is remarkable, in view of the fact that sized papers do not show this behaviour.

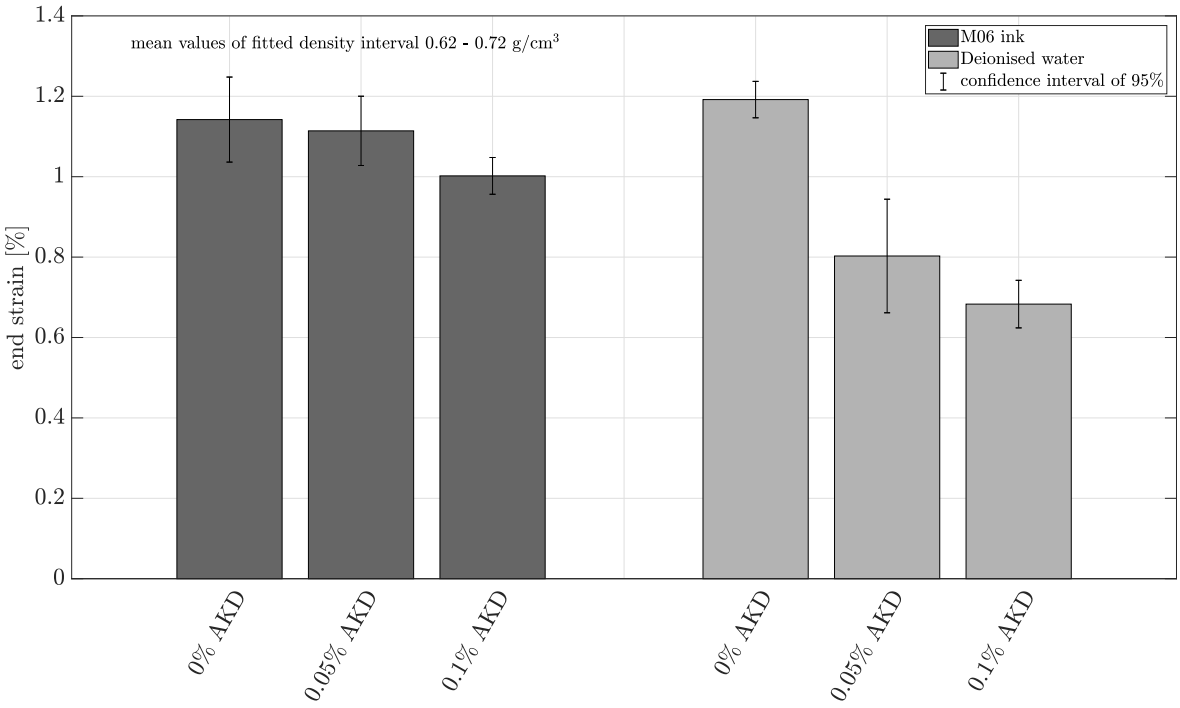

Figure 72. Comparison of wet expansion in ink vs deionised water for *Sizing* trial.

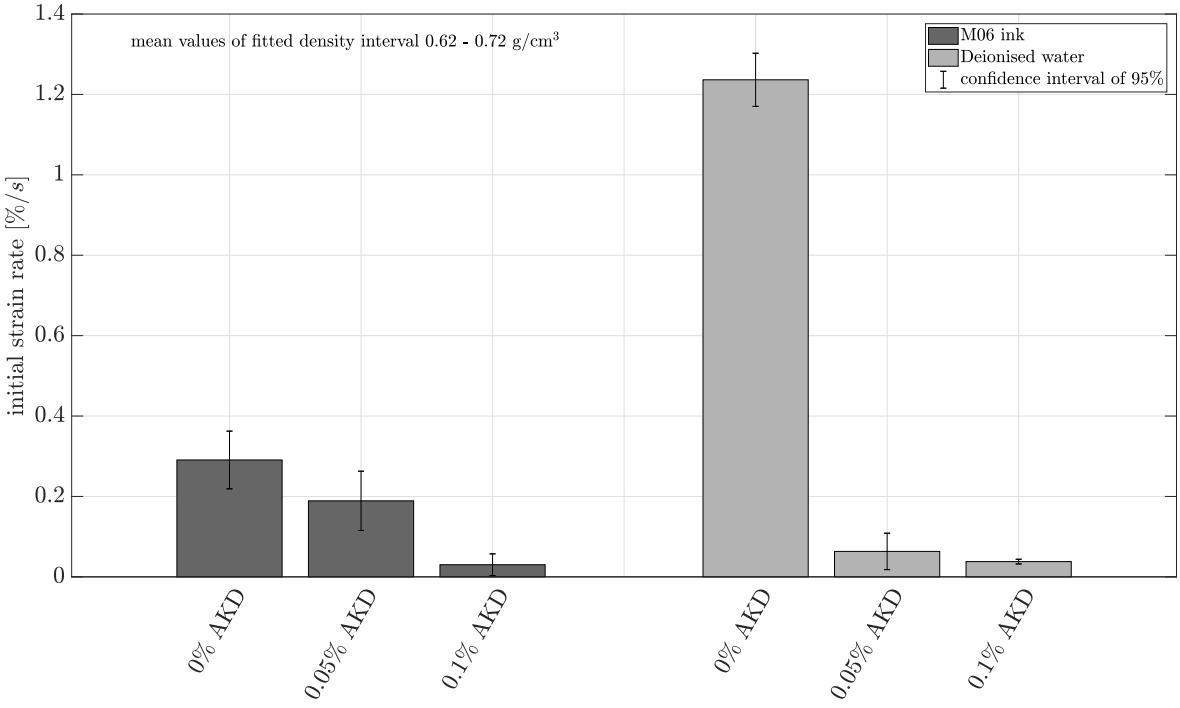

Figure 73. Comparison of wet expansion rate in ink vs deionised water for *Sizing* trial.

Conclusion of *Sizing* trial

Regarding the entire test series, papers with an enhanced water repellency due to sizing performed in the expected manner. The straight-forward interpretation here is a lower water uptake leading to a reduced deformation of the overall fiber network. Consequently, all investigated KPIs diminish by increasing the sizing degree. The higher resistance towards wetting and penetration is caused by hydrophobic functional groups attached to the fiber surfaces. Thus, a significant amount of water is evaporated on the paper surface before penetrating in, or less water is penetrating into the fibers and more into the pores between the fibers.

Investigations on the influence of various liquids used within the hydroexpansion tests show extraordinary high differences between ink and water. Though the ink is water based with a water content of approximately 60%, the initial strain rate of pure water is four times the speed of ink if testing conventional not sized handsheets. However, in case of sized papers, the end strain of an expansion in water is lower than in ink. This outcomes emphasize the significance of ink properties and compositions regarding paper deformation issues.

4.6 Results for trial 6: Fiber orientation - DSF

Handsheets for the previously discussed trials were entirely produced on a Rapid Köthen Sheetformer. In order to investigate the impact of a preferential fiber alignment on curl, a trial with sheets manufactured on a Dynamic Sheet Former (DSF) was conducted. Mechanical properties of the corresponding lab sheets are given in Table 14. Dynamic sheets which were not wet pressed show extra ordinary high thickness values of 244 to 264 μm and thus a dramatically reduced density lower than 0.35 g/cm^3. If pressed, they are compacted to roughly equal levels as exhibited by isotropic sheets. It is concluded that the sheet compression due to centrifugal drainage in a DSF is lower compared to vacuum drainage in a conventional handsheet former.

The MD/CD ratio regarding TI for sheets pressed with 4 bar is similar to the TSI measured with the L&W TSO tester. More precisely, the 750 m/min specification has a ratio of 1.7 compared to 1.9 obtained with 1000 m/min. At a higher density the TI ratio increases to 1.8 and 2.2, respectively. Regarding the modulus of elasticity out of bending stiffness shown in Figure 74, ratios for the 4 bar pressed sheets are marginally higher than for 8 bar. Conventional sheets have an E^b adjacent to the corresponding MD values, but in contrast a TI closer to the CD values of oriented sheets.

$TSI_{MD/CD}$ ratios for the manufactured lab sheets are basically in the range of cut sheet copy papers (1.4 - 2.2) [40].

Table 14. Mechanical properties of papers of trial 6: Fiber orientation.

Specification	ρ [g/cm^3]	d [μm]	bw [g/m^2]	S^b [Nmm]	E^b [N/mm^2]	TI [Nm/g]	E^t [N/mm^2]
RK-SF_{0bar}	0.601	128±2	77.1±0.2	0.407±0.019	2317±110	37.0±2.0	4651±399
RK-SF_{4bar}	0.623	126±3	78.6±0.3	0.395±0.019	2364±115	41.2±1.3	4830±323
RK-SF_{8bar}	0.634	124±3	78.6±0.2	0.405±0.009	2554±56	41.0±3.2	4757±148
$DSF750_{0bar\ CD}$	0.336	244±9	82.0±0.5	0.667±0.085	552±71	19.5±1.0	1354±209
$DSF750_{0bar\ MD}$				1.181±0.079	977±65	33.1±2.6	2849±350
$DSF750_{4bar\ CD}$	0.589	133±6	78.3±1.7	0.282±0.018	1443±94	30.3±1.2	2964±175
$DSF750_{4bar\ MD}$				0.473±0.053	2419±269	50.5±2.6	5490±521
$DSF750_{8bar\ CD}$	0.631	127±4	79.9±1.1	0.289±0.034	1704±198	34.6±1.7	3440±503
$DSF750_{8bar\ MD}$				0.474±0.029	2798±172	62.4±9.4	6459±1061
$DSF1000_{0bar\ CD}$	0.343	264±19	91.0±2.8	0.723±0.031	470±20	20.3±1.1	1381±112
$DSF1000_{0bar\ MD}$				1.812±0.195	1177±127	31.7±4.9	2728±382
$DSF1000_{4bar\ CD}$	0.591	139±6	82.0±0.6	0.318±0.036	1432±162	30.3±2.4	2866±258
$DSF1000_{4bar\ MD}$				0.654±0.091	2941±407	58.4±2.5	5484±118
$DSF1000_{8bar\ CD}$	0.632	131±5	82.6±3.8	0.266±0.012	1428±64	33.1±0.4	3121±331
$DSF1000_{8bar\ MD}$				0.496±0.056	2659±299	74.6±7.7	6509±147

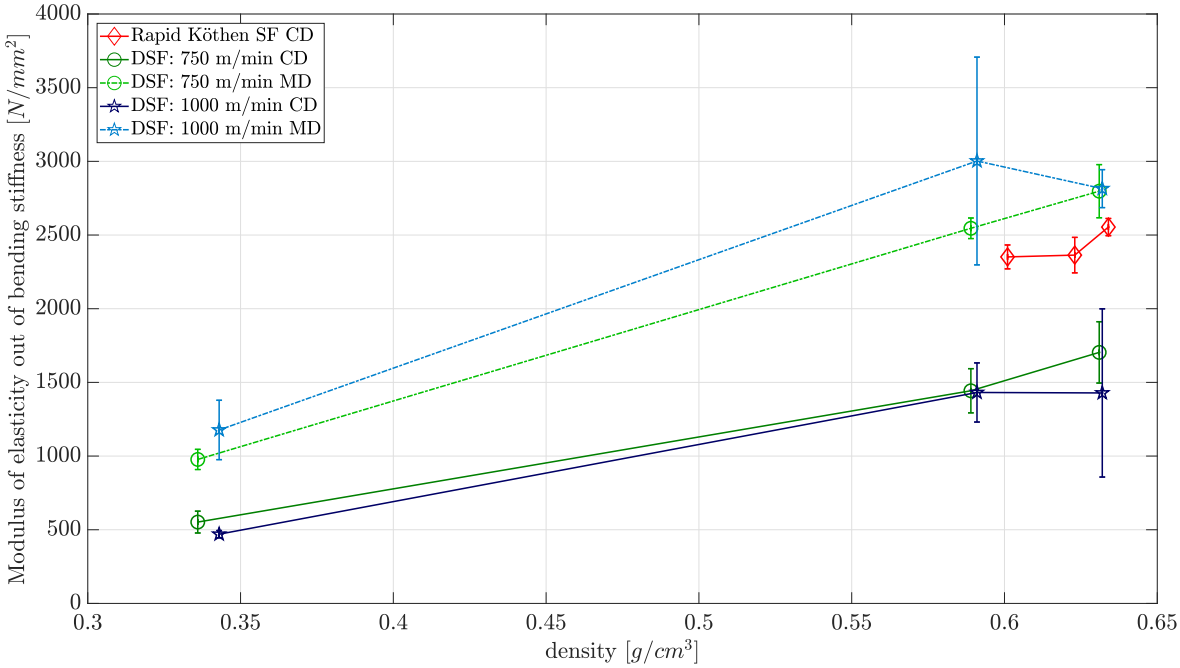

Figure 74. Modulus of elasticity over density for *Fiber orientation* trial.

4.6.1 Maximum, end curl and curl rate

The assumptions for this trial were a stronger and faster curl formation for specimens cut in CD due to a preferential fiber swelling in transverse direction. Indeed, a difference in maximum curvature of approximately 70% to 120% referring to MD samples is found in Figure 75. Samples of Rapid Köthen sheets show an initial curl after printing similar to dynamic sheet specimens in MD. Differences for TS and BS printed are not significant, which is in accordance with the sheet splitting results in 3.1.6. Neither a FO-angle nor anisotropy two sidedness was observed there. The occasionally appearing variation is most likely structure related, e.g. inhomogeneous distribution of fines, or just a randomized fluctuation.

In Figure 76, a remarkable similarity of end curvature values for both MD and CD samples is found. Over the whole density range specimens end up at a final curl height close to 0. The Rapid Köthen sheets reach an up to 4 times higher end curvature. Comparing maximum and end curl, the latter seems to be fully independent of the intensity of the first. Additionally, a distinctive fiber alignment results in hardly any remaining curl or curl upwards to the printed side.

The FO-anisotropy of 1.7-2.2 leads to differences in the orientation directions:

MD - low swelling force, high stiffness of not wetted (back) side

CD - high swelling force, low stiffness of not wetted (back) side

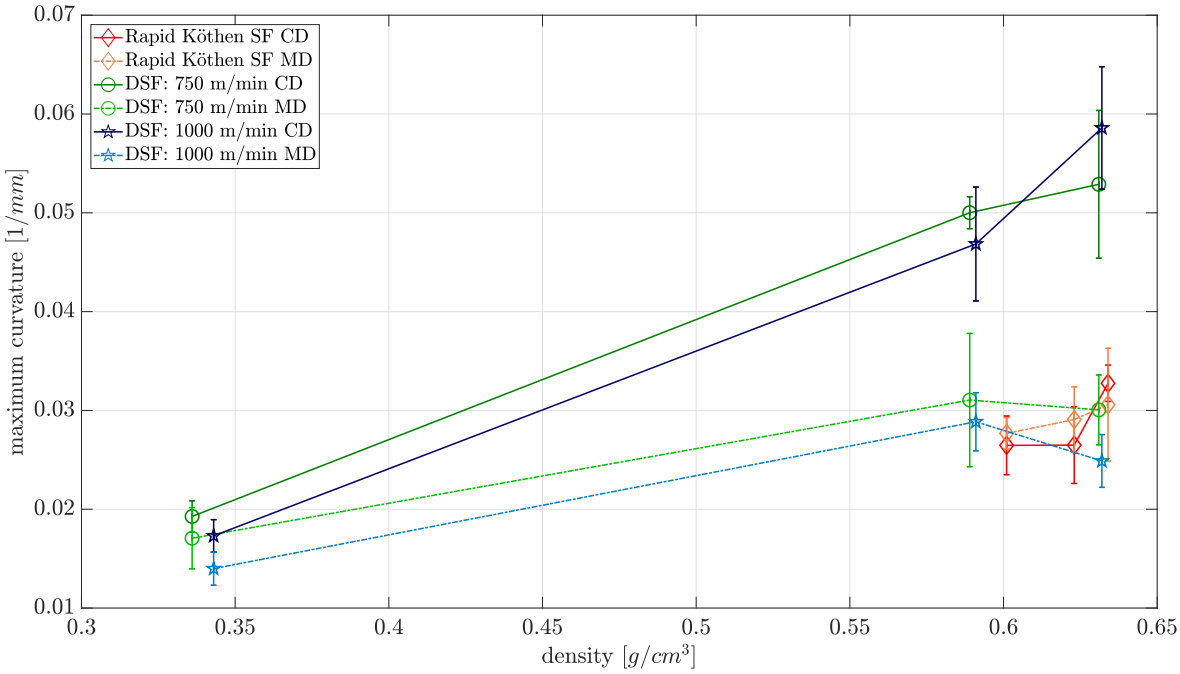

Figure 75. Maximum curvature over density for *Fiber orientation* trial.

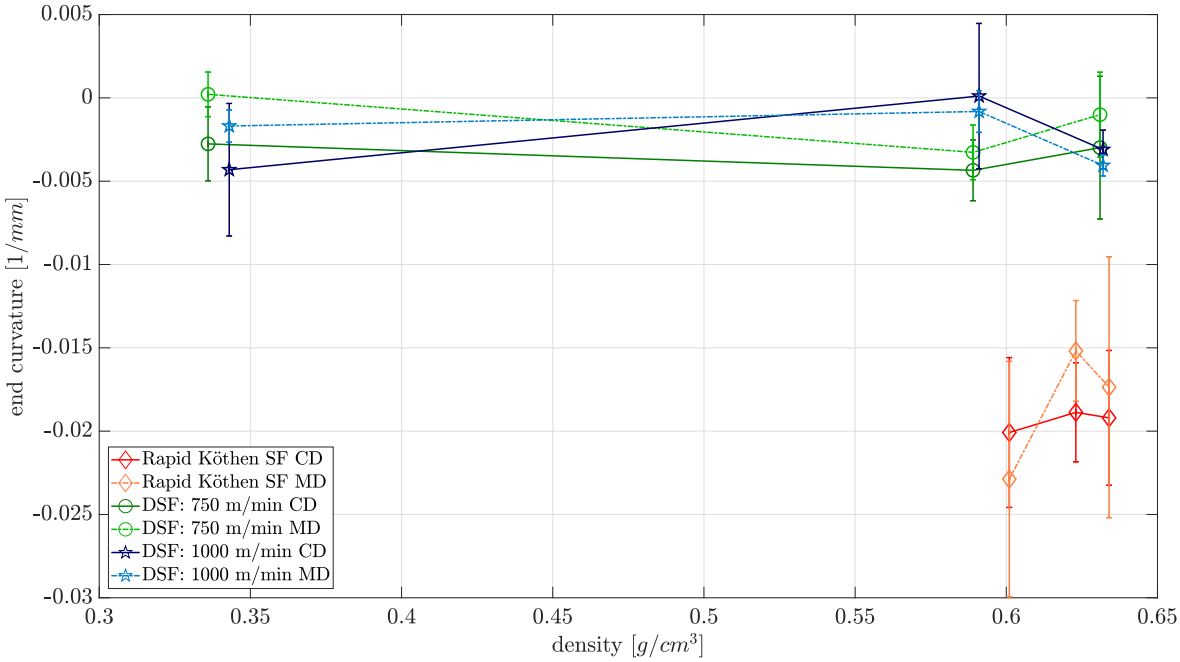

Figure 76. End curvature over density for *Fiber orientation* trial.

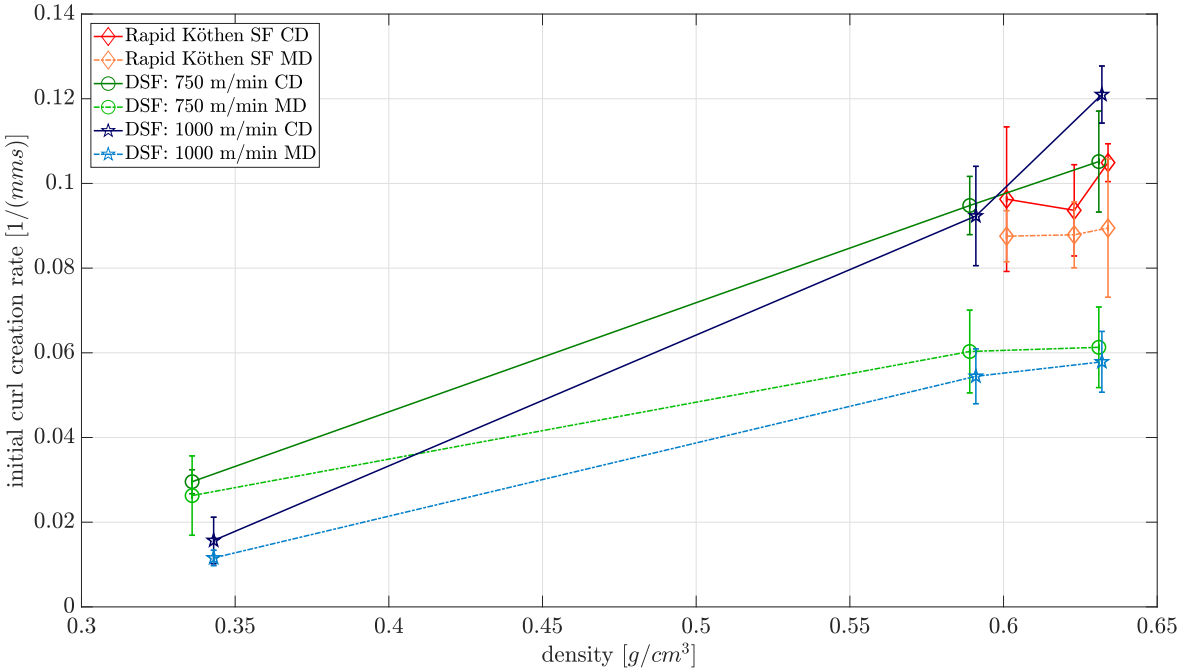

Figure 77. Initial curl creation rate over density for *Fiber orientation* trial.

It is very interesting and remains unclear, why the end curl is the same anyway. The sheet-splitting results in Fig. 25 and 26 do not show any FO two-sidedness excluding any impact from that side. All other influences regarding sheet structure, fines, filler, density, fibers, etc. can be neglected here due to the fact that the same sheets were tested in cross and machine direction.

The curves in Figure 77 for the initial curl creation rate resemble the respective graphs of the maximum curvature (Figure 75) with exception of the isotropic sheets. Specimens of dynamic sheets in cross direction curl faster than samples in machine direction and almost equally to papers produced on a Rapid Köthen SF.

4.6.2 Hydroexpansion in MD vs CD

The density interval used for calculating overall mean values of hydroexpansion and stiffness reduction was 0.6 - 0.63 g/cm^3 in this trial. Thus, only the range where density values of Rapid Köthen sheets and DSF sheets overlap was considered. The fits for KPIs of hydroexpansion over density based on six measurements, except for the Rapid Köthen sheets, were only three tests were conducted. CIs are thus elevated.

Figure 78 shows a comparison between the wet strain in ink obtained for samples in MD vs samples in CD. The expansion in cross direction was on average twice as high as in machine direction. This is a plausible value for the present but not excessive fiber orientation. A corresponding behaviour is detected by looking on the initial strain rate in Figure 79. CD specimens elongate with a higher initial speed than MD samples, though some observations are less reliable due to extraordinary high CIs.

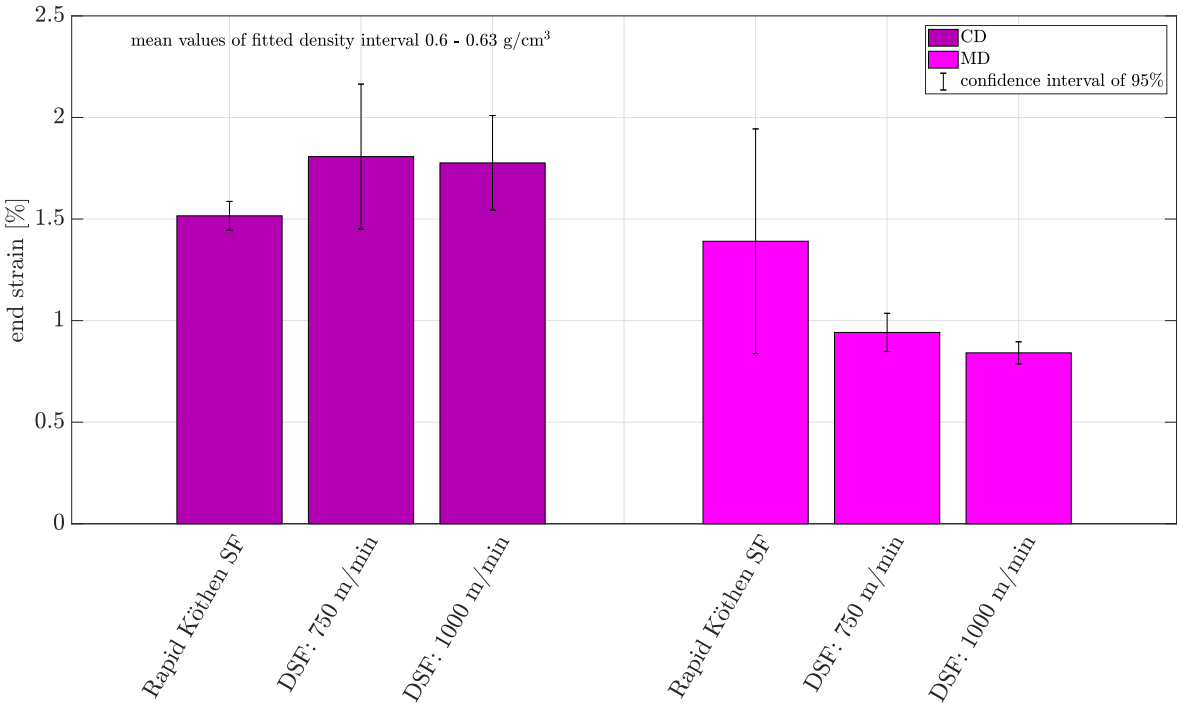

Figure 78. Comparison of wet expansion in ink for MD vs CD samples.

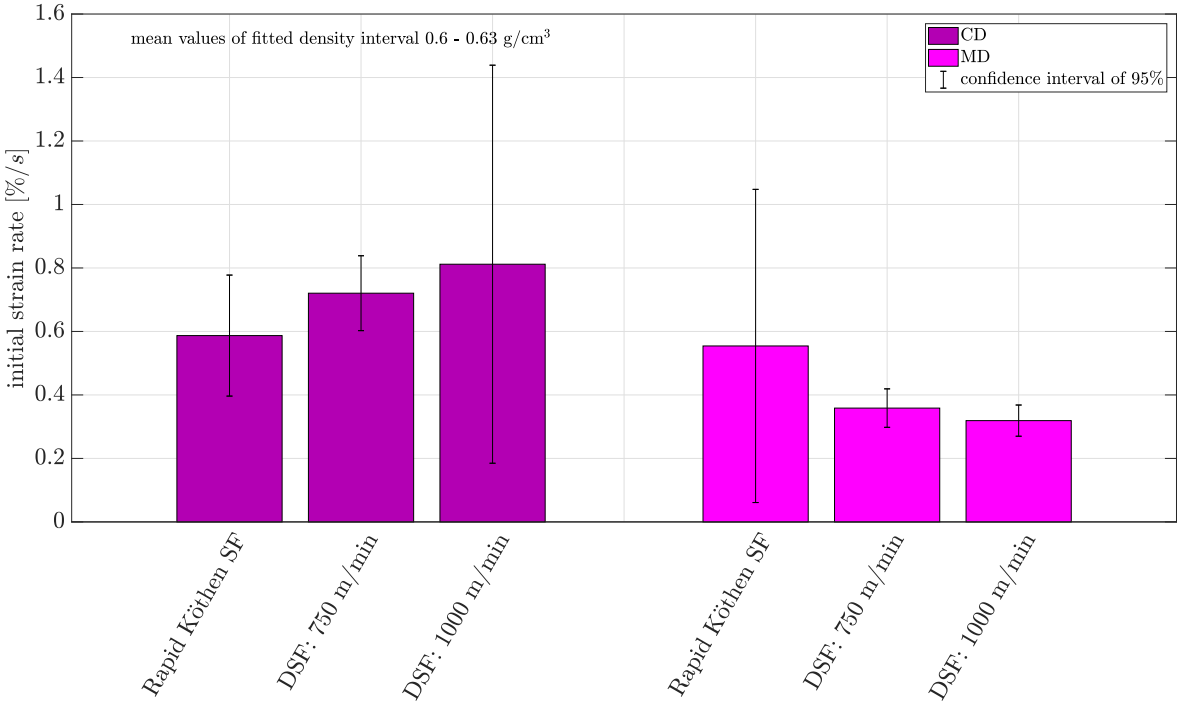

Figure 79. Comparison of wet expansion rate in ink for MD vs CD samples.

4.6.3 Stiffness reduction in MD vs CD

Figure 80 demonstrates the dimensionless stiffness reduction factor of paper samples triggered by printing ink on it. Here, the fits for calculating mean values of KPIs in the defined density interval based on 12 measurements. Nevertheless, variations are considerable. On average, stiffness of a specimen cut in MD deteriorate less than a specimen cut in CD. It is not clear, why isotropic sheets show an equal behaviour. The stiffness reduction factor of dynamic sheets in CD was expected to be higher than for sheets produced on a Rapid Köthen sheetformer, but this is not seen here. Actually, the mean values decrease with higher orientation.

Regarding the time constant $\tau_{stiffness\ reduction}$ in Figure 81, there is a correlation for mean values of oriented sheets showing a slower stiffness reduction (higher τ) in MD. However, if the error bars are considered, no statistically significant statement can be derived. Analysis of stiffness reduction was inconclusive.

Conclusion of *Fiber orientation* trial

Sheets with a preferential fiber alignment in machine direction perform essentially as expected before. Swelling due to liquid uptake is higher in transversal direction of the fiber, i.e. in cross direction of the paper sheet. Considering the increased FO-anisotropy in the oriented sheets, an escalating maximum curvature in CD corresponds with theory. Observations for hydroexpansion are plausible. A lower stiffness reduction in CD of oriented sheets than of isotropic sheets is not plausible.

It remains unclear why the final curl in MD and in CD is the same in spite of a FO-anisotropy of 1.8-2.1, which is in the range of an industrial copy paper. To seek a negligible upwards curl, oriented sheets seem to be favoured. Although, the maximum curvature in CD is up to twice as high as in MD, observations for the end curvature do not show any differences between these orientation directions.

However, the sheet forming process of a DSF is fundamentally different compared to a Rapid Köthen Sheetformer. The spraying of a pulp suspension onto a rotating wire causes a more layered than felted sheet structure with different network effects.

A sometimes observed difference between TS and BS printed can not be related to a FO-two-sidedness as shown by sheet splitting results. It is rather credible, that inhomogeneities in e.g. porosity, fines content or local density over the z-direction of the sheet are responsible for these variations.

The equivalent end curvature in CD and MD samples can not be explained by these structural variations. If present, there would be any difference between CD and MD apart form the fiber orientation.

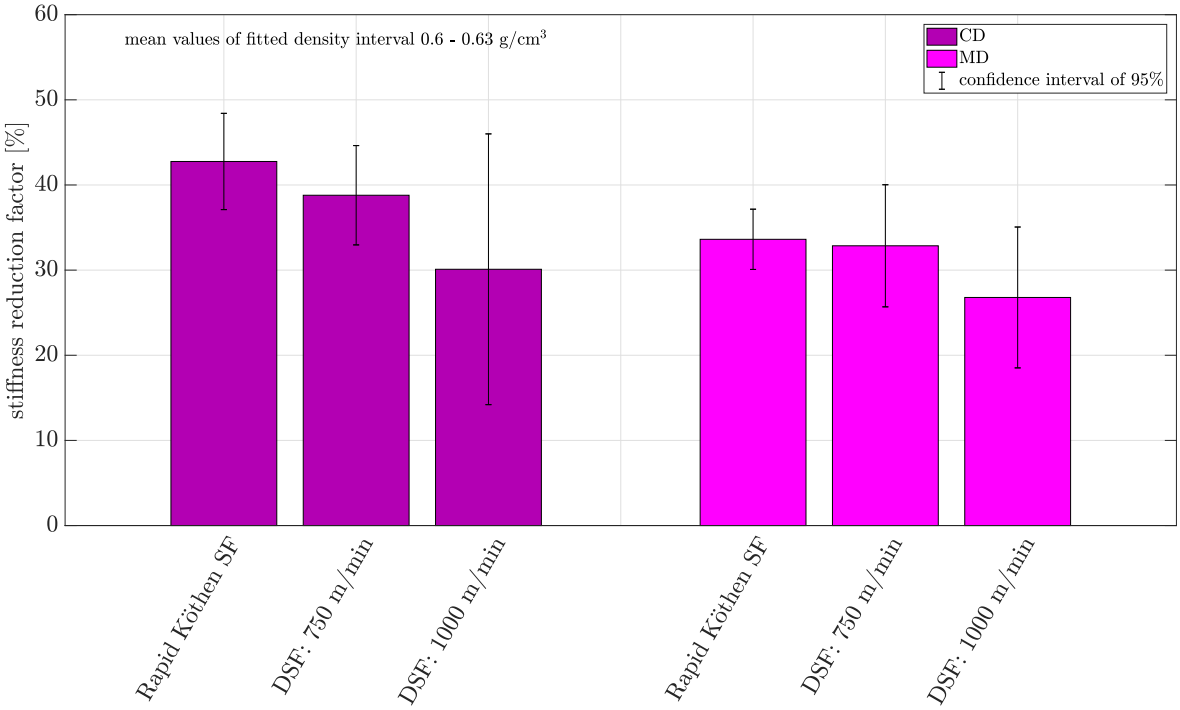

Figure 80. Comparison of stiffness reduction in MD vs CD.

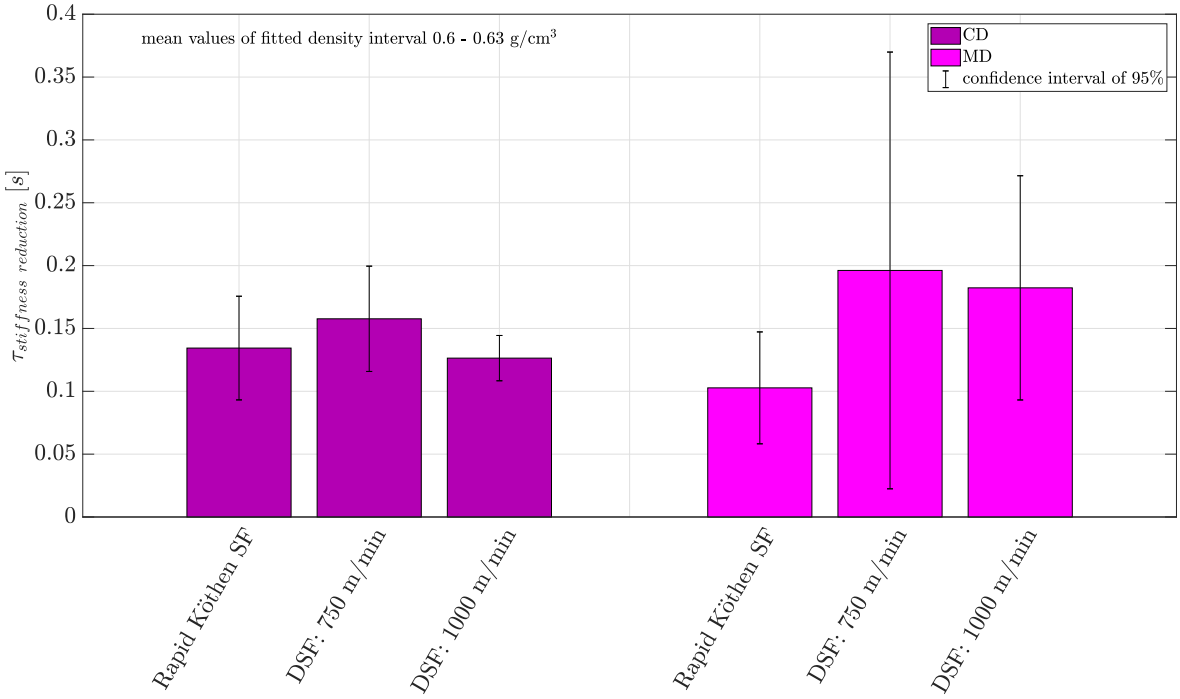

Figure 81. Comparison of time constant of stiffness reduction in MD vs CD.

4.7 Comparison of various trials

In this section, the entire test series of all six individual trials is analysed by means of the method described in section 3.4. The summarising plots contain mean values for the investigated KPIs in a defined density interval of 0.6-0.75 g/cm^3. In order to achieve a qualitative estimation how the chosen KPI develops by changing a specific paper component, a normalisation relative to the *zero point* was done. The *zero point* is defined in line 1 of Table 2 in section 3.1. Only results for measurements in CD are considered in this context.

As observable in Figure 82 and 83, curl results for the initial point of the second to the sixth trial differ from the 1000 rev PFI specification. Regarding the BCTMP trial the variation is attributed somehow to the deficient refining, thus a similarity with 0 rev PFI would be expected. It is indeed observed for the maximum curvature but the end curvature deviates, although density values of the respective samples are comparable. The error made by the fit is minor in this case, in contrast to the *Fiber orientation* trial, where the available density values of Rapid Köthen sheets are close together between 0.6 and 0.63 g/cm^3. The apparent variation of the *zero point* has to be considered when examining the following diagrams. The mean values for 0% PCC, 0% Fines and 0% AKD are comparable, but the difference to the 1000 rev PFI is not explainable. If the mean of e.g. the maximum curvature for this point was lower, the influence of refining would be more significant.

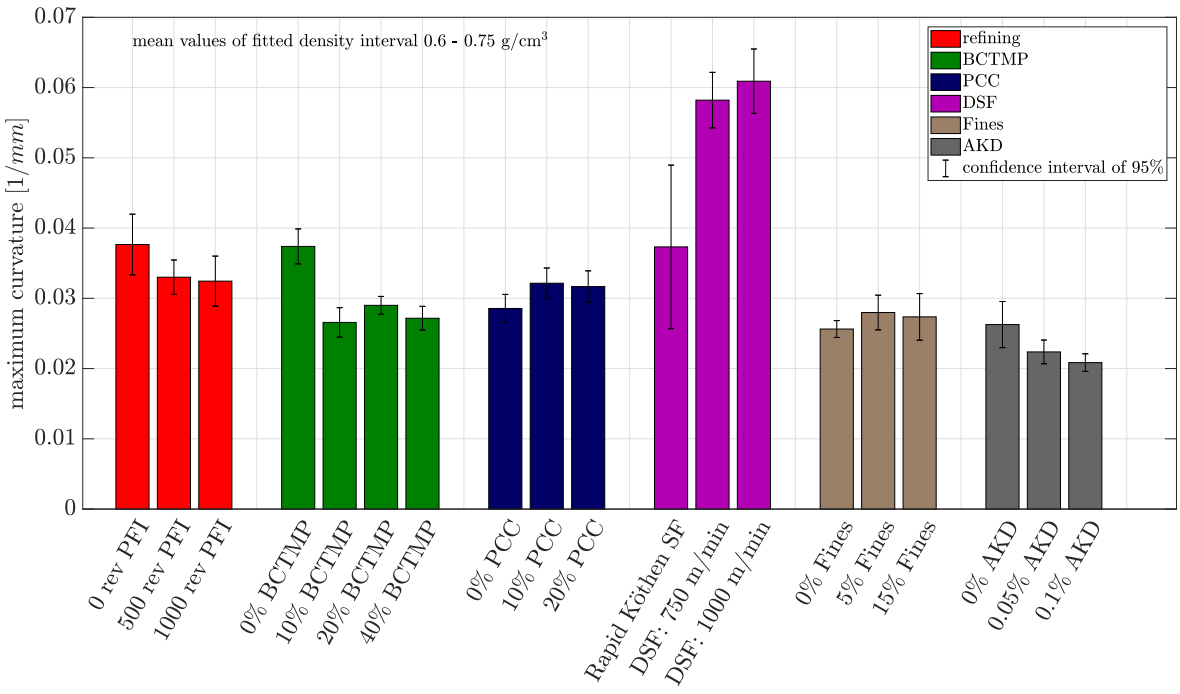

Figure 82. Maximum curvature for all trials.

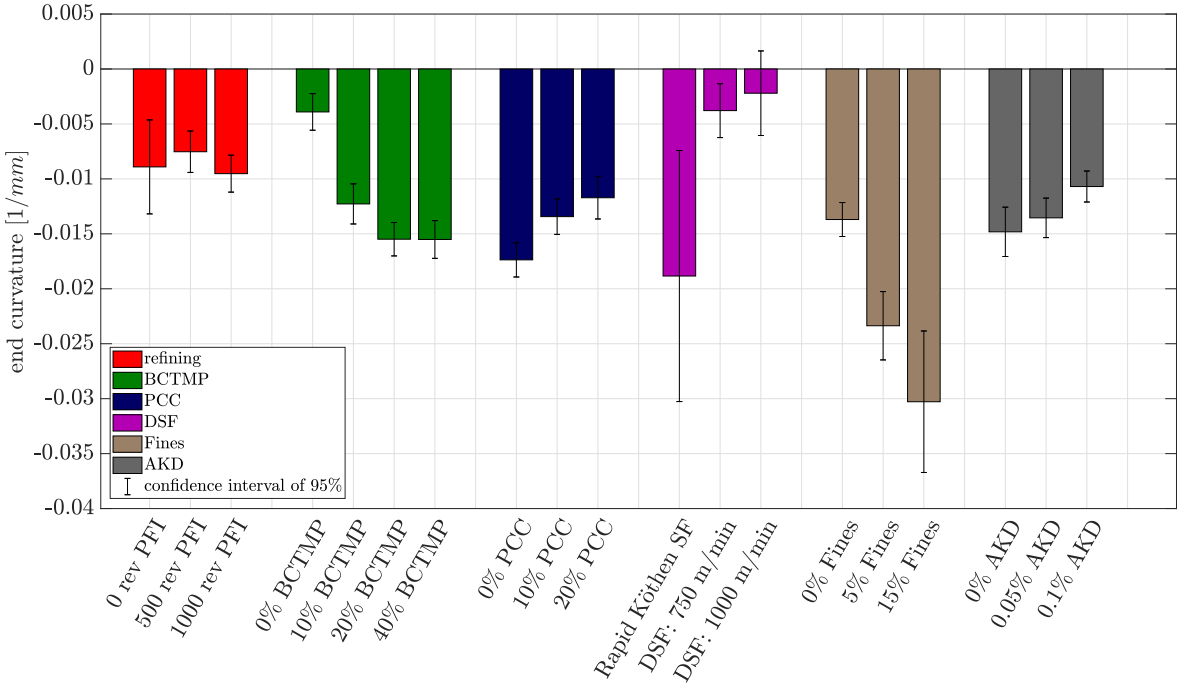

Figure 83. End curvature for all trials.

4.7.1 Maximum curvature vs end curvature

Figure 84 depicts the evolution of both maximum and end curvature for all investigated paper components proceeding from the *zero point*: 100% Santa Fe: 1000 rev PFI. The data points here are the normalized data from Fig. 82 and 83. Supporting information on these type of plot is given in 3.4.

While four trials show a negative correlation between maximum and end curvature, the *Fines* and *AKD* trial behave contrarily. A higher refining degree leads to a lower maximum curl towards non printed side but has barely any impact on end curl. Sheets with mechanical pulp fractions (BCTMP) show a reduced maximum curl but a high end curl towards printed side. The oriented sheets curl substantially more in CD but show a back curl close to 0 for both directions (compare 4.6). A fines content higher than average provokes a slight rise of initial curl and a considerable increase of end curl within this density interval. For densities over 0.75 g/cm^3, the maximum curl for 15% Fines is below the *zero point*.

Adding PCC to the furnish seems to be less crucial for the curl development, but this is only applicable if neglecting the influence of printed side as demonstrated in Figure 85. The graph split up for TS and BS printed indicate a stronger end and maximum curl for TS printed PCC sheets. Fines also show a measurable two-sidedness but with a lack of consistency between 5% and 15% fines content. The remarkable variation within the *Refining* trial might be caused by fine material on the BS of the sheet. However, observations for the *Fines* trial are different and again, no systematic behaviour is visible. BCTMP do not show variations regarding the maximum curvature but the end curvature increases if printed on BS.

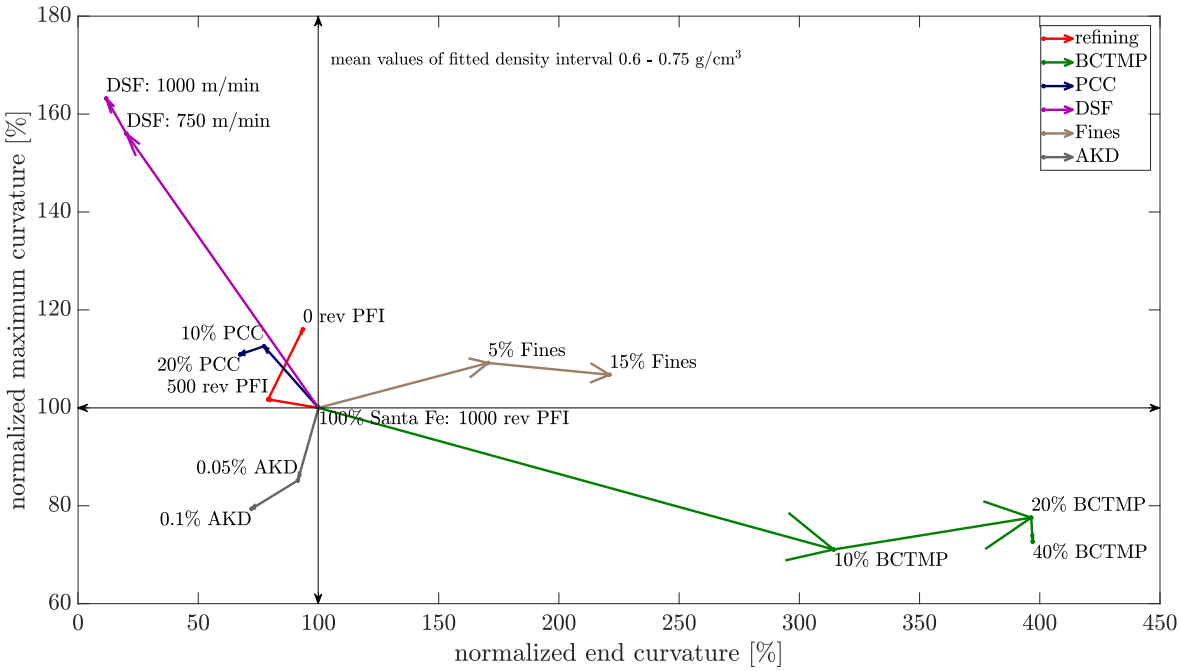

Figure 84. Maximum vs end curvature for all trials.

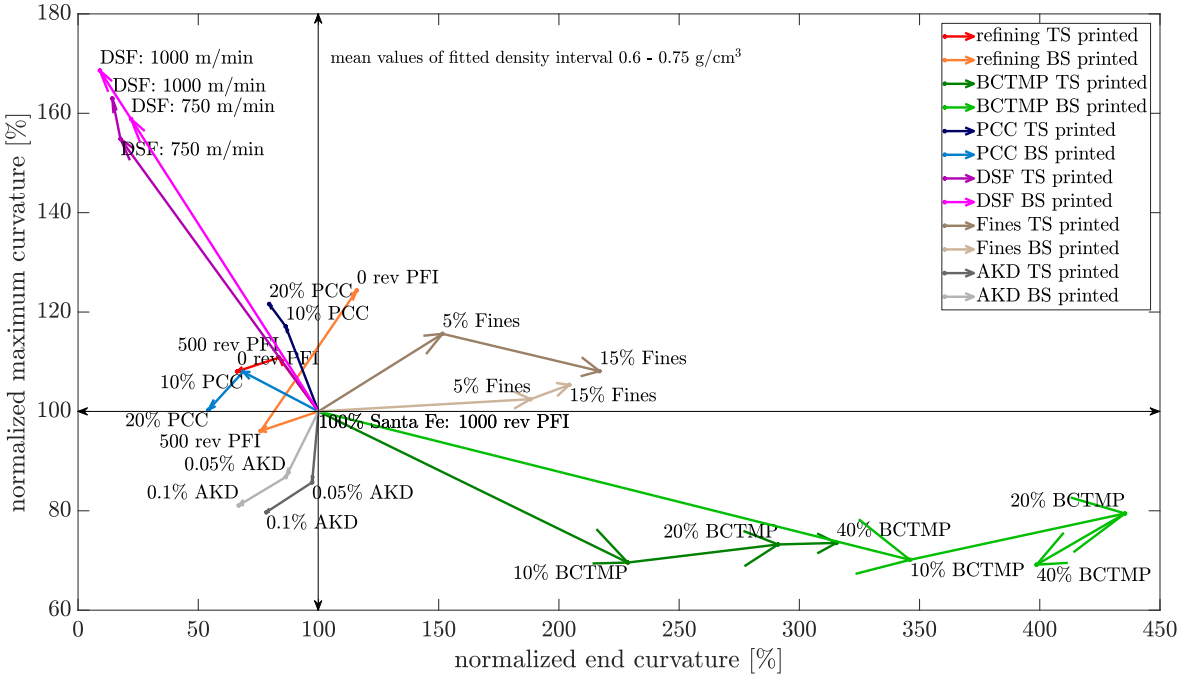

Figure 85. Maximum vs end curvature for all trials, TS & BS printed.

Mechanical fines may contribute to this effect enhancing swelling on BS and thus lead to a more severe overexpansion on TS.

The only trial located in the *"Quadrant of desire"*, i.e. reduction of initial and final curl, is the *Sizing* trial. Both the initial maximum curl and the subsequent end curl are reduced by the improved water repellency of the *AKD* sized papers. Little variations between TS and BS are explained by differences in $Cobb_{60}$ values (compare Table 4 in subsection 3.1.5).

Key conclusions of maximum curvature vs end curvature

- Maximum and end end curvature are not related for most of the influence factors (DSF, PCC, refining, BCTMP) i.e. improving one of the curl types leads to a deterioration of the other.
- Only for Fines and AKD the results are consistent: improvement of both curl types for AKD and deterioration for sheets with additional fines.
- Initial and end curl are controlled by different drivers.

4.7.2 Initial curl rate and time constants of curl tests

The initial curl rate is determined by the slope of a linear fit to the curl curve obtained by the laser sensor. Data points less than 40% of the maximum curl are considered for this calculation. The parameter describes the curl development within the first 1-2 seconds.

In Figure 86 the maximum curvature is compared to the initial curl rate divided into TS and BS printed. Obviously, no correlation between the velocity and the extent of the maximum curl can be derived due to entirely diverse observations. Papers of the *Refining* trial and sized papers show a rather linear relation towards lower and slower curl formation with higher refining or AKD content, respectively. Sheets with filler and fines deform slower and weaker if printed on BS where the majority of these constituents is supposed to be located. If printed on TS, however, the speed is comparable with conventional sheets except of the 15% Fines point. As expected, the dynamic sheets curl faster and stronger in cross direction. BCTMP fractions show a relatively high rise in velocity of up to 30% but simultaneously a decrease in maximum curvature. The actual amount of BCTMP added to the furnish seems to be hardly relevant.

Results regarding the time constant $\tau_{curl\ creation}$ in Figure 87 show equal relations except for the *Fiber orientation* trial. For the other five trials a higher $\tau_{curl\ creation}$ correlates with a slower initial curl rate. The dynamic sheets exhibit a higher time constant and a faster initial curl development.

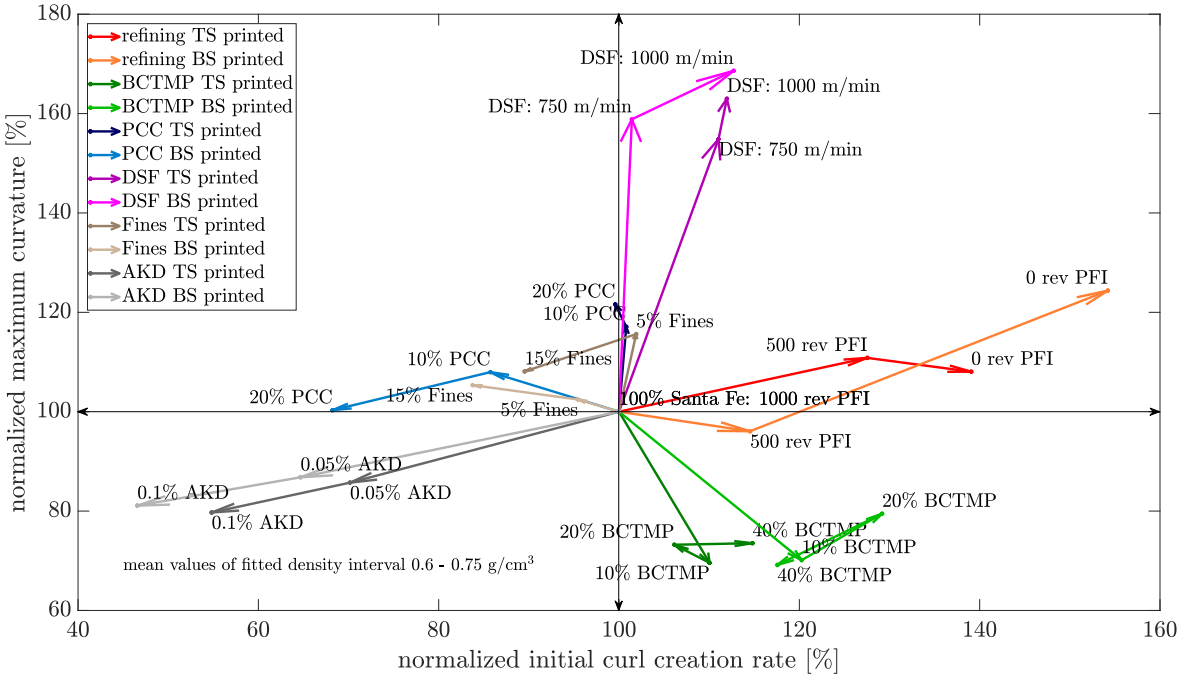

Figure 86. Maximum curvature vs initial curl rate for all trials.

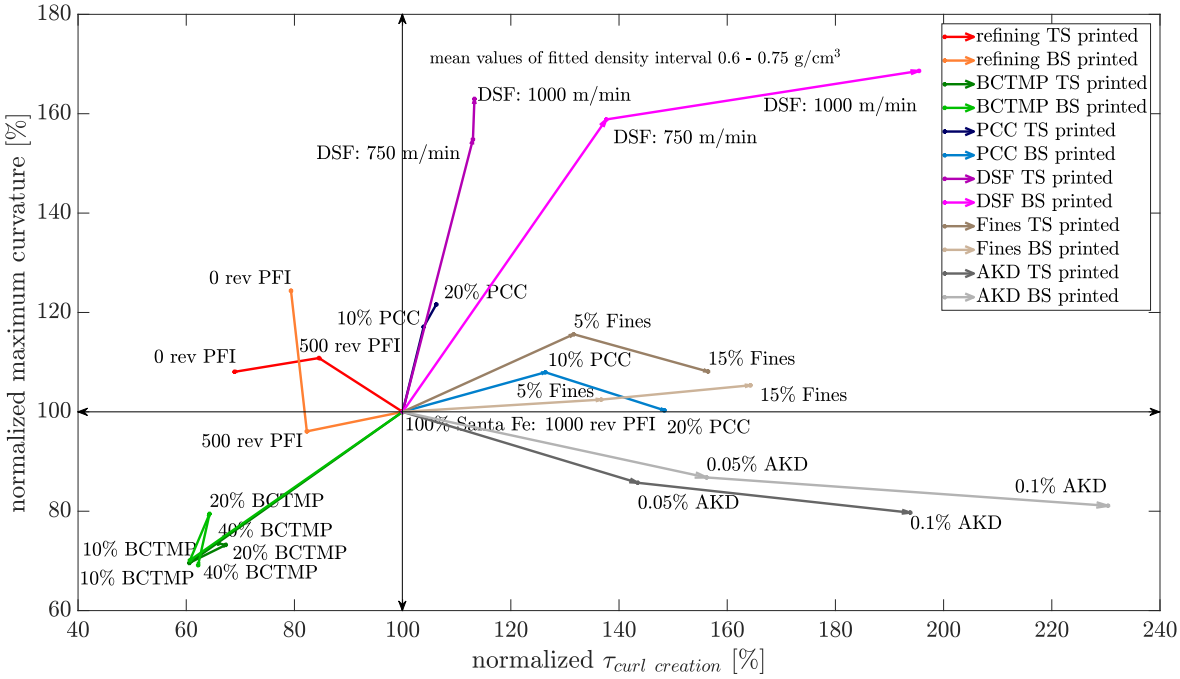

Figure 87. Maximum curvature vs $\tau_{curl\ creation}$ for all trials.

The connection between the end curvature towards printed side and the time constant $\tau_{curl\ reduction}$ is illustrated in Figure 88. For *AKD* and *DSF* trial, curl reduction lasts longer and leads to a less severe back curl. While the *Refining* trial do not exhibit a significant tendency, *PCC*, *BCTMP* and *Fines* show an unambiguous trend towards a stronger back curl if the reduction needs more time.

Comparing both time constants $\tau_{curl\ creation}$ and $\tau_{curl\ reduction}$ in Figure 89, no correlation can be found. This coincides with the findings in 4.7.1 that maximum and final curl are two different mechanisms.

Key conclusions of kinetics of curl

- No correlation is observed between initial curl creation rate or $\tau_{curl\ creation}$ and maximum curvature. The speed of the curl creation and the magnitude are unrelated.
- Interestingly there is a correlation between $\tau_{curl\ reduction}$ and end curvature: slower reduction of curl leads to higher end curl.
- The time constants $\tau_{curl\ creation}$ and $\tau_{curl\ reduction}$ are not correlated emphasizing the observations of maximum curvature vs end curvature in 4.7.1. These curl phenomenons are independent from each other.

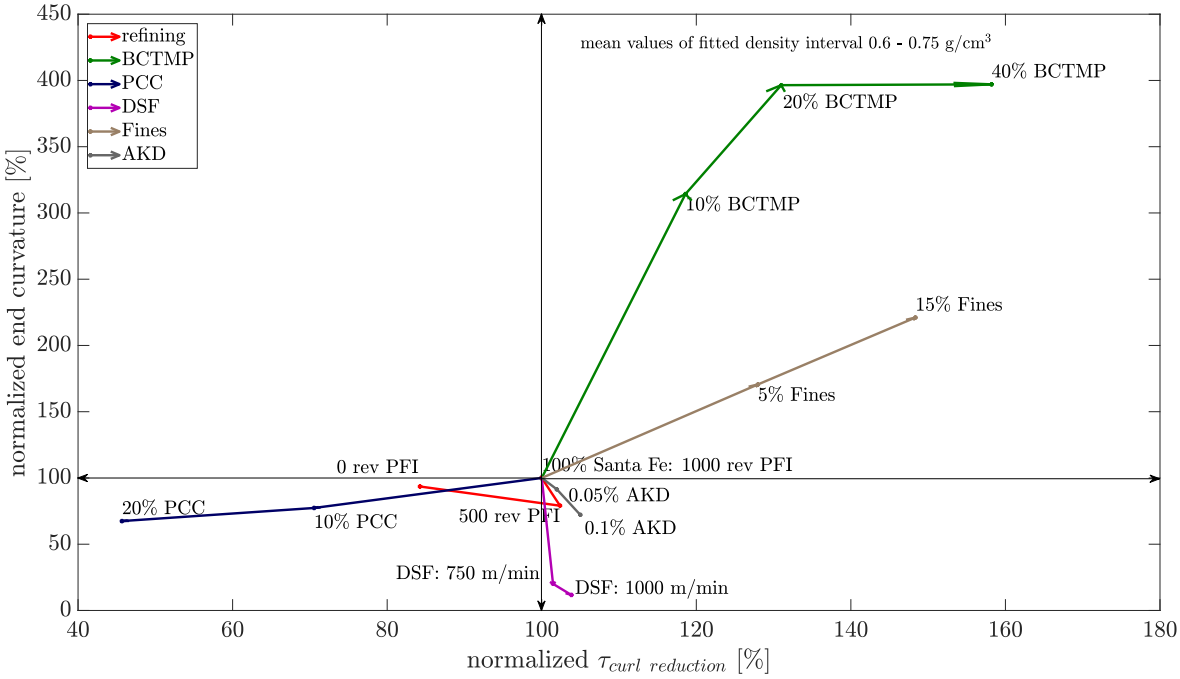

Figure 88. End curvature vs $\tau_{curl\ reduction}$ for all trials.

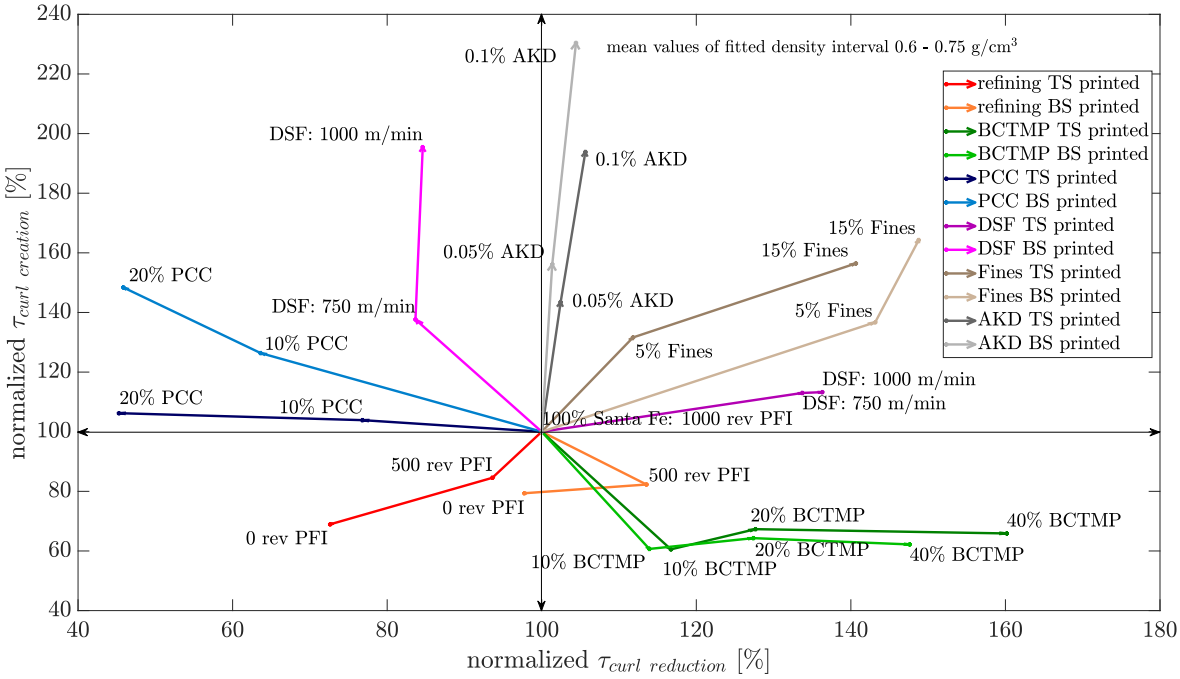

Figure 89. $\tau_{curl\ creation}$ vs $\tau_{curl\ reduction}$ for all trials.

4.7.3 Curl vs modulus of elasticity and bending stiffness

Modulus of elasticity was considered an appropriate material parameter to correlate with the curl values for maximum and end curvature. In Figure 90 the maximum curvature is plotted over modulus of elasticity out of bending stiffness E^b. Apart from the *Fines* trial a negative correlation can be detected here. Papers show a reduced initial curl away from printed side if modulus of elasticity increases. This fairly intuitive relation can be found for all trials, except for the sheets with higher fines content. Though stiffness increases, paper curls about 10% stronger.

Figure 91 shows that the relations for maximum curvature vs bending stiffness correlate to a high extent with the observations for maximum curvature vs modulus of elasticity. Due to the fact that the mean values are fitted for equal sheet densities and grammage was comparable, the thickness influence is not seen here.

Regarding the end curvature to printed side, a positive correlation with modulus of elasticity and bending stiffness can be seen in Figure 92 and 93. In case of the *Refining* trial, it is relatively weak but all other trials except of AKD show a clear tendency towards higher end curl with increasing stiffness. Sized papers have a lower back curl even though stiffness values slightly augment.

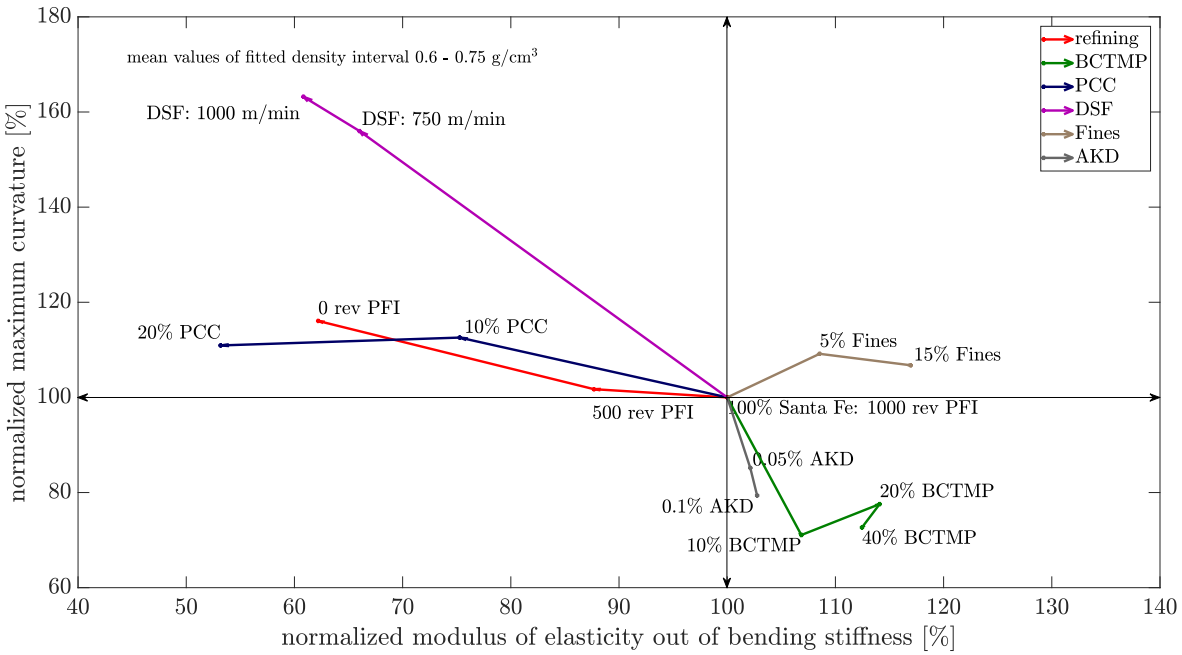

Figure 90. Maximum curvature vs modulus of elasticity for all trials.

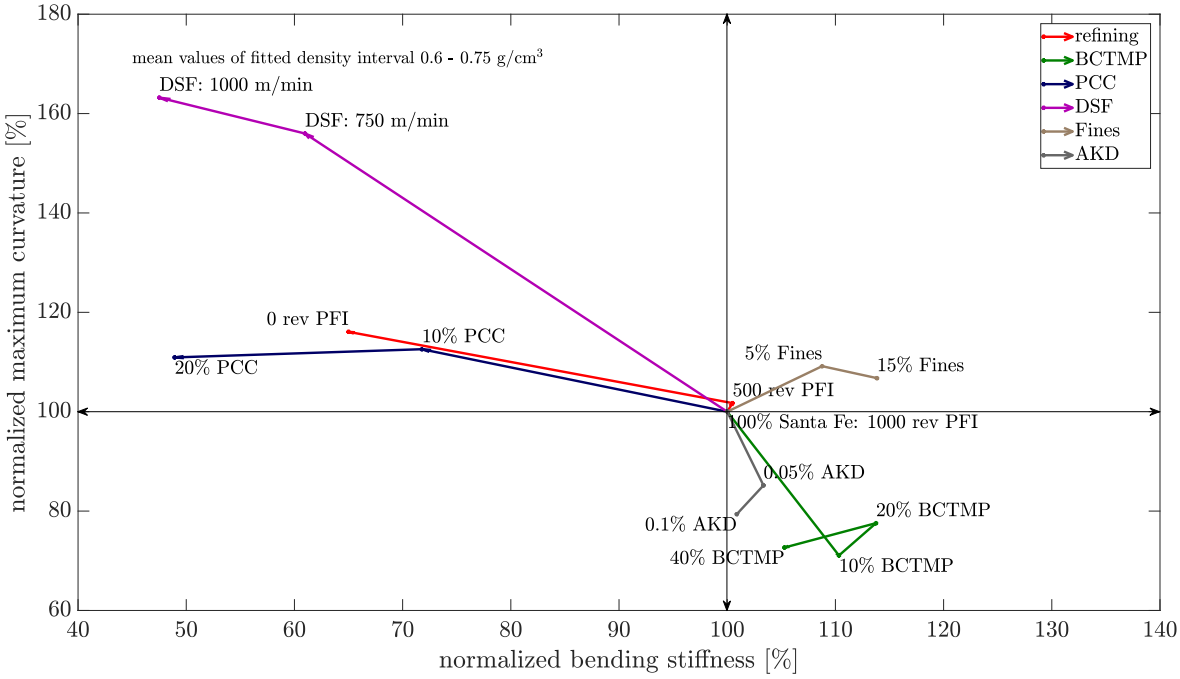

Figure 91. Maximum curvature vs bending stiffness for all trials.

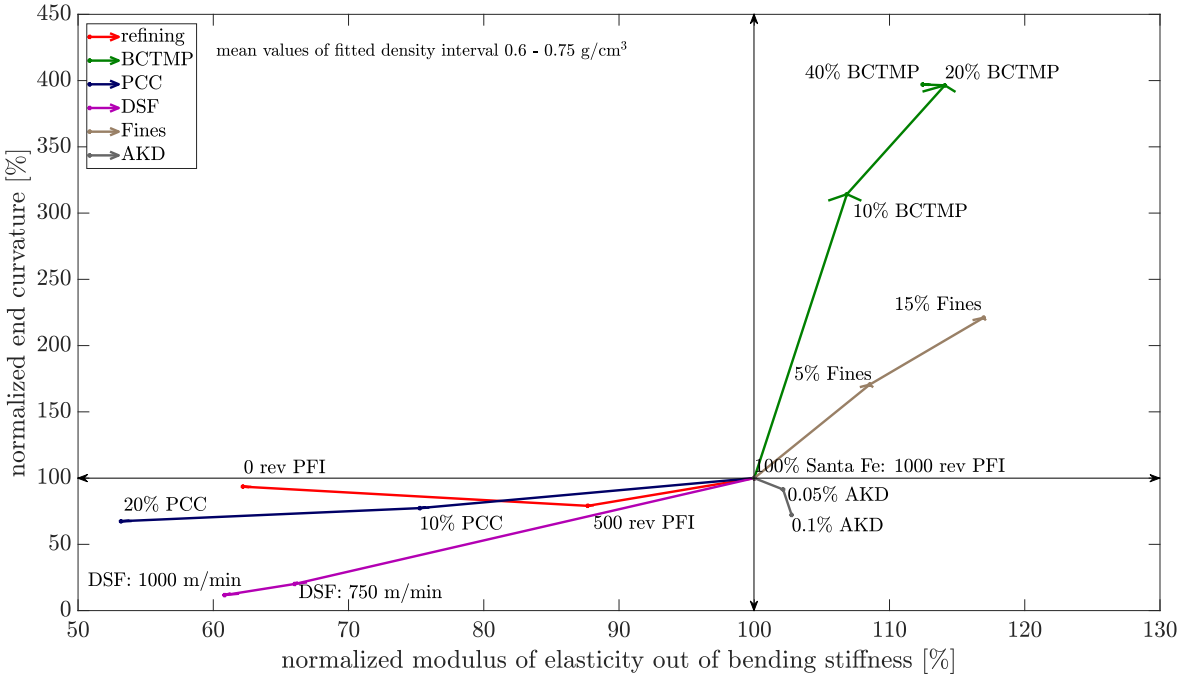

Figure 92. End curvature vs modulus of elasticity for all trials.

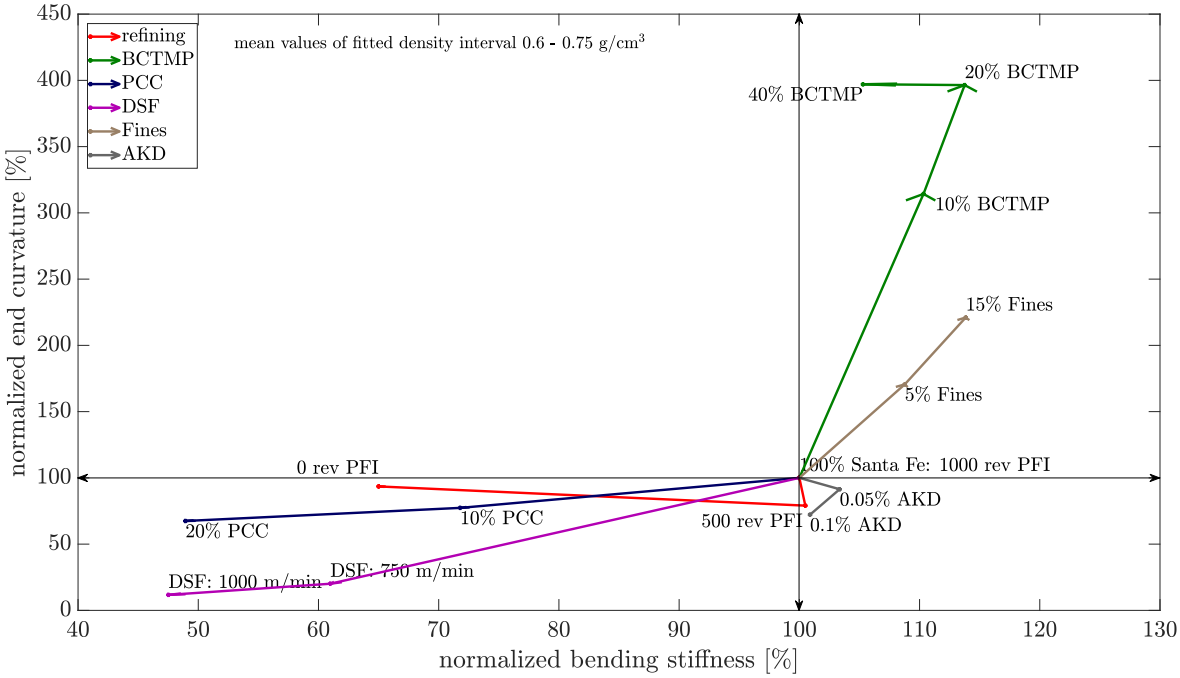

Figure 93. End curvature vs bending stiffness for all trials.

It is assumed that a higher sheet stiffness improves resistance against an initial print curl. The end curl in turn rises due to softening of the printed side and a subsequent amplified curl moment towards printed side. The findings further emphasize the significance of a suitable hydrophobisation of papers, leading to minor alterations of paper properties and thus enhanced dimensional stability.

Key conclusion of curl vs sheet stiffness

- Overexpansion of the not wetted side may not be the driving mechanism for the end curvature. If this side was highly expanded due to swelling of the fibers on the printed side, the end curl would be stronger for less stiffer sheets. However, a contrary correlation is found here. The end curl is stronger at higher stiffness values.

4.7.4 Curl vs hydroexpansion tests

Although only six hydroexpansion tests per point (e.g. 15% Fines) were conducted and thus the statistical significance is inferior, a comparison with curl results is made. The majority of handsheets submerged into ink expand between 1 and 1.5% in CD as shown in Figure 94. The value for Rapid Köthen SF of the *Fiber orientation* trial is possibly too high due to restricted data points in the considered density interval. More reliable results on this topic are shown in 4.6.2. In general, wet expansion in ink tend to increase with:

- lower refining degree
- higher filler content
- higher BCTMP content
- higher fiber orientation
- lower sizing degree

If looking on the speed of wet deformation in Figure 95, the calculated mean values depict occasionally expanded error bars but considerable tendencies regarding three trials. Mechanical pulp and AKD sizing decelerate the expansion, whereas PCC accelerates it. For the remaining trials, no significant change can be determined.

Fines seem to barely contribute to any alteration in trends referring to hydroexpansion.

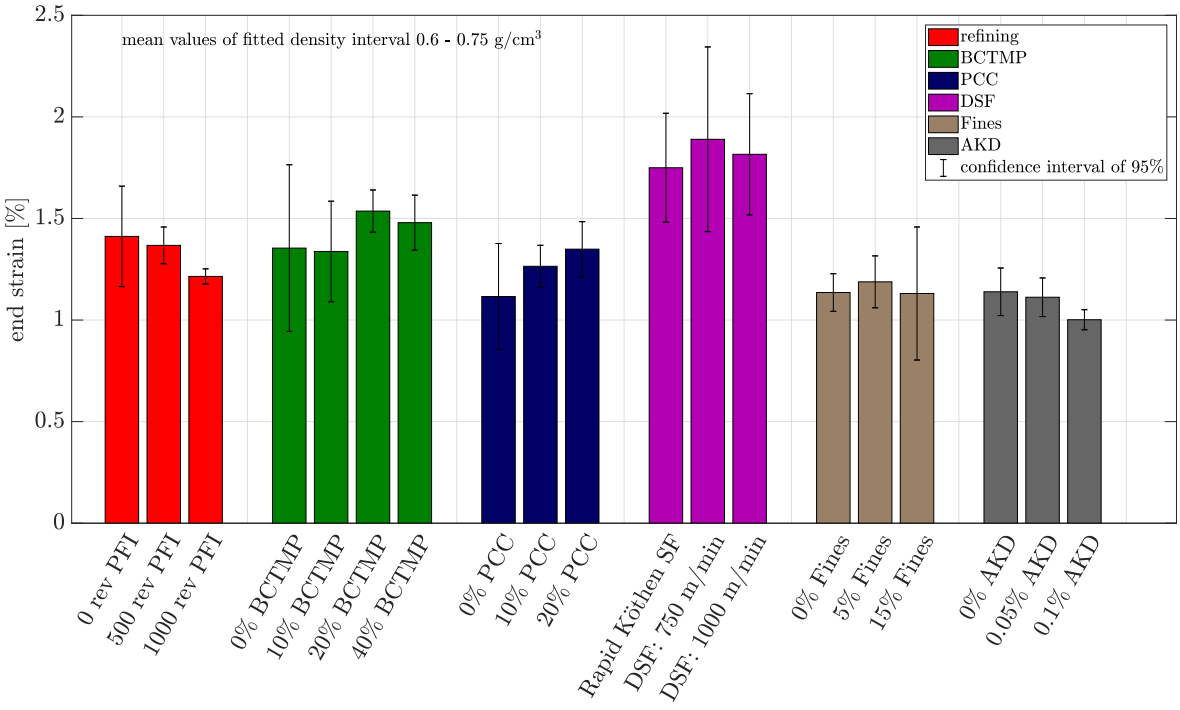

Figure 94. End strain for all trials.

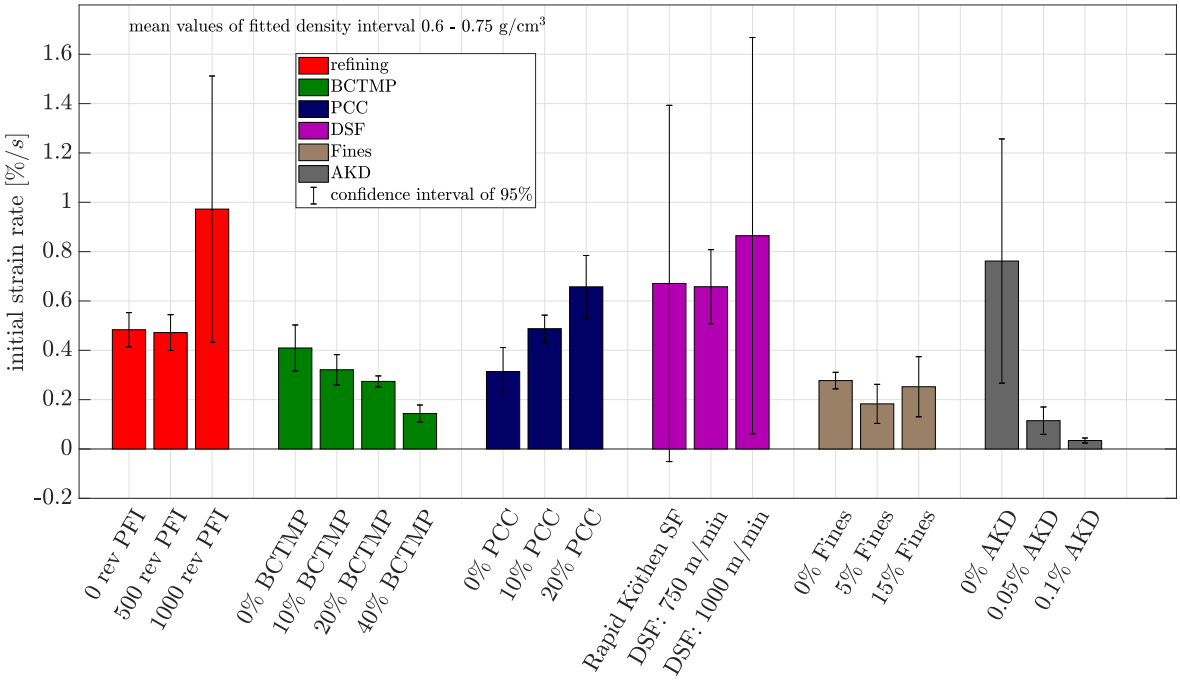

Figure 95. Initial strain rate for all trials.

In order to compare curl and hydroexpansion tests, the maximum curvature is plotted over the observed end strain in Figure 96. An extended expansion is expected to provoke a stronger initial curl, what is observable for four of six trials. If more fines a present in sheets, the curl increases slightly, but the strain is comparable to conventional handsheets. Papers with BCTMP fractions of 20 and 40% curl less but expand to a higher extent than pure kraft pulp paper. While no unambiguous correlation can be derived here, there seems to be a trend that higher wet strain is indeed somewhat related to high maximum curl.

The end curvature shown in Figure 97 is not clearly influenced by end strain. Sizing diminishes both end curvature and end strain. Adding BCTMP to the furnish leads to a rise in both KPIs. An increased fines content exhibits a distinct amplification of end curvature but no systematic impact on wet strain. Unrefined and filler containing sheets show the highest increment of end strain with simultaneous low back curl. Oriented sheets expand relatively stronger in CD than observable in this chart, as previously mentioned. The practically vanishing end curl here is astonishing by all means.

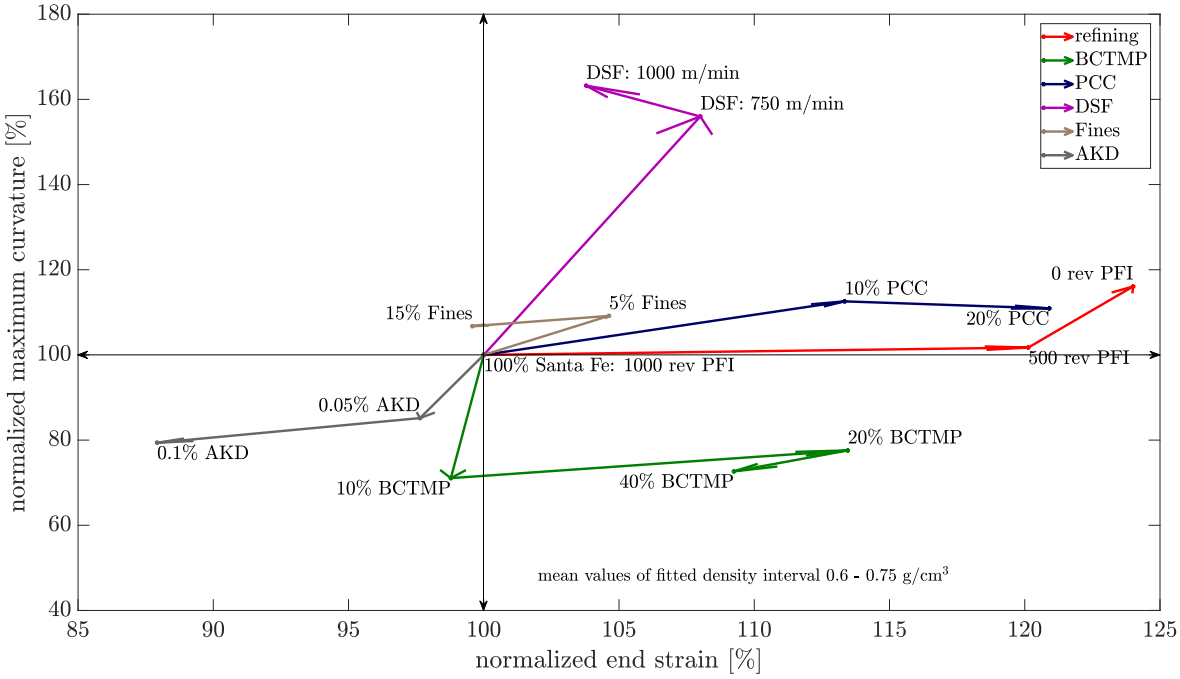

Figure 96. Maximum curvature vs end strain of all trials.

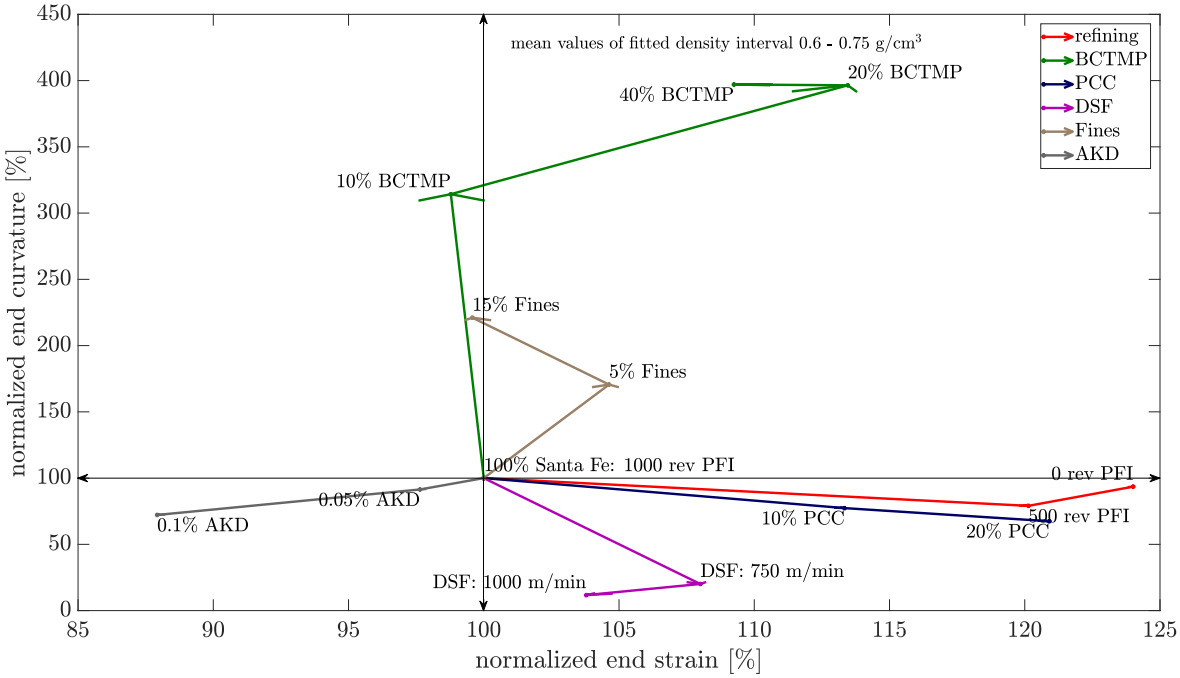

Figure 97. End curvature vs end strain of all trials.

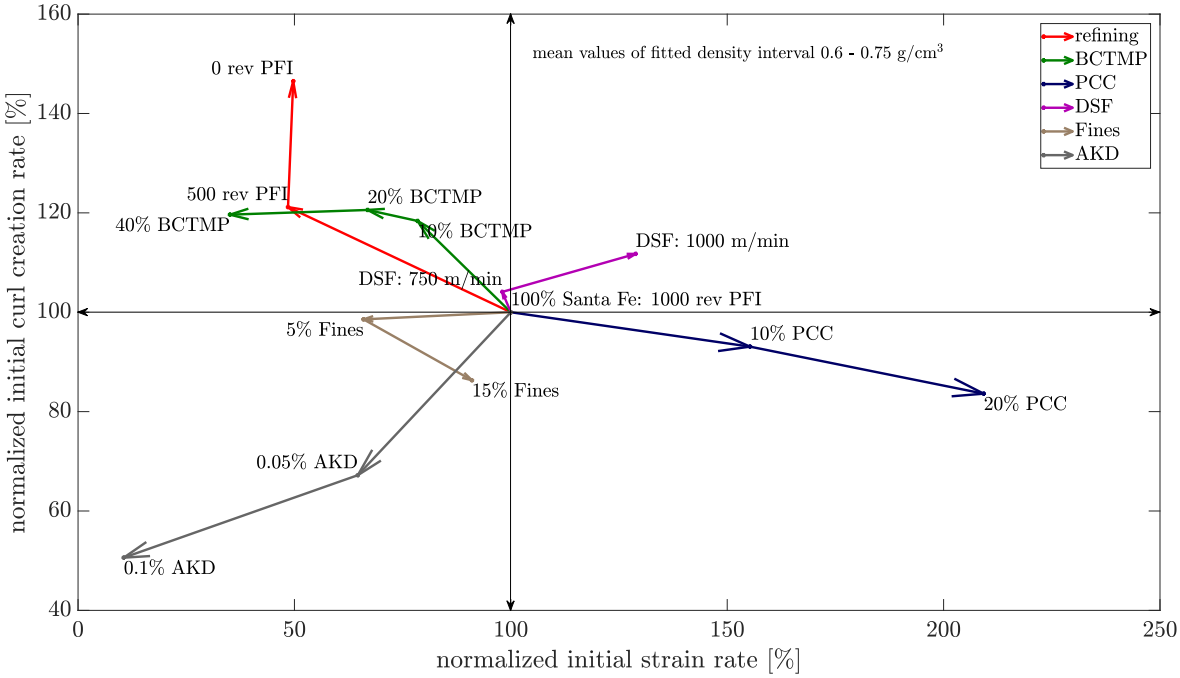

Figure 98. Initial curl rate vs initial strain rate for all trials.

In Figure 98 the initial curl creation rate and the initial strain rate are compared. For AKD and dynamic sheets, the expected synchronous development is observed. Sheets with additional fines curl and swell slower but no linear trend regarding the percentage of fines can be seen.

The remaining three trials demonstrate a contrary behaviour, though variation within the *Refining* trial is error-prone as shown in Figure 95. While an elevated BCTMP fraction lead to a quicker curl creation and slower strain, more PCC reduces the curl formation speed but nearly doubles the initial strain rate.

Key conclusions of curl vs hydroexpansion

- Wet strain seems to be somewhat related to maximum curvature.
- There is no correlation found between hydroexpansion and end curvature or between initial strain rate and curl creation rate.

4.7.5 Curl vs stiffness reduction tests

The stiffness reduction due to printing was measured on a pilot setup by means of applying a specific pre-load and recording the drop of force signal during printing. The experimental method was described in 3.6.

Figure 99 summarises the obtained results of the dimensionless stiffness reduction factor. It consistently amounts to 30 - 40% with considerable variations for the *Fiber orientation* trial. On average, BCTMP, PCC and fines contribute to a relatively higher stiffness loss. Dynamic sheets tend to better preserve the initial stiffness value previous to printing than isotropic sheets.

The time constant $\tau_{stiffness\ reduction}$ for the entire handsheet series is shown in Figure 100. Clear tendencies can be identified regarding refining, filler content and sizing degree. More intense refining lead to a slower stiffness reduction correlating with a generally improved stiffness due to beating. As expected, also sized papers need more time to lose stiffness. A remarkable fast drop in stiffness is observed for papers with an increasing amount of PCC. The time constant reduces to about 10% of its initial value.

Curl and stiffness reduction tests are compared in terms of the respective time constants in Figure 101. The star shape of the arrows indicates a lack of correlation regarding the investigated KPIs.

A higher refining as well as increased sizing degree lead to a simultaneous slower curl creation and stiffness reduction. The differences between TS and BS printed for AKD sized papers are partly explainable by variations in $Cobb_{60}$ values.

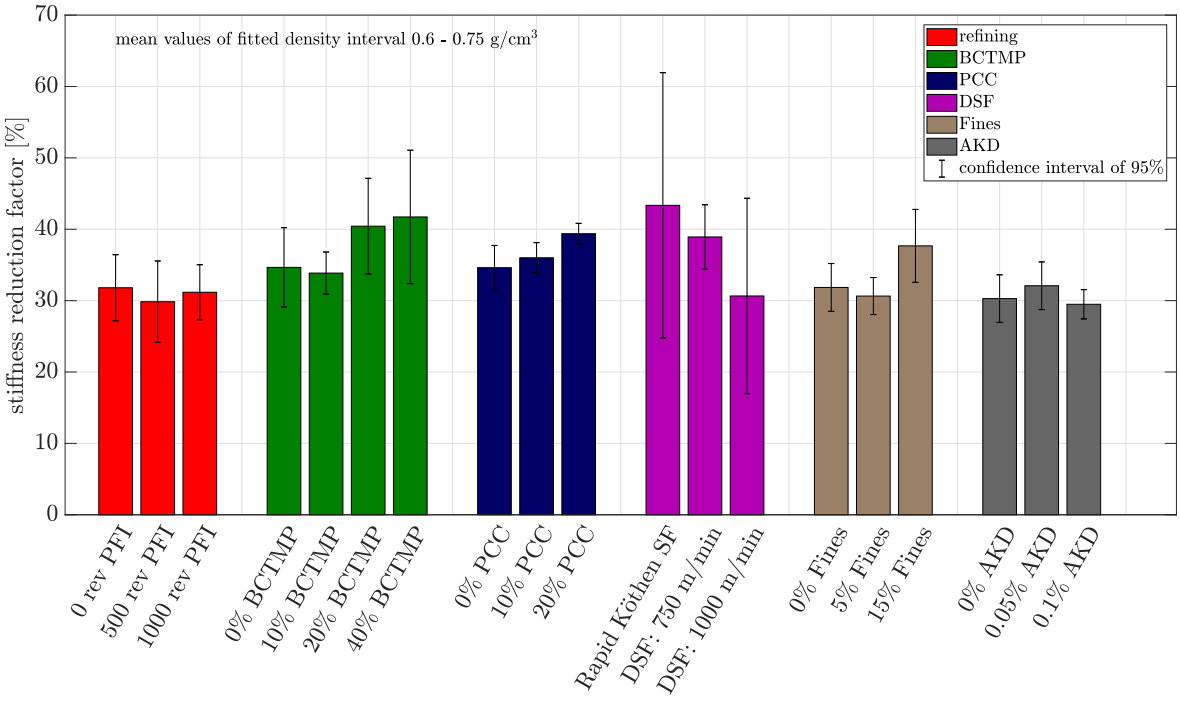

Figure 99. Stiffness reduction factor for all trials.

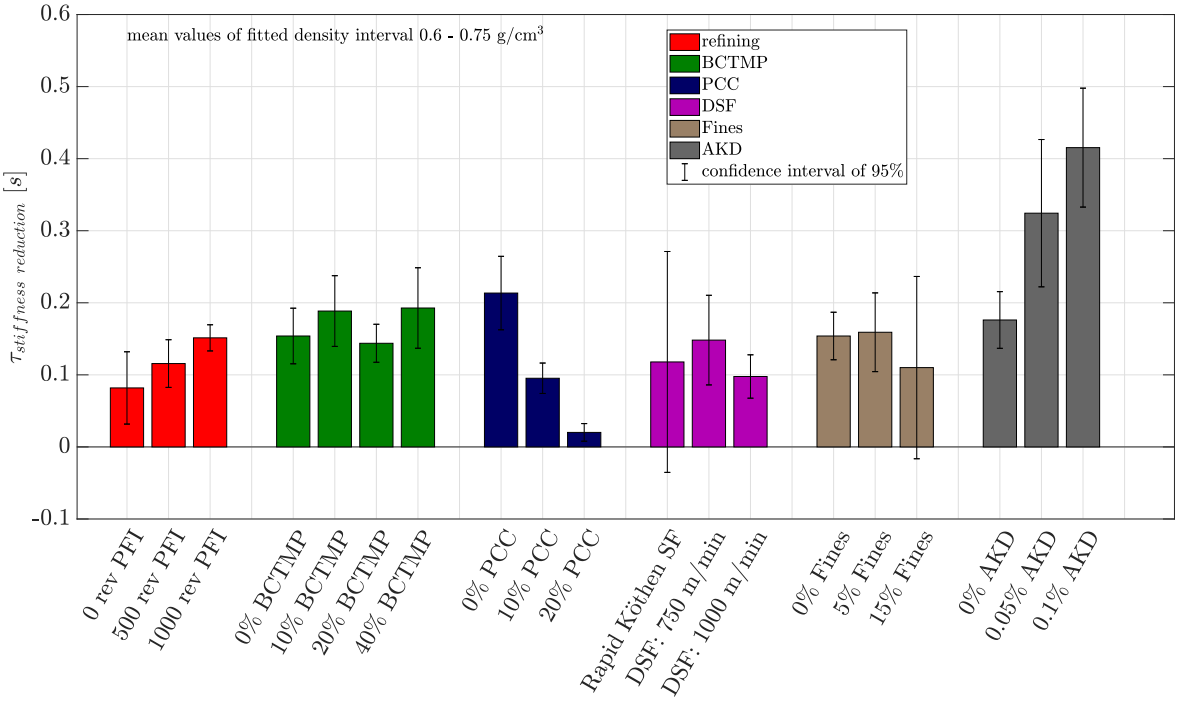

Figure 100. $\tau_{stiffness\ reduction}$ for all trials.

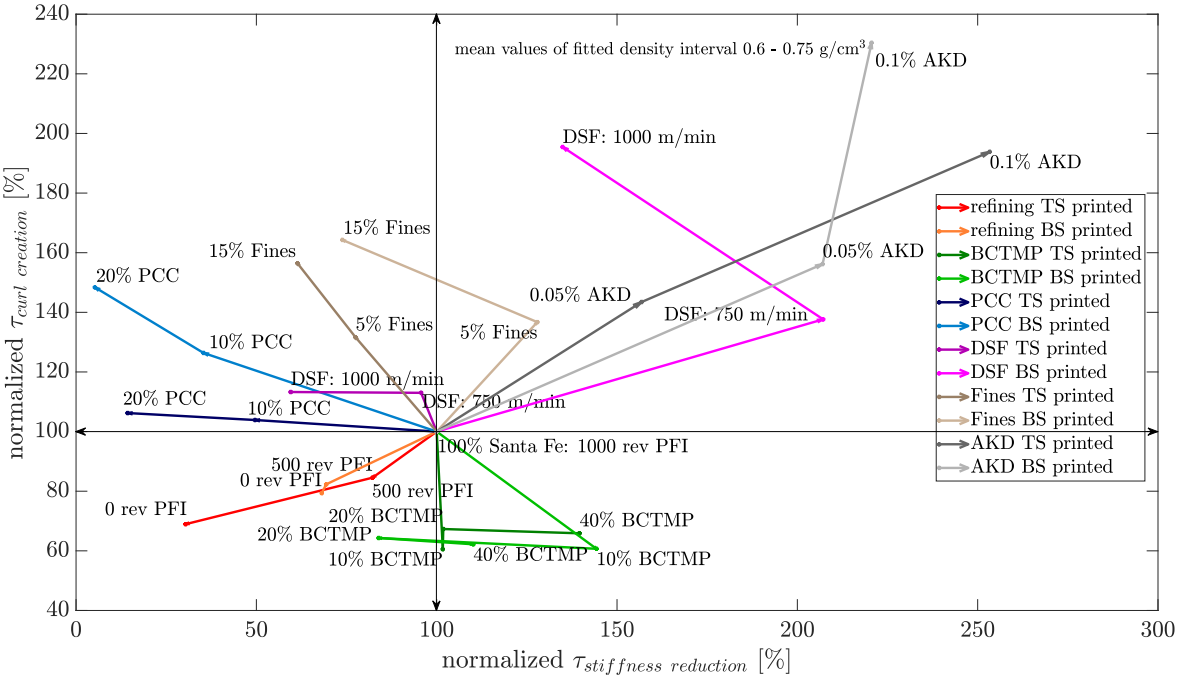

Figure 101. $\tau_{curl\ reduction}$ vs $\tau_{stiffness\ reduction}$ for all trials.

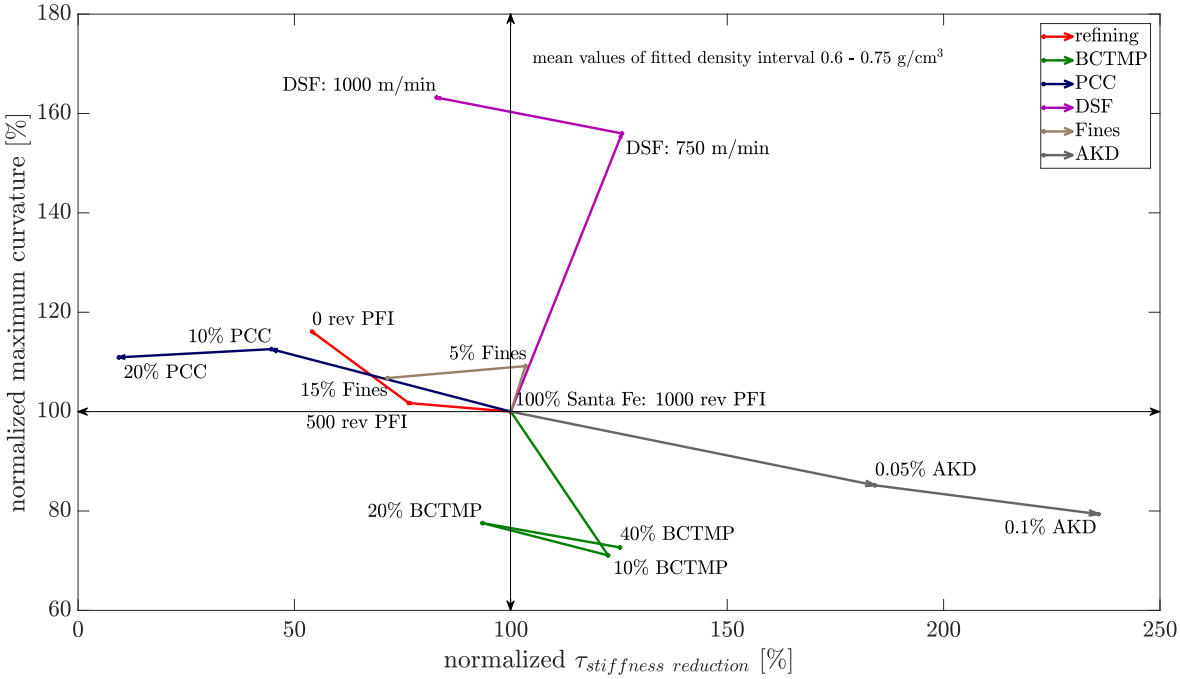

Figure 102. Maximum curvature vs $\tau_{stiffness\ reduction}$ for all trials.

BCTMP sheets are prone to a quick curl formation implying a lower time constant. Results for $\tau_{stiffness\ reduction}$ are contradictory for various mechanical pulp ratios and printing on top or bottom side.

Papers filled with PCC exhibit an accelerated stiffness reduction but a slower curl creation. Considering the printed side, this discrepancy further intensifies. While TS printed sheets have a $\tau_{curl\ creation}$ similar to unfilled sheets, $\tau_{stiffness\ reduction}$ is heavily decreased. For BS printed sheets, $\tau_{stiffness\ reduction}$ diminishes even more and $\tau_{curl\ creation}$ increases, signifying a decelerated curl development and a quicker stiffness reduction.

Referring to the *Fines* trial, general observations are to a certain extent similar to PCC sheets if printing mode is neglected. Differences between TS and BS arise particularly for the 5% Fines configuration. Stiffness of BS printed sheets drops slower than if printed on TS.

Extended variations are observed for the dynamic sheets. However, the estimations for this trial and KPIs are not fully reliable due to high error bars of the initial point (Rapid Köthen SF).

Figure 102 shows that maximum curvature and $\tau_{stiffness\ reduction}$ are roughly correlated. If the time constant increases, i.e. stiffness of specimens slower diminishes, the obtained maximum curl value is lower. As already mentioned, an appropriate evaluation of oriented sheets is not possible in this case.

5 Conclusions

The purpose of this thesis was to investigate paper-related reasons for High Speed Inkjet printing curl by means of a wide range of handsheet specifications. An experimental design was created including six individual trials, namely *Refining*, *Furnish-BCTMP*, *Fillers-PCC*, *Fines*, *Sizing-AKD* and *Fiber orientation-DSF*. Handsheets for each trial were produced at three or four different levels of the respective paper constituent or property starting with a conventional handsheet made of beaten Eucalyptus kraft pulp.

The approach of adapting one single production parameter referring to the *zero point* enabled examination of the relative influence of each parameter on paper curl triggered by inkjet printing. A pilot curl test setup was used to evaluate the curl performance of the manufactured laboratory sheets in terms of magnitude and rate of the deformation. Measurements of wet expansion in ink and stiffness reduction due to printing were additionally conducted.

A summary of the major observations regarding defined Key Performance Indicators (KPIs) is given in Table 15. The arrows ↘ or ↗ indicate a negative or positive correlation to the respective paper property. The magnitude of the influence is shown by two different sizes of the arrows. A line – signifies that there is no correlation.

For instance, a higher level of refining, sizing or BCTMP content leads to a decreasing maximum curvature which points towards non printed side and immediately develops after applying ink onto the sample. An increasing amount of PCC or fines within the paper structure has a negative effect on the initial curl. Sheets with a distinctive fiber alignment in machine direction show a strong maximum curl in CD, whereas specimens in MD achieve comparable results to isotropic sheets.

Table 15. Summary of major observations.

KPI	Refining	BCTMP	PCC	Fines	Sizing	Fiber orientation	
						CD	MD
Maximum curvature	↘	↘	↗	↗	↘	↗	–
End curvature	–	↗	↘	↗	↘	↘	↘
Initial curl creation rate	↘	↗	↘	↘	↘	↗	↘
End strain	↘	↗	↗	–	↘	↗	↘
Initial strain rate	↗	↘	↗	↘	↘	↗	↘
$\tau_{stiffness\ reduction}$	↗	↗	↘	↘	↗	–	↗
Modulus of elasticity E^b	↗	↗	↘	↗	–	↘	↗

The maximum curl shortly after printing and the end curl after four minutes of free drying do not show any systematic correlation. Specimens of the entire handsheet series exhibit an upwards curl towards printed side. The degree of refining is barely relevant regarding the end curvature, whereas oriented sheets show an end curl close to 0, regardless if cutting samples in CD or MD. This is one of the major findings of this work, taking into account that fibers are stiffer and have a lower swelling capacity in longitudinal direction than in transverse direction. However, the end curl is not related to either of these parameters.

A reduced initial curl creation rate is not necessarily accompanied by a lower maximum curvature as particularly observed within the *PCC* and *Fines* trial. In case of BCTMP, a considerable faster curl development do not contribute to a higher maximum curl. The actual proportion of mechanical pulp between 10-40% in the furnish mixture seems to be less significant regarding the majority of investigated KPIs.

Systematic differences between TS and BS printed specimens are essentially seen in case of PCC and to some extent in papers with additional fines content. The occurring variation is related to a structural two-sidedness of papers created during the sheet-forming process. If printed on TS, the mentioned sheets curl initially stronger than if printed on BS where the fine material is located. However, the deformation is in both cases more severe than for conventional handsheets without fillers or additional fines. Regarding the end curvature, fines and fillers behave contrarily.

The oriented sheets produced on a dynamic sheet former do not have any fiber orientation anisotropy two-sidedness, why occasionally appearing differences between top and bottom side printing can not be linked to this type of inhomogeneities over sheet thickness.

The extent of wet strain seems to be somewhat related to maximum curvature but the initial strain rate does not correlate with the initial curl rate.

The modulus of elasticity E^b calculated from bending stiffness and the time constant $\tau_{stiffness\ reduction}$ of the stiffness reduction measurement fairly correlate with the magnitude of the maximum curvature. First, a stiffer sheet counteracts a fast stiffness loss and second, prevents a more severe initial curl. Nevertheless, it simultaneously tend to lead to a more critical end curl. Thus, overexpansion of the not wetted side may not be the reason for a final curl towards printed side. It would be only plausible if the end curl is higher for sheets with lower stiffness. Considering the fact that the *Fines* and *Sizing* trial only exhibit one of these behaviours, print curl is a combination of many individual effects.

A positive impact of increasing the water repellency of papers by sizing agents and thus inhibiting swelling of the pulp fibers is unambiguously detected in all experiments. The lower water uptake into the sheet structure is responsible for a generally enhanced dimensional stability.

Due to the fact that samples were freely dried after printing, the obtained results are hardly comparable to the observations of Hunstein [2] investigating short-term curl of printed paper with included vacuum drying.

To conclude, the following crucial points are observed within the presented thesis:

- Initial maximum curl after printing and short term curl after drying are two different mechanisms.
- A high modulus of elasticity mostly favours a lower maximum curvature and a higher end curvature.
- Higher sheet density leads to an increase of maximum curl but has barely any influence on end curl.
- AKD sized papers show the best performance regarding all investigated deformation issues.
- A distinctive fiber orientation leads to a high maximum curvature in CD but results in an equivalent low end curl in CD and MD.

Outlook

It is evident, that even changing just one paper constituent results in a simultaneous alteration of multiple paper properties. For instance, adding fillers to the paper modifies thickness, porosity, modulus of elasticity, bonding strength, roughness, etc.

Feyrer [3] showed that no substantial correlation between deformation issues and isolated properties of industrial paper sheets can be derived. Thus, a multi-parameter analysis combined with a simulation model would be useful to understand the underlying mechanisms of the liquid-paper interactions causing print curl.

It is proposed to conduct curl tests on the curl test setup at Océ Venlo and on the IPTS [2] with the same set of papers. In this way, the influence of the vacuum drying on the IPTS could be detected and it would be possible to discover if the same mechanisms are effective for print curl with and without drying.

6 Bibliography

[1] T. Harter. "Einflüsse und Ursachen für reversible und irreversible Wölbung von Kopierpapier". MA thesis. TU Graz, Institute of Paper, Pulp and Fiber Technology, Jan. 2018.

[2] O. Hunstein. "Long and short term measurements of printed uncoated fine papers using a high speed inkjet testing setup". MA thesis. TU Graz, Institute of Paper, Pulp and Fiber Technology, July 2017.

[3] S. Feyrer. "Out-of-Plane Deformation Behavior in High-Speed Inkjet cut-sheet Printing". MA thesis. TU Graz, Institute of Paper, Pulp and Fiber Technology, Feb. 2018.

[4] U. Hirn. "Paper Structure at Different Length Scales and its Influence on Paper Properties". Habilitation Thesis. TU Graz, Institute of Paper, Pulp and Fiber Technology, June 2015.

[5] K. Niskanen and P. Pakarinen. "Paper structure". In: *Paper Physics. Book 16 of Papermaking Science and Technology*. Ed. by K. Niskanen. 2nd ed. Paperi ja Puu Oy, 2008. Chap. 1, pp. 11–58. ISBN: 978-952-5216-29-5.

[6] B. Norman. "Web forming". In: *Stock Preparation and Wet End. Book 8 of Papermaking Science and Technology*. Ed. by H. Paulapuro. 2nd ed. Paperi ja Puu Oy, 2007. Chap. 6, pp. 216–288. ISBN: 978-952-5216-25-7.

[7] C.J. Biermann. "Paper Manufacture". In: *Handbook of Pulping and Papermaking*. 2nd ed. Academic Press, 1996. Chap. 9, pp. 209–262. ISBN: 978-0-12-097362-0.

[8] J.D. Parker. *The Sheet-Forming Process*. A Project of the Fluid Mechanics Commitee. TAPPI, 1972.

[9] C. Sörenmark, G. Johansson, and A. Kiviranta. "Charakterization and elimination of fiber orientation streaks". In: *Tappi Engineering Conference 1994*. 1994, pp. 97–104.

[10] J. Blechschmidt, ed. *Taschenbuch der Papiertechnik*. 2nd ed. Hanser, 2013. ISBN: 987-3-446-43802-6.

[11] U. Hirn and W. Bauer. "Evaluating an Improved Method to Determine Layered Fibre Orientation by Sheet Splitting". In: *Proceedings of the 61st Annual APPITA Conference & 2007 Paper Physics Conference*. Vol. 2. 2007, pp. 71–80.

[12] B. Krogerus. "Papermaking Additives". In: *Papermaking Chemistry. Book 4 of Papermaking Science and Technology*. Ed. by R. Alén. 2nd ed. Paperi ja Puu Oy, 2007. Chap. 3, pp. 56–121. ISBN: 978-952-5216-24-0.

[13] J. Sirviö. “Fibres and bonds”. In: *Paper Physics. Book 16 of Papermaking Science and Technology*. Ed. by K. Niskanen. 2nd ed. Paperi ja Puu Oy, 2008. Chap. 2, pp. 60–92. ISBN: 978-952-5216-29-5.

[14] W. Brecht and K. Klemm. “The structural mixture of groundwood as key to understand its technological properties”. In: *Wochenblatt für Papierfabrikation* 80.11 (1952), pp. 364–370.

[15] A. Heikkurinen and L. Leskelä. “The character and properties of mechanical pulps”. In: *Mechanical Pulping. Book 5 of Papermaking Science and Technology*. Ed. by B. Lönnberg. 2nd ed. Paperi ja Puu Oy, 2009. Chap. 15, pp. 458–514. ISBN: 978-952-5216-35-6.

[16] J. Paltakari and E. Lehtinen. “Surface sizing chemicals”. In: *Pigment Coating and Surface Sizing of Paper. Book 11 of Papermaking Science and Technology*. Ed. by J. Paltakari. 2nd ed. Paperi ja Puu Oy, 2009. Chap. 9, pp. 309–315. ISBN: 978-952-5216-27-1.

[17] J. Laine and P. Stenius. “Internal sizing of paper”. In: *Papermaking Chemistry. Book 4 of Papermaking Science and Technology*. Ed. by R. Alén. 2nd ed. Paperi ja Puu Oy, 2007. Chap. 4, pp. 122–162. ISBN: 978-952-5216-24-0.

[18] T. Kilpeläinen and H. Manner. “Internal and surface sizing of inkjet printing papers”. In: *2000 International Printing & Graphic Arts Conference Proceedings*. TAPPI Press, 2000.

[19] D. Glittenberg and N.O. Bergh. “Oberflächenleimungsstrategien für Ink-Jet geeignete Büropapiere”. In: *Wochenblatt für Papierfabrikation* 5 (1995), pp. 182–189.

[20] M. Stankovská, J. Gigac, M. Letko, and E. Opálená. “The effect of surface sizing on paper wettability and on properties of inkjet prints”. In: *Wood Research* 59.1 (2014), pp. 67–76.

[21] S.J. Bares and K.D. Rennels. “Paper compatibility with next generation ink-jet printers”. In: *Tappi Journal* 73.1 (1990), pp. 123–125.

[22] P. Oittinen and H. Saarelma. “Mechanisms of digital printing”. In: *Print Media - Principles, Processes and Quality. Book 13 of Papermaking Science and Technology*. Ed. by P. Oittinen. 2nd ed. Paperi ja Puu Oy, 2009. Chap. 5, pp. 173–210. ISBN: 978-952-5216-33-2.

[23] J. Ketoja. “Dimensional stability”. In: *Paper Physics. Book 16 of Papermaking Science and Technology*. Ed. by K. Niskanen. 2nd ed. Paperi ja Puu Oy, 2008. Chap. 9, pp. 319–350. ISBN: 978-952-5216-29-5.

[24] M. Lindner. “Factors affecting the hygroexpansion of Paper”. In: *Journal of Materials Science* 53 (2018), pp. 1–26.

[25] A. Kulachenko. "Moisture-induced deformations". In: *Mechanics of Paper Products*. Ed. by K. Niskanen. De Gruyter, 2012. Chap. 9, pp. 164–179.

[26] P. Larsson. "Hygro- and hydroexpansion of paper. Influence of fibre-joint formation and fibre sorptivity". PhD thesis. KTH Royal Institute of Technology Stockholm, Department of Fibre and Polymer Technology, Oct. 2010.

[27] T. Uesaka. "Dimensional stability and environmental effects on paper Properties". In: *Handbook of Physical Testing of Paper*. Ed. by R.E. Mark, C.C. Habeger, J. Borch, and B. Lyne. Vol. 1. Marcel Dekker AG, 2001. Chap. 3, pp. 115–171.

[28] L. Carlsson, C. Fellers, and M. Htun. "Curl and two-sidedness of paper". In: *Svensk Papprstiding* 83.7 (1980), pp. 194–197.

[29] U. Hirn and W. Bauer. "Investigating paper curl by sheet splitting". In: *Proceedings of the 2006 Eucepa supported conference: Challenges in Pulp- and Papermaking Technology*. Bratislava, Nov. 2006, pp. 1–18.

[30] M. Schuller. "Untersuchung von Zweiseitigkeiten und Trocknungsspannungen auf das Wölbungsverhalten von Kopierpapieren". MA thesis. TU Graz, Institute of Paper, Pulp and Fiber Technology, Sept. 2016.

[31] G.K. Lau and M. Shrestha. "Ink-Jet Printing of Micro-Electro-Mechanical Systems (MEMS)". In: *Micromachines* 8.6 (2017). Ed. by H. Jiang, pp. 194–213.

[32] E. Hakola and P. Oittinen. "Principles of digital printing". In: *Print Media - Principles, Processes and Quality. Book 13 of Papermaking Science and Technology*. Ed. by P. Oittinen. 2nd ed. Paperi ja Puu Oy, 2009. Chap. 4, pp. 148–172. ISBN: 978-952-5216-33-2.

[33] A. Hudd. "Inkjet Printing Technologies". In: *The Chemistry of Inkjet Inks*. Ed. by S. Magdassi. World Scientific Publishing Co. Pte. Ltd., 2010. Chap. 1, pp. 3–18. ISBN: 978-981-281-821-8.

[34] C. Schmid. "Formulation and Properties of Waterborne Inkjet Inks". In: *The Chemistry of Inkjet Inks*. Ed. by S. Magdassi. World Scientific Publishing Co. Pte. Ltd, 2010. Chap. 7, pp. 123–140. ISBN: 978-981-281-821-8.

[35] S. Krainer. "Evaluierung verschiedener Messmethoden und Testflüssigkeiten zur Bewertung der Druckfarbenpenetration im High Speed Inkjet - Druck". MA thesis. TU Graz, Institute of Paper, Pulp and Fiber Technology, Nov. 2016.

[36] K. Koskenhely. "Refining of chemical pulp fibres". In: *Stock Preparation and Wet End. Book 8 of Papermaking Science and Technology*. Ed. by H. Paulapuro. 2nd ed. Paperi ja Puu Oy, 2007. Chap. 4, pp. 92–139. ISBN: 978-952-5216-25-7.

[37] P. Leuk, M. Schneeberger, U. Hirn, and W. Bauer. "Heat of sorption: A comparison between isotherm models and calorimeter measurements of wood pulp". In: *Drying Technology* 34.5, 563-573 (2016).

[38] L. Jagiello. “Separation and Thickening of Pulp Fibres and Fines in the Lab Scale and Application Thereof”. PhD thesis. TU Graz, Institute of Paper, Pulp and Fiber Technology, 2017.

[39] R. Giner Tovar, W.J. Fischer, R. Eckhart, and W. Bauer. “White Water Recirculation Method as a Means to Evaluate the Influence of Fines on the Properties of Handsheets”. In: *BioResources* 10.4 (2015), pp. 7242–7251.

[40] G. Lindblad and T. Fürst. *The Ultrasonic Measuring Technology on Paper and Board*. 2nd ed. AB Lorentzen & Wettre, 2007.

[41] R.C. Neagu, E.K. Gamstedt, and M. Lindström. “Influence of wood-fibre hygroexpansion on the dimensional instability of fibre mats and composites”. In: *Composites: Part A* 36 (2005), pp. 772–788.

[42] C. Leys et al. “Detecting outliers: Do not use standard deviation around the mean, use absolute deviation around the median”. In: *Journal of Experimental Social Psychology* 49 (2012), pp. 764–766.

[43] K. Luukko and T.C. Maloney. “Swelling of mechanical pulp fines”. In: *Cellulose* 6 (1999), pp. 123–135.

[44] B. Andreasson, J. Forsström, and L. Wågberg. “The porous structure of pulp fibres with different yields and its influence on paper strength”. In: *Cellulose* 10 (2003), pp. 111–123.

[45] M. Bäckström, M.C. Kolar, and M. Htun. “Characterisation of fines from unbleached kraft pulps and their impact on sheet properties”. In: *Holzforschung* 62 (2008), pp. 546–552.

List of Figures

List of Tables

Appendix

A Further results

A.1 Correlation of moduli of elasticity

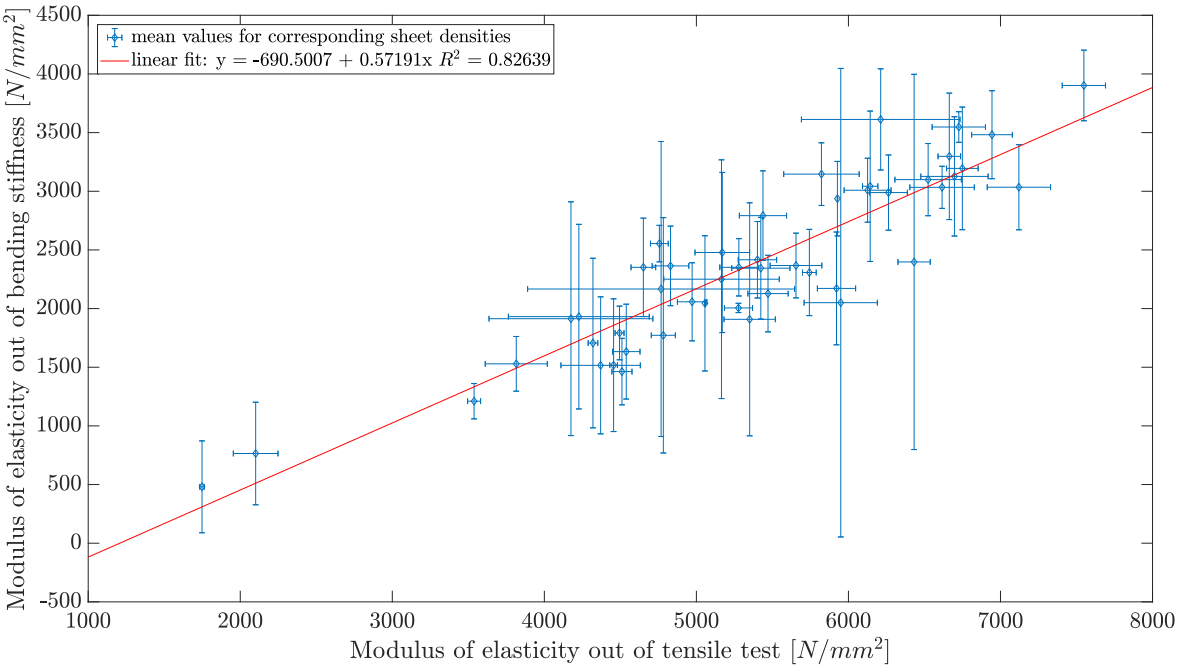

Figure 103. Correlation between modulus of elasticity out of bending stiffness E^b vs modulus of elasticity out of tensile test E^t.

A.2 Comparison of KPIs

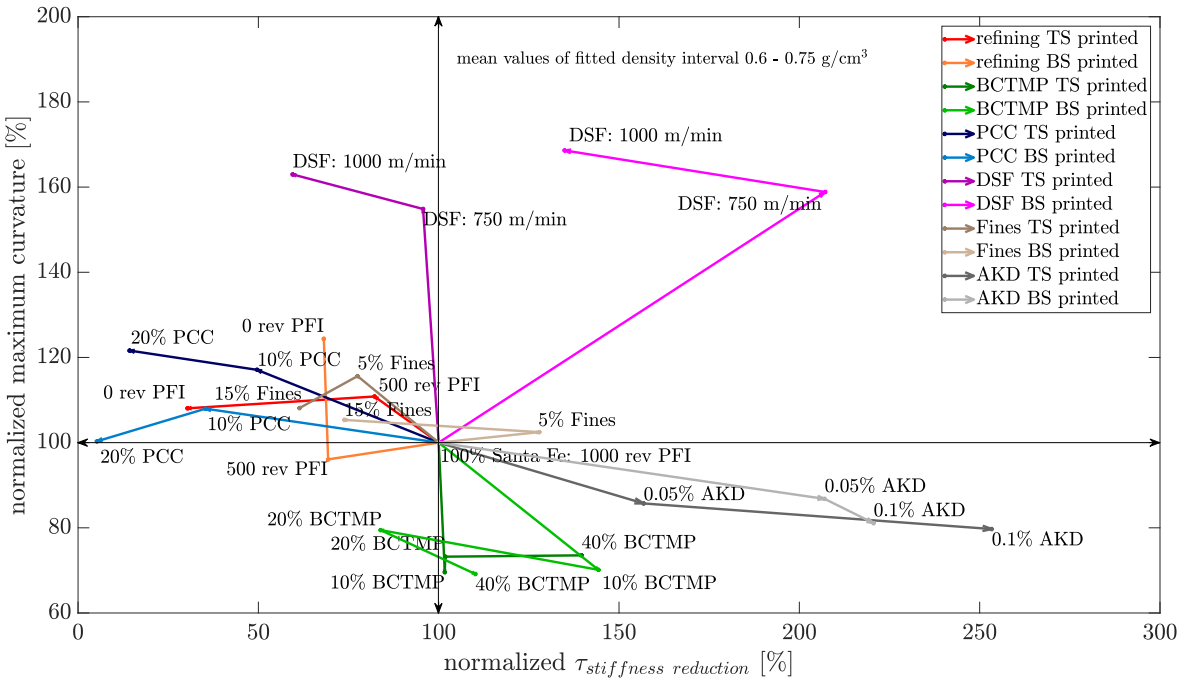

Figure 104. Maximum curvature vs $\tau_{stiffness\ reduction}$ for all trials, TS vs BS.

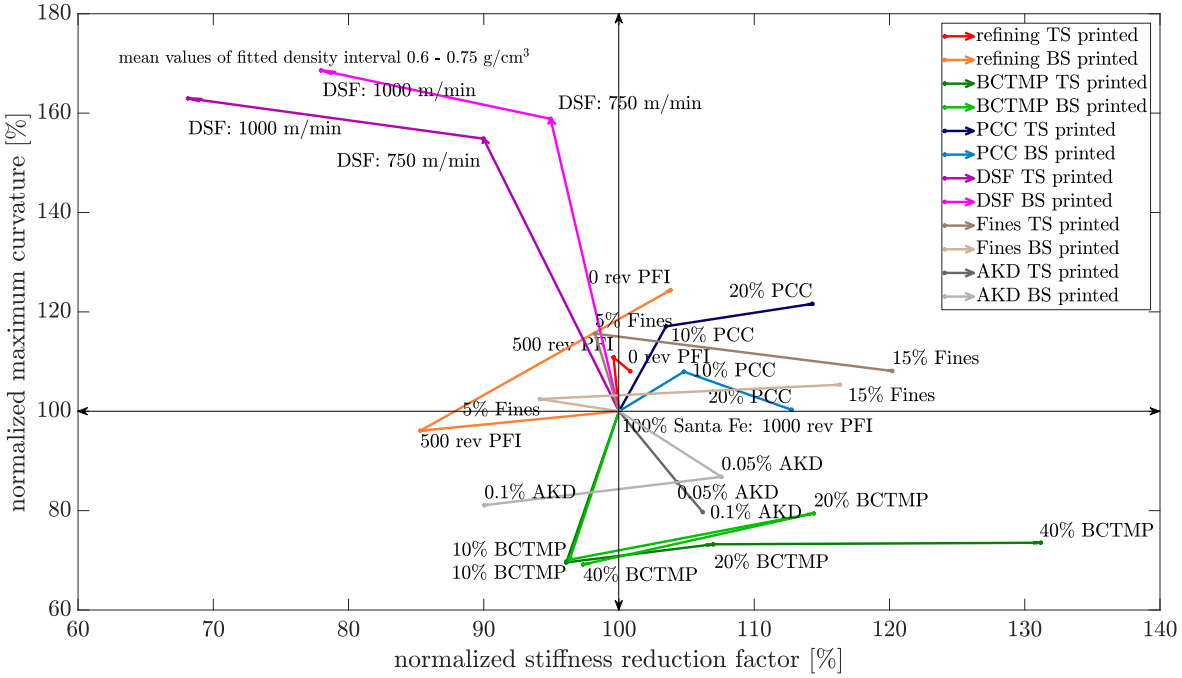

Figure 105. Maximum curvature vs stiffness reduction factor for all trials, TS vs BS.

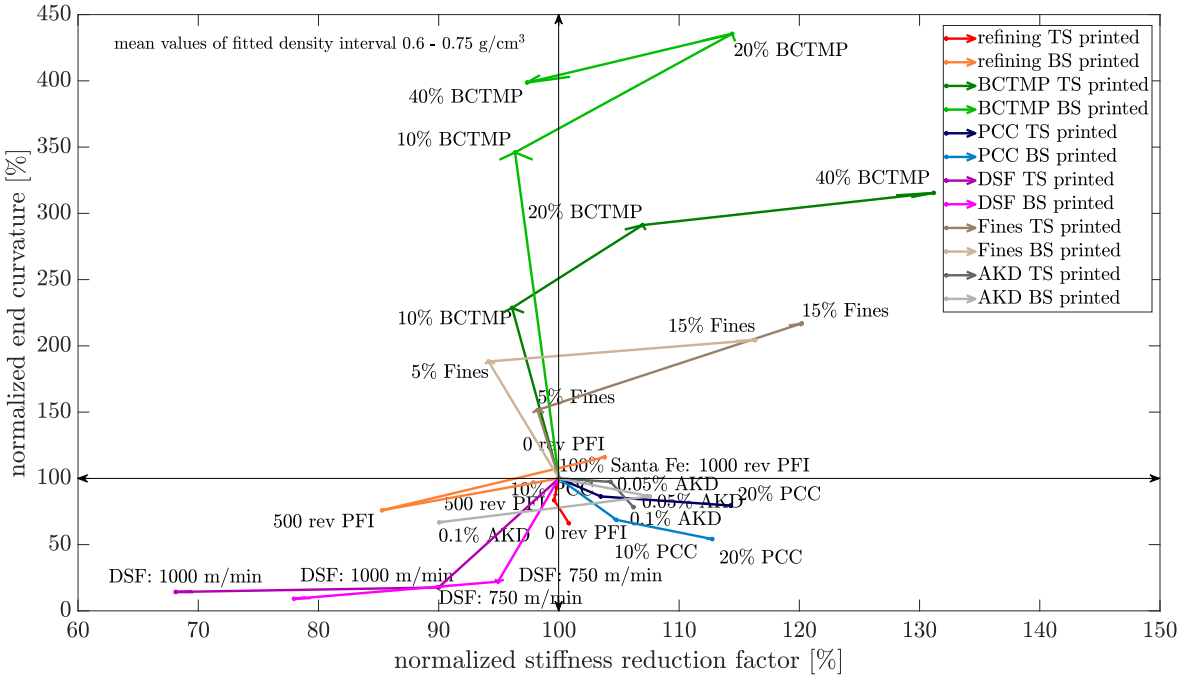

Figure 106. End curvature vs stiffness reduction factor for all trials.

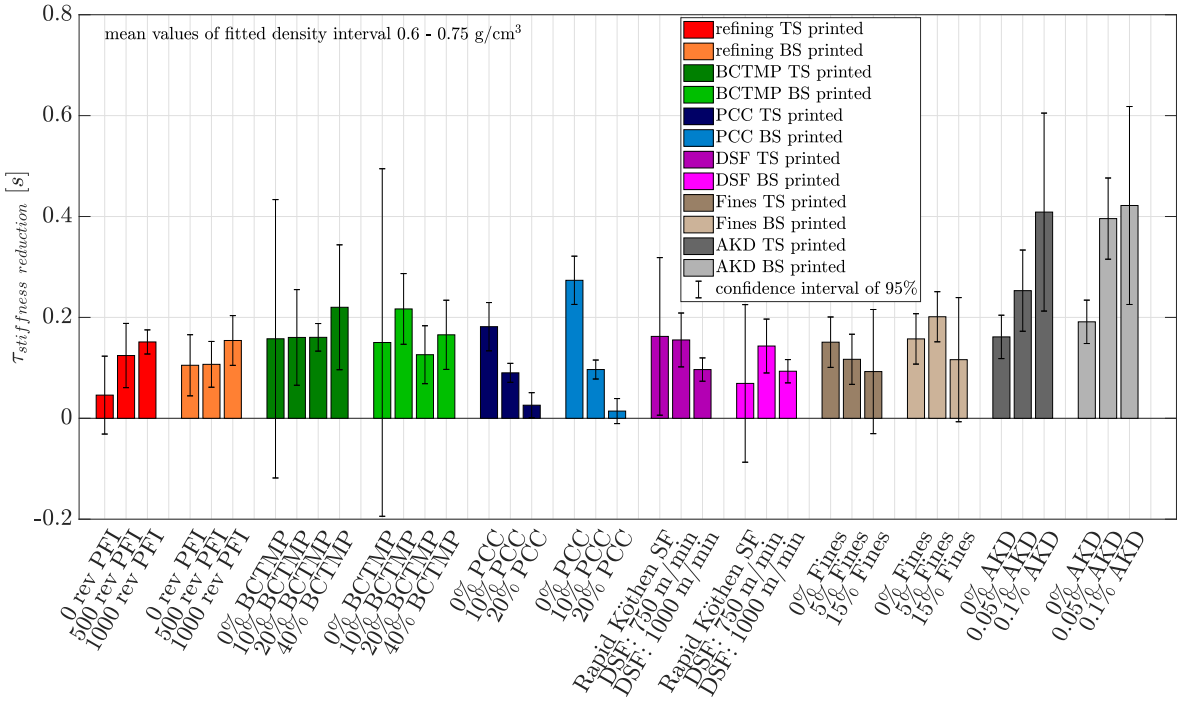

Figure 107. $\tau_{stiffness\ reduction}$ for all trials, TS vs BS.

A.3 Fits of maximum curvature vs density

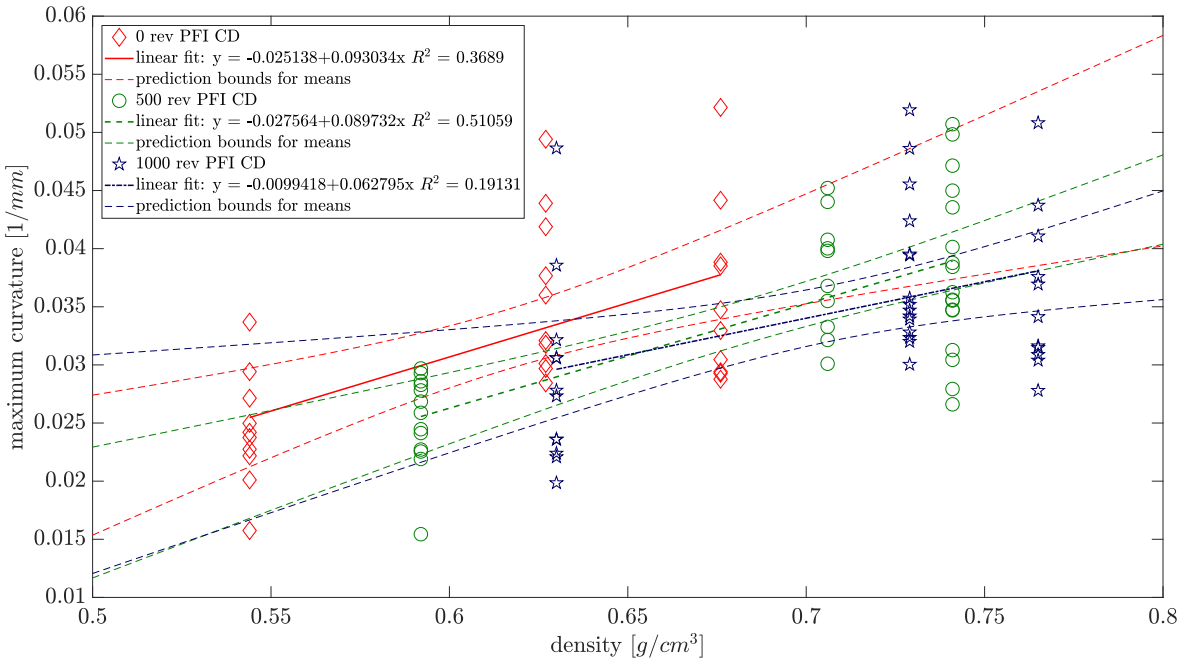

Figure 108. Fit of maximum curvature vs density for *Refining* trial.

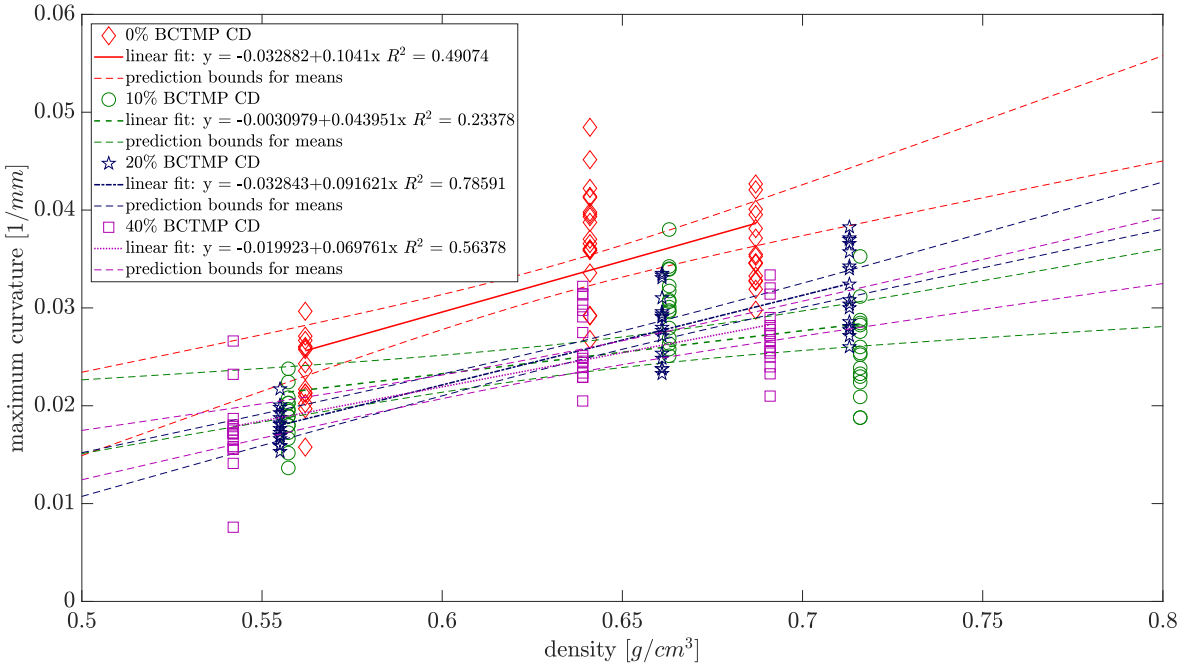

Figure 109. Fit of maximum curvature vs density for *BCTMP* trial.

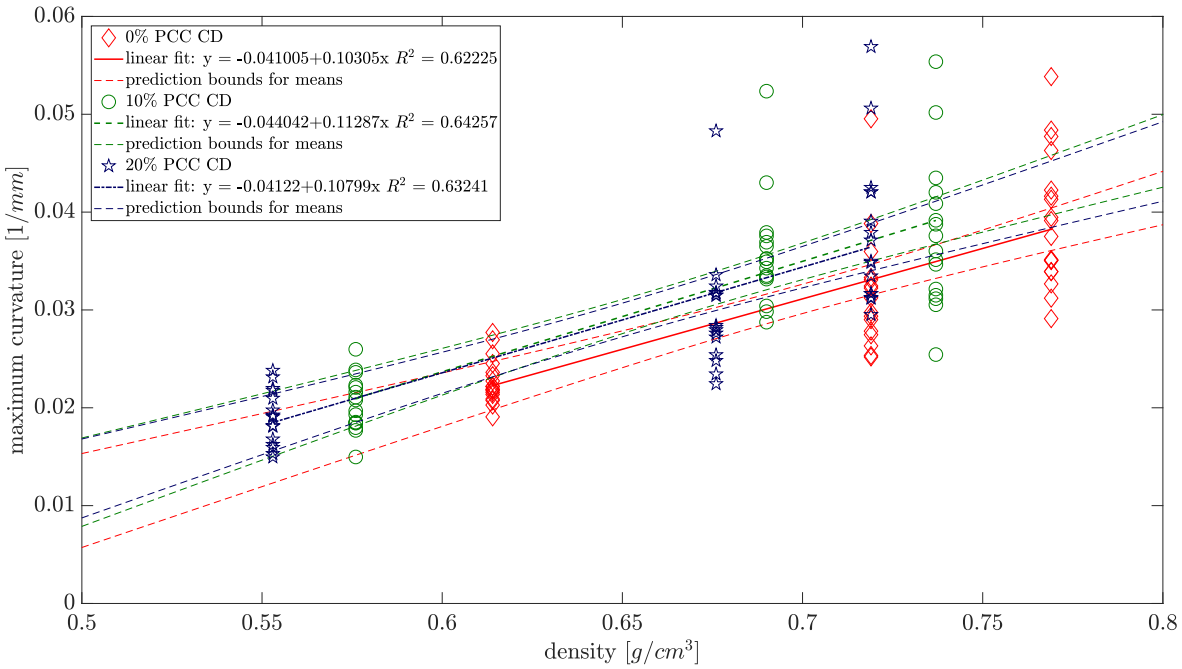

Figure 110. Fit of maximum curvature vs density for *PCC* trial.

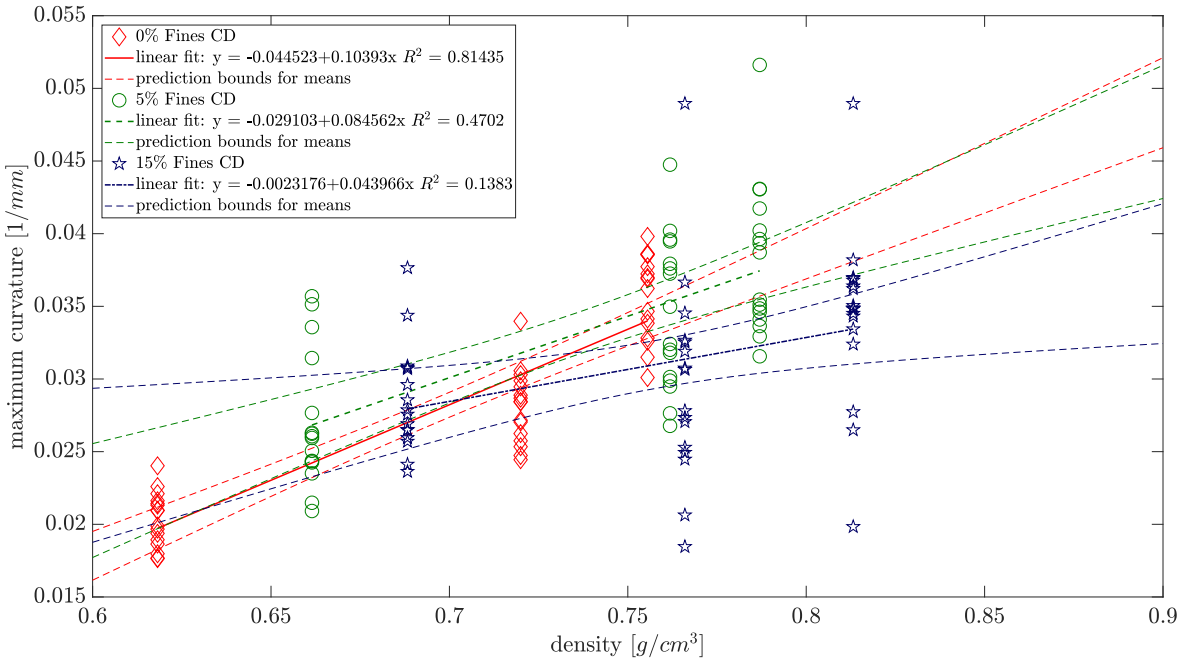

Figure 111. Fit of maximum curvature vs density for *Fines* trial.

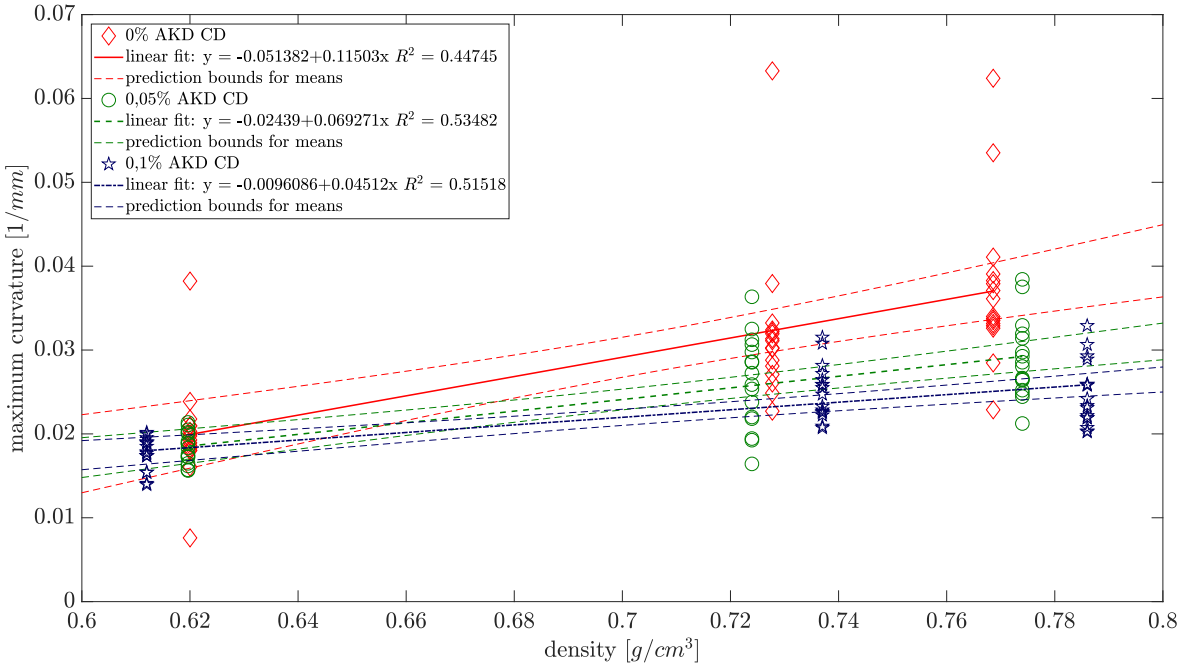

Figure 112. Fit of maximum curvature vs density for *AKD* trial.

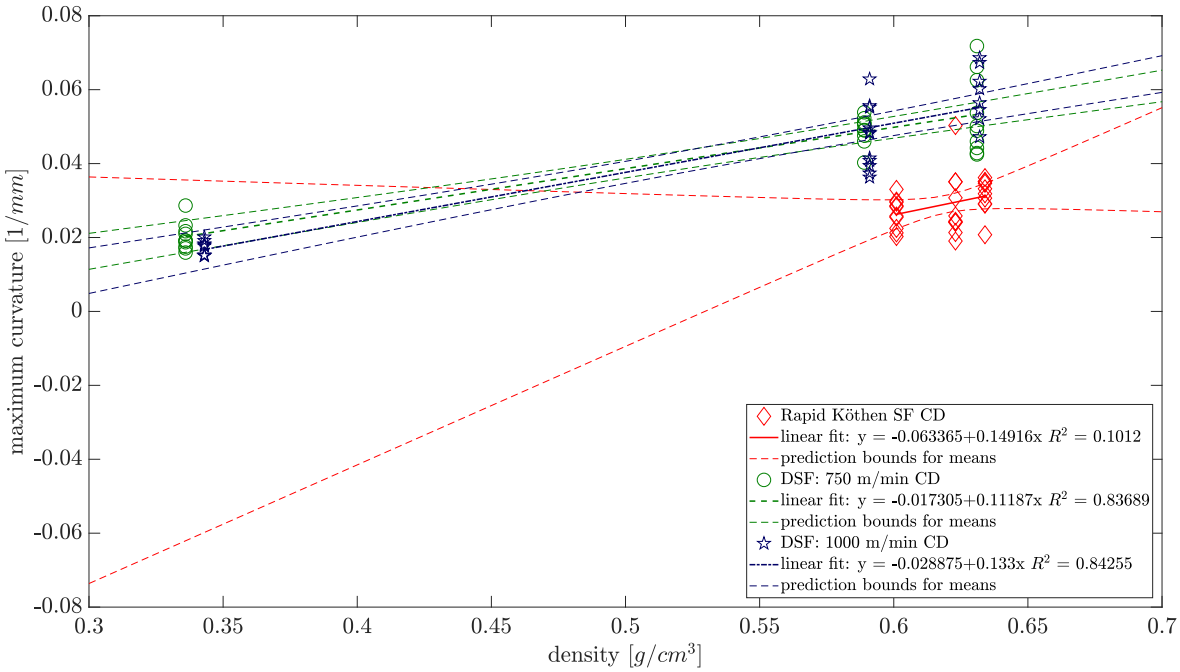

Figure 113. Fit of maximum curvature vs density for *DSF* trial.